Electrical Engineering and Automation

Magneto-vibro-acoustic Computational Techniques for Electrical Machines

Sabin Sathyan

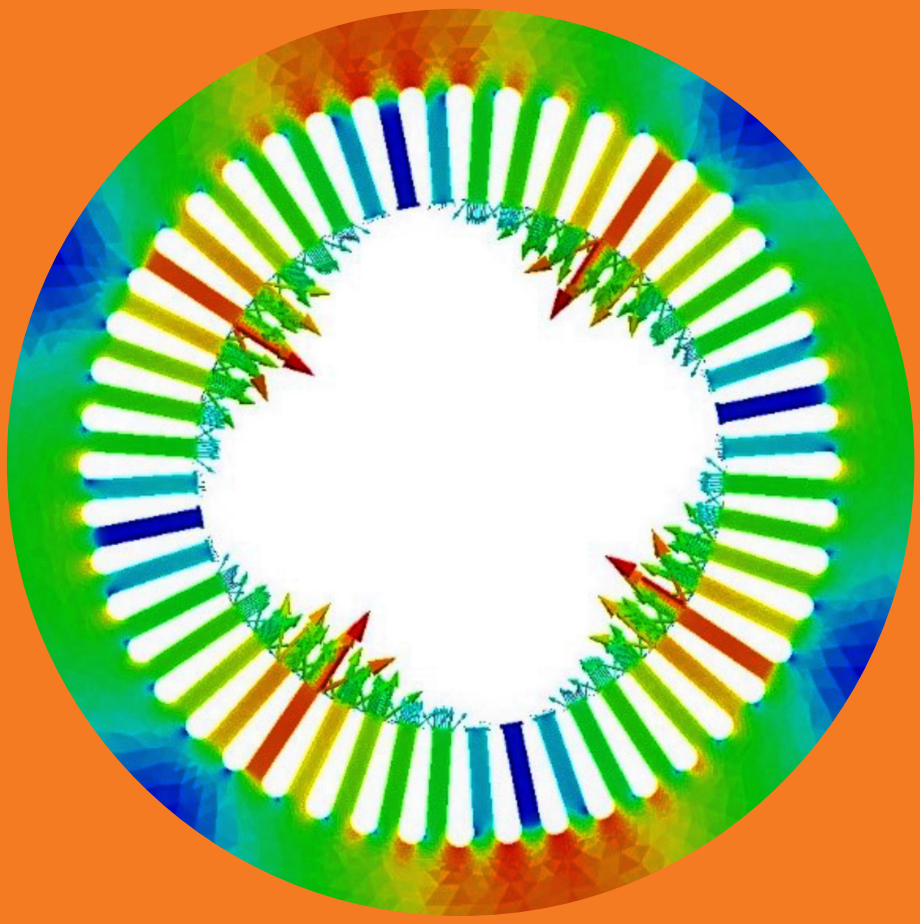

Aalto University

DOCTORAL DISSERTATIONS

Aalto University publication series
DOCTORAL DISSERTATIONS 34/2020

Magneto-vibro-acoustic Computational Techniques for Electrical Machines

Sabin Sathyan

A doctoral dissertation completed for the degree of Doctor of Science (Technology) to be defended, with the permission of the Aalto University School of Electrical Engineering, at a public examination held at the lecture hall AS2 of the school on 13 March 2020 at 12 noon.

Aalto University
School of Electrical Engineering
Electrical Engineering and Automation
Electromechanics

Supervising professor
Prof. Anouar Belahcen

Preliminary examiners
Prof. Youguang Guo, University of Technology Sydney, Australia
Prof. Guillaume Krebs, University of Paris-Sud, France

Opponent
Prof. Chris Gerada, University of Nottingham, United Kingdom

Aalto University publication series
DOCTORAL DISSERTATIONS 34/2020

ISBN 978-952-60-8969-0 (printed)
ISBN 978-952-60-8970-6 (pdf)
ISSN 1799-4934 (printed)
ISSN 1799-4942 (pdf)
http://urn.fi/URN:ISBN:978-952-60-8970-6

Unigrafia Oy
Helsinki 2020

Finland

NORDIC SWAN ECOLABEL
Printed matter
4041-0619

Aalto University

Abstract

Aalto University, P.O. Box 11000, FI-00076 Aalto www.aalto.fi

Author
Sabin Sathyan

Name of the doctoral dissertation
Magneto-vibro-acoustic Computational Techniques for Electrical Machines

Publisher School of Electrical Engineering

Unit Electrical Engineering and Automation

Series Aalto University publication series DOCTORAL DISSERTATIONS 34/2020

Field of research Electromechanics

Manuscript submitted 14 October 2019 **Date of the defence** 13 March 2020

Permission for public defence granted (date) 31 January 2020 **Language** English

☐ **Monograph** ☒ **Article dissertation** ☐ **Essay dissertation**

Abstract

This thesis investigates the electromagnetic, magnetomechanical and vibro-acoustic interactions in an electrical machine, and proposes numerical computational tools and experimental techniques for modeling these phenomena in electrical motors. In an electrical motor, the supplied electrical energy goes through different physical domains in the form of magnetic, mechanical, acoustic and thermal energy. In this thesis, computational methods for magnetic forces, magnetostriction, mechanical deformations, vibrations, and finally the acoustic sound produced by electrical motors are successfully implemented.

The study starts with the analysis of magnetic forces in ferromagnetic materials and electrical motors by crafting finite element methods for computing these forces and validating them with experiments. From there, the investigations proceed to structural mechanics zone, where the effects of magnetic forces and magnetostriction on the deformations and vibrations of electrical steel sheets and the stator core of electrical motors are studied using numerical methods and experimental justifications. The causes of vibrations in two induction motors were examined with computational and experimental methodologies. The generation of acoustic noise due to mechanical vibrations is modeled using a numerical method that is based on a combination of the finite-element and boundary-element methods.

The results and findings in the thesis from numerical and experimental studies provide efficient tools for analyzing and computing various quantities pertaining to the behavior of ferromagnetic materials and electrical motors. These methods can be applied in practical facets such as the design and condition-monitoring stages of electrical motors. This thesis has succeeded in addressing different domains of energy conversions and their effects in electrical machines by developing reliable and proficient computational tools and experimental methods in the realms of magnetics, mechanics and acoustics.

Keywords Electrical machines, Finite Element Analysis, Magnetic Forces, Magnetostriction, Vibrations, Acoustics

ISBN (printed) 978-952-60-8969-0 **ISBN (pdf)** 978-952-60-8970-6

ISSN (printed) 1799-4934 **ISSN (pdf)** 1799-4942

Location of publisher Helsinki **Location of printing** Helsinki **Year** 2020

Pages 181 **urn** http://urn.fi/URN:ISBN:978-952-60-8970-6

Preface

This PhD project was carried out at the Research Group of Computational Electromechanics in the Department of Electrical Engineering and Automation, Aalto University School of Electrical Engineering, between June 2015 and September 2019. I am greatly thankful to my supervisor Prof. Anouar Belahcen for the support, guidance, motivation and inspiration that he has given during my tenure as a PhD candidate. I would also like to thank Prof. Antero Arkkio for his help and support since I joined in Aalto University. I am grateful to Dr. Juhani Kataja from CSC for his guidance and advice concerning my work. I am very appreciative to my colleagues Dr. Antti Lehikoinen and Dr. Ugur Aydin for their help in many crucial tasks. I extend my gratitude to Mr. Ari Haavisto for his help at the laboratory. In addition to the people from Aalto, I would like to thank Prof. Jianguo Zhu from the University of Technology Sydney for his support and hosting me as an exchange researcher.

The pre-examination of this thesis was done by Prof. Youguang Guo from University of Technology Sydney, Australia and Prof. Guillaume Krebs from GeePs and Paris-Sud University, France to whom I am thankful for the constructive feedbacks and comments that helped to improve the thesis manuscript.

I would like to acknowledge the financial support from the projects SEMTEC, CEM3D, MORE and Oy Strömberg Ab. Besides, I would like to thank VTT and Ingersoll Rand Oy for their collaboration in laboratory experiments and measurement projects.

My colleagues at the Research group of Electromechanics have supported and encouraged me to succeed and flourish as a PhD student, and I am indebted to everyone at the group for every moment that I have spent with them. I want to extend my thanks to my friends and colleagues Devi Nair, Mehrnaz Farzam Far, Toni Tukia, Simo Uimonen, Mikael Kauppinen, Sasu Tamminen, Ravi Sundaria, Aswin Balasubrahmanian, Osaruyi Osemwenyan, Brijesh Upadhyaya, Floran

Martin, John Ocsalev, Sahas Bikram Shah and countless others for their companionship and support. It has been truly joyous and exuberant to spend time with all of you during numerous occasions like our coffee breaks, international lunch and sit-sit parties, after-work beers and so forth. I have been fortunate to have worked with many professionals from outside the university and I am thankful to Dr. Janne Keränen, Dr. Paavo Rasilo, Dr. Fredrik Boxberg, Dr. Pavel Ponomarev and Dr. Ahmed Hedeida for their valued guidance.

Finally, I want to thank my family; my parents Bindu and Sathyan, my sister Sukanya and brother Bibin for their unconditional love and care. I am presenting this thesis with the joy of seeing the smile of my niece Nila.

Espoo, 14 October 2019
Sabin Sathyan

Contents

List of Publications

This doctoral dissertation consists of a summary of the following publications, which are referred to in the text by their Roman numerals.

I. Sabin Sathyan, Anouar Belahcen, Juhani Kataja, Francois Henrotte, Abdelkader Benabou, and Yvonnick Le Menach. Computation of Magnetic Forces using Degenerated Airgap Element. *IEEE Transaction on Magnetics*, Volume 53, June 2017.

II. Sabin Sathyan, Anouar Belahcen, Ugur Aydin, Juhani Kataja, Vesa Nieminen and Janne Keränen. Computational and Experimental Segregation of Deformations due to Magnetic Forces and Magnetostriction. In *The 20th International Conference on Electrical Machines and Systems (ICEMS 2017)*, Sydney, Australia, August 2017.

III. Janne Keränen, Pavel Ponomarev, Sabin Sathyan, Juhani Kataja and Anouar Belahcen. Magneto-structural Simulation of an Induction Motor Start-up using Nodal Magnetic Forces in Elmer. *Journal of Structural Mechanics*, Volume 50, pp. 296-299, August 2017.

IV. Sabin Sathyan, Ugur Aydin, Antti Lehikoinen, Anouar Belahcen, Toomas Vaimann and Juhani Kataja. Influence of Magnetic Forces and Magnetostriction on the Vibration behavior of an Induction Motor. *International Journal of Applied Electromagnetics and Mechanics*, Volume 59, pp. 825-834, December 2018.

V. Sabin Sathyan, Antti Lehikoinen, Ugur Aydin, Anouar Belahcen and Fredrik Boxberg. Investigation of the Causes behind the Vibrations of a High-Speed Solid-Rotor Induction Motor. *Journal of Sound and Vibration,* Volume 463, September 2019.

VI. Sabin Sathyan, Ugur Aydin and Anouar Belahcen. Acoustic Noise Computation of Electrical Motors using the Boundary Element Method. *Energies*, Volume 13, December 2019.

Author's Contribution

Publication 1: "Computation of Magnetic Forces using Degenerated Airgap-Element"

In this paper, an efficient method to calculate the magnetic forces on bodies in contact is presented. The results from this method are validated with measurements on a permanent magnet setup. The degenerated airgap element method facilitates a cost effective and effectual platform for electromechanical computation of electromechanical devices and magnetic materials. This method noticeably reduces the computational load of heavy meshing and pricey finite element simulations. For applications where accurate force computations are essential, the degenerated air-gap element method is a brilliant choice, as one does not have to concentrate on complex meshing at contacts of complex structures.

This publication is a joint work among the other co-authors. The theoretical background of the force computation method was developed in close collaboration between Sabin Sathyan and Juhani Kataja, who also implemented the model in a finite element open-source software tool *Elmer*. Anouar Belahcen gave valuable contribution through advice and suggestions. Abdelkader Benabou and Yvonnick Le Menach conducted the experiments and measurements and Francois Henrotte did the eggshell method modeling. Sabin performed all the simulations, postprocessing and design of the example models and machines given in the paper. He also wrote the manusctript for the paper.

Publication 2: "Computational and Experimental Segregation of Deformations due to Magnetic Forces and Magnetostriction"

In this paper, an original experimental setup to measure the deformation in an iron sheet under the influence of an electromagnetic field is presented. The

measurement results of the strain in the sheet are compared with the simulation results and then postprocessed to separate the effects of magnetic forces and magnetostriction on the deformation of the sheet. These experimental and numerical studies provide insight on how magnetic forces and magnetostriction primarily affect the mechanical behavior of magnetic materials. The results can be used as reference for further extensive studies on electrical machines.

This publication is a joint work among the other co-authors. Sabin Sathyan designed the experimental setup and the test specimen and performed all the simulations presented in the paper. Ugur Aydin identified the parameters for the magnetomechanical model and Anouar Belahcen contributed in both design and model implementation processes. Juhani Kataja implemented the model in the open-source software. Vesa Nieminen and Janne Keränen both supported and participated in the experiment at the laboratory. Sabin Sathyan also wrote the manuscript for the paper.

Publication 3: "Magneto-structural Simulation of an Induction Motor Start-up using Nodal Magnetic Forces in Elmer"

In this paper, the Generalised Nodal Forces implemented in the open-source finite-element software tool *Elmer* are used for studying the vibration behavior of an induction motor during the start-up stage. A direct coupling method is used to couple the nodal magnetic forces to the structural solver in *Elmer* to compute the deformation of the stator core of the motor. One major outcome of the paper is the successful demonstration of the capability of the open-source multiphysics FEM software tool *Elmer* in magnetomechanical computations of electrical motors.

This publication is a joint work among the other co-authors. Janne Keränen is the corresponding author of the paper, along with Pavel Ponomarev who contributed to the simulations and postprocessing of the results. Sabin Sathyan contributed significantly in the computation of nodal forces in *Elmer* and the implementation of the magnetomechanical coupling method to calculate the deformations. Juhani Kataja performed the nodal force computation coding in *Elm*er. Anouar Belahcen participated in the development of the numerical methods for computing forces.

Publication 4: "Influence of Magnetic Forces and Magnetostriction on the Vibration behavior of an Induction Motor"

In this paper, the effect of both the magnetic forces and magnetostriction are inspected and differentiated based on their contribution to the vibration behavior of an induction motor. The results of the study reveal that the effect of magnetic forces and magnetostriction can have a varying influence on different kinds of machines, as they can either strengthen or counteract each other, and affect the amount of deformation and vibrations in opposite ways. It has been inferred that, in magnetomechanical studies of electrical motors such as stress and noise analysis, magnetostriction is an inevitable factor. The proposed magnetomechanical models successfully modeled the vibration spectra of the motor, which is an important factor in the noise analysis of electrical machines.

This publication is a joint work among the other co-authors. Sabin Sathyan formulated and developed the framework of the study, including the types of motors to be inspected, various parameters to be analyzed and did all the simulations, post-processing and inferences of the results. Antti Lehikionen did the Matlab implementation of the magnetomechanical model, the parameters of which were developed by Ugur Aydin. Anouar Belahcen was part of both measurement and simulation studies as he advised and suggested techniques to be undertaken. Juhani Kataja performed the open-source implementation of force computation and Toomas Vaimann did the vibration measurements. Sabin Sathyan also wrote the manuscript for the paper.

Publication 5: "Investigation of the Causes behind the Vibrations of a High-speed Solid-Rotor Induction Motor"

In this paper, the vibrations from a high-speed solid-rotor induction motor were studied by measurement data and finite element simulations. The study considered the effect of magnetic forces, magnetostriction, power supply and the presence of a rotor eccentricity fault on the vibration behavior of the motor. The presence of rotor dynamic eccentricity was found to be a major cause in creating additional frequency components in the frequency spectra of the vibrations, compared to normal, non-faulty operation of the machine. A close agreement was achieved in terms of the frequency components present in the simulated

vibration spectra using the energy-based magnetomechanical model and the measured vibrations.

This publication is a joint work among the other co-authors. Sabin Sathyan performed the magnetomechanical simulations, postprocessing of the frequency components, the theoretical derivations and analytical interpretations of electromagnetic stress, the faults and their connection with the vibrations. The parameters for the energy-based model were formulated by Ugur Aydin through measurements and fitting, and Antti Lehikoinen performed the Matlab implementation of the coupled model. Anouar Belahcen helped create the research methods and contributed to the tactics of analysis of the vibration problem in the motor. Fredrik Boxberg had the major role in vibration measurements. Sabin Sathyan also wrote the manuscript for the paper.

Publication 6: "Acoustic Noise Computation of Electrical Motors using the Boundary Element Method"

In this paper, the sound pressure level produced by a high-speed solid rotor induction motor is calculated using a numerical simulation method based on a combined finite element and boundary element methods. The electromagnetic finite element simulation calculates magnetic forces; the magnetomechanical coupling in structural mechanics simulation is used for the computation of stator deformations and vibrations; and, finally, the boundary element method is employed for the acoustic computations, where a vibro-acoustics connection is illustrated using an acoustic-structure boundary condition. This multi-level coupling approach is an efficient technique for vibro-acoustic computations of electrical motors.

In this study, Sabin Sathyan conceptualized the framework of numerical computations. He made the geometries, meshes and created the numerical model using a commercial software. Ugur Aydin contributed in the structural mechanics part of the study and Anouar Belahcen supervised the work with valuable advice on the format of magnetomechanical and vibro-acoustic computations. Sabin Sathyan performed the results visualizations and postprocessing and he wrote the entire manuscript.

List of Abbreviations and Symbols

$\boldsymbol{A}$	Magnetic vector potential
$\boldsymbol{B}$	Magnetic flux density
$\boldsymbol{C}$	Elastic modulus
c	Speed of sound
$\boldsymbol{d}$	Displacement field
d_{e}	Degree of dynamic eccentricity
$\boldsymbol{E}$	Electric field strength
$\boldsymbol{F}$	Total magnetic force
$\boldsymbol{f}$	Volume force
G	Shear modulus
g	Average airgap length
$\boldsymbol{H}$	Magnetic field strength
$\boldsymbol{I}$	Unit tensor
I_i	ith Invariant
J	Current density
$\boldsymbol{J}_{\mathbf{s}}$	Jacobian matrix in FEM
K	Boundary element
$\boldsymbol{M}$	Magnetization
Q	Monopole domain source
q_d	Dipole domain source
m	Space harmonic number
$\boldsymbol{N}$	Nodal shape function
n	Time harmonic number
P_{s}	Sound pressure

p	Number of pole pairs
p_t	Acoustic pressure
T	Temperature
t	Time
$\boldsymbol{u}$	Unit vector
V	Volume
v	Velocity
W_s	Magnetic energy
β	Heat expansion tensor
β_S	Adiabatic compressibility coefficient
ε	Strain
λ	Lamé constant
Λ	Permeance
μ	Magnetic permeability
μ_0	Permeability of vacuum
ν	Magnetic reluctivity
ν_0	Reluctivity of free space
ρ	Mass density
σ	Stress
σ_e	Electric conductivity
σ_r	Radial stress
σ_ϕ	Shear
$\boldsymbol{\tau}$	Maxwell stress tensor
ϕ	Reduced electric scalar potential
φ	Angular position
Ω	Area
ω	Angular frequency

∇	Gradient operator
$\nabla \cdot$	Divergence operator
$\nabla \times$	Curl operator
$\|\|$	Determinant of a matrix

2D	Two dimensional
3D	Three dimensional
BEM	Boundary Element Method
FE	Finite Element
FEA	Finite Element Analysis
FEM	Finite Element Method
GNF	Generalised Nodal Forces
MS	Magnetostriction
PWM	Pulse-width modulation

The subscripts r and ϕ within a vector quantity refer respectively to the radial and circumferential component of that quantity in a polar coordinate system.

Superscript e within a quantity refers to the same quantity at the element level.

The subscripts n and t within a vector quantity refer respectively to the normal and tangential component of that quantity with respect to a given surface.

The quantities representing vectors, tensors and matrices are denoted by bold face in the text.

1. Introduction

1.1 Background

Since their invention in the beginning of the 19th century, electromechanical energy converters, such as electrical generators and motors, have been a prevalent factor of industrial and infrastructure development around the globe. There have been numerous types of electrical machines developed for different kinds of applications, and the research and development of electrical machines technology remain as a significant area in electrical engineering. The term electrical machines in electrical engineering generally indicates any machine that uses electromagnetic forces as the principle behind their operation. Hence, the backbone of design, development and analysis of electrical machines comprises the study of electromagnetic forces and associated electromechanical phenomena.

Electrical generators produce nearly all the electrical power on the planet and electrical motors driven systems consume around 45% of this power. The present world electrical machines have attained more than 95% efficiency with innovative designs and control algorithms. Electrical machines are the linchpins in the engineering driving force of industrial, commercial, automotive and residential sectors. Industrial development has taken its toll on the planet in the form of pollution, climate change and related negative impacts on the environment. The conservation of the environment and reduction of fossil fuels point to green energy and alternative forms of energy technologies that are sustainable and eco-friendly. Switching to electrical machines from fuel-based technologies reduces the negative environmental impact, although electrical machines are not entirely free from polluting effects and carbon footprints. However, in recent years, there has been a world-wide increase in the use of electrical machines in place of traditional fuel engines. One chief area is the automotive in-

dusty, where the development of electric and hybrid vehicles has escalated massively in the last decade. Since the development of global infrastructure relies heavily on electrical machines, the focus on developing highly efficient machines with minimal polluting effects is of critical importance.

The reduction in electrical machine losses - such as load losses, iron losses, mechanical losses and additional losses - is attained by advanced optimization techniques in terms of machine design, manufacturing processes and the selection of materials for different parts of the machine. Besides the electrical machine itself, other components in a power train, such as frequency converters and related drive modules, all contribute to the performance of the machine. One major consequence of the operation of electrical machines is their vibration and subsequent acoustic noise. The causes of vibration and noise can be divided into different categories such as electromagnetic, mechanical and aerodynamic facets. The electromagnetic causes of vibrations were found to be magnetic forces and magnetostriction. The magnetomechanical phenomenon that causes geometrical deformation in a ferromagnetic material under the influence of an external magnetic field is called magnetostriction. The mechanical components such as the bearings and cooling systems also contribute to unwanted vibrations and noise. A solid grasp of the magnetic forces and magnetostriction and ways to mitigate their undesirable effects are hence critical factors in vibro-acoustic studies of electrical machines. The study of these phenomena includes the analytical and numerical modeling of magnetic forces, magnetostriction, vibration and noise through electromagnetic, magnetomechanical and vibro-acoustic models.

The vibrations in electrical machines produce undesirable acoustic noise in nearby environments and it can also cause weakened performance and lifespan of the machines and associated systems. Analytical and numerical modeling, investigation of causes of vibration and noise, and development of methods to reduce the vibro-acoustic phenomena in machines are hence significant in machine design and condition-monitoring phases. Accurate models of magnetic forces, forces of bodies in contact, electromechanial coupling phenomenon and acoustic noise are indispensable in such studies. This thesis attempts to develop computational methods for electromagnetic phenomena such as magnetic forces and magnetostriction, and apply those models for the analysis of vibration and acoustic characteristics of electrical machines. The major attention will

be on the calculation of magnetic forces and implementing those using Finite Element Analysis (FEA) software tools. Furthermore, the use of magnetic forces in vibration analysis and the development of magnetomechanical coupled models, including magnetostriction in detailed vibration analysis of electrical motors, are presented. Finally, the outputs from the magnetomechanical models are taken into the acoustic realm for the computation of noise.

1.2 Objectives and Focus of the Thesis

The main aim of the thesis is to develop magnetic and magnetomechanical computational methods for electrical machines by implementing calculation models for magnetic forces, magnetostriction, vibration and noise. The Finite Element Method (FEM) is the numerical tool used for electromagnetic and magnetomechanical computations, and for acoustic studies, the Boundary Element Method (BEM) is employed. The major focus has been given to applying the models in different kinds of electrical motors, articulating extensive investigation methods both computationally and experimentally to understand the electromagnetic phenomena behind vibrations and noise. The study covers the examination of both material level and component level features of the machines.

The electromagnetic forces are computed using methods that suit the application of magnetic forces to vibration analysis and for special cases like two bodies in contact, where an infinitesimally small airgap is present in a machine. The vibrations of electrical motors are examined with different magnetomechanical coupling methods to understand the effect of both magnetic forces and magnetostriction. The sound produced by vibrations, or the noise, is calculated by coupling the finite element and boundary element methods.

The major focus of this thesis is on studying the vibrations in electrical motors due to the inherent properties of iron, such as electromagnetic forces and magnetostriction. These two phenomena are extensively analyzed and the thesis reviews how they contribute to the mechanical deformations and vibrations. Despite having done the study of vibrations using measurements and frequency analysis, the mechanical aspects related to vibrations - such as modal analysis and the influence of frame and mechanical bearings - are beyond the scope of this thesis because the author has concentrated on investigating the mechanics

and vibrations of machines predominantly from an electromagnetic standpoint. Besides, an expansive examination of vibro-acoustics and noise analysis is also beyond the space constraints of this thesis. The acoustic noise analysis is presented in the final part of the thesis primarily to establish the interconnected nature of the magnetic, mechanical and acoustic properties of an electrical machine, and hence to demonstrate the importance of electromagnetics in vibro-acoustic studies.

The main scientific contributions of this thesis are summarized as follows:

- The computation of electromagnetic forces using the Virtual work principle is successfully implemented in this thesis to calculate the Generalized Nodal Forces (GNF). The nodal forces are crucial in vibration studies as they are localized forces on nodes that facilitate accurate computation of deformations in machine geometries and resulting vibrations. The nodal magnetic forces are utilized in a direct magnetomechanical coupling to compute the vibrations and stress distribution in electric motors and end windings, and it has been found to be a simple but efficient method for the calculation of mechanical quantities such as stress, deformations and vibrations in different parts of a machine. Moreover, the implementation of both 2D and 3D computational models in an open-source finite element software tool that has been originally done for this thesis provides a cost-effective, yet efficient means for numerical computations of electrical machines.
- An effectual method to compute the magnetic forces on bodies in contact is developed and proved to be very accurate from the comparison between experimental and numerical calculation results. As a contribution of this thesis, the application of the Virtual work principle is extended to the so-called degenerated air-gap elements to calculate the magnetic forces where an infinitesimal air gap is present. This method reduces the finite element computational burden associated with heavy meshing of thin layers in intricate parts of the machines, without compromising the accuracy of the results.

- A free-energy based coupled magnetomechanical model to consider magnetostriction is employed for studying the deformations and vibrations in electrical motors, with experimental verificatios. This improves the accuracy of vibration computations, because the dependency on magnetic material properties on magnetostrictive stress is considered in this model. Besides, the computational results using this model indicate that the interaction of magnetic forces and magnetostriction changes the deformation behavior of the core material and hence the magnitude of vibrations in electrical motors. The magnetomechanical simulation results were compared with vibration measurements and proved to be reliable.
- The interaction and effect of magnetic forces and magnetostriction in electrical steel sheets is studied through an original experiment to analyze how these two phenomena contribute to the mechanical deformation of ferromagnetic materials. This study gives light on how different parameters, such as the structure of a material sample, and the method of electromagnetic excitation affect the geometric deformations of the material. In any scenario where a ferromagnetic material is electromagnetically excited, the defining factors that determine which phenomenon among magnetic forces and magnetostriction dominates over the other are the shape of the material, especially whether an air gap is present or not, and the manner in which the material is magnetically excited.
- The electromagnetically-induced vibrations and noise in high speed electrical machines are extensively analyzed with the help of magnetic and magnetomechanical models and simulations. The study on a high-speed solid-rotor induction motor has helped to understand the causes of deformations and vibration in the motor. This study has examined and been successful in finding out how the magnetic forces, magnetostriction, the means of power supply (like frequency converters) and the presence of faults (such as eccentricity) influence the vibration behavior and acoustic noise in high-speed motors. A combined FEA and measurement-based magnetomechanical vibration analysis of high-speed industrial motors is an originality component of this study.

- In the final phase of the thesis, the acoustic noise in electrical motors is studied using a coupled analysis of the Finite Element and Boundary Element Methods. The Boundary Element Method is a cost-efficient and accurate scheme for acoustic studies because it reduces the computation time and storage requirements of simulations compared to Finite Element Analysis. The sound pressure produced by the vibrations in a motor is successfully computed with the Boundary Element Method. This study brings an original contribution through a full numerical analysis presenting the preparation of theoretical equations, coupling methods and a multi-stage simulation of magneto-vibro-acoustic chanarecteristics of a machine.

1.3 Outline of the Thesis

This thesis is divided into five chapters. In the current chapter, the author introduces the research topic and explains the objectives of the research and the scientific contributions of this work. The second chapter consists of the literature review of the research topic which is relevant to this thesis. In Chapter 3, the experimental and numerical models and methods used in this thesis are explained. Chapter 4 presents the results of the computational and experimental studies. Finally, in Chapter 5, these results are discussed and concluded with suggestions for potential future research related to the topics covered in this thesis.

2. Review of Relevant Research

This chapter presents the most appropriate and significant research that has been done over the past years related to the topic of this thesis. First, the basic theory of electromagnetic forces is presented with explanations on the importance and effect of magnetic forces in the operation of electrical machines and various computational methods for these forces. Then a review on the topic of magnetostriction is given with brief descriptions of various magnetomechanical models to calculate the magnetostrictive effect in materials and machines. After that, the vibration phenomenon in electrical motors is explained and different causes behind the vibrations are described. Finally, the vibro-acoustic studies into electrical machines are presented and the computational techniques for acoustic noise in the preceding literature review are depicted.

2.1 Ferromagnetism and Magnetic Forces

2.1.1 Ferromagnetic Materials

This thesis studies extensively the magnetic forces in ferromagnetic materials and electrical machines using analytical, numerical and experimental procedures. Before pitching into the studies and literature on magnetic forces, a review of ferromagnetism and ferromagnetic materials is essential. Ferromagnetism is the property of some materials such as iron that enables these materials to form magnetic properties. The ferromagnetic property of such materials is characterized by their crystalline structure and microstructure. The elements found in nature such as iron, cobalt and nickel all exhibit ferromagnetic properties. The alignment patterns of their atoms contribute to the magnetic properties of these materials, as these atoms can act as elementary electromagnets having magnetic moments. In terms of their crystalline structure, it can be

stated that they are formed of grains with a uniform crystal structure but different magnetic dipole moments. The application of an external field enables the magnetic dipoles to align in a way that the magnetic fields reinforce each other. However, this magnetic property of ferromagnetic materials exists only below the Curie temperature, above which they lose their magnetic characteristics. Above the Curie temperature, the magnetization of the ferromagnetic material disappears, and it becomes paramagnetic. The Curie temperatures for iron is 1043 K, for cobalt it is 1394 K, and for nickel, 631 K.

The magnetic domain theory was developed by the French physicist Pierre-Ernest Weiss in 1907, according to which the ferromagnetic solids consist of regions called domains. The Barkhausen effect (coined by the German physicist Heinrich Barkhausen in 1919) explains the changes in the size and orientation of magnetic domains of ferromagnetic materials such as iron when it is subjected to an external field. The Barkhausen effect provided direct evidence on the existence of ferromagnetic domains. By the 1940s, many physicists in Europe had already explored the phenomenon of Ferromagnetism and Ferromagnetic materials. The layers between the domains in ferromagnetic materials are known as the Bloch wall, named after the scientist Bloch (1932) who had done a great amount of studies on ferromagnetic materials and their domain structure. The basic problem regarding the origin of magnetic domains in ferromagnetic material was solved by L. Landau and E. Lifshitz in 1935. The paper entitled *The Physical Theory of Ferromagnetic Domain* by Kittel in 1949 extensively explained the domain theory to the world.

2.1.2 Forces

The term force(s) has a broad meaning in electromagnetic studies, as it can be interpreted in different ways depending on the scenario. In general, forces can be divided into total force(s) and distributed force(s) according to the standard of mechanical terminology (IEC 60027-1 1992). In the case of magnetic force(s), terminologies such as nodal force(s) and force distribution can also be seen in the literature.

There are different formulations developed by researchers for the computation of magnetic forces (Carpenter 1959), and all those formulations result in the same total force acting on a part of the machine (Muller 1990). The method

for computation of distributed forces is different in all the established formulations and there is no explicit proof showing which formulation is the best way to calculate the forces. According to Melcher (1981), magnetic force can be defined as the rate of change in magnetic energy when the magnetic medium is undergoing an incremental displacement, with the magnetic excitation held fixed. The book *Continuum Electromechanics* (1981) by Melcher is a significant contribution to the electromechanics field, detailing electromagnetic forces, force densities and stress tensors.

In the context of an electrical machine, three types of forces exist, viz, Reluctance forces, Lorentz forces and Magnetostrictive forces. Reluctance forces can also be termed as Maxwell forces as the force density is proportional to the normal component of the Maxwell stress tensor (Carpenter 1959, Melcher 1981), and the force can be calculated by integrating the Maxwell stress on a closed surface located in air. These forces are called Reluctance forces because they are forces acting on the boundaries between materials having different reluctivities. Lorentz forces are produced by the current flow in conductors when they are placed in a magnetic field. And Magnetostrictive forces act inside the iron core of machines arising from the intrinsic characteristic of the iron, magnetostriction.

The force computation using Maxwell stress tensor was studied and implemented for the total force computation in the rotor and torque computation in electrical motors by Arkkio in 1987 in his PhD thesis. Later on, Belahcen et al. (1999, 2001) developed the radial component of the Maxwell stress tensor into the Fourier series for vibration studies. The surface integral of the normal component of the stress on a surface encircling the volume under consideration gives the force density. Hu, Guo et al. developed an analytical model to calculate the magnetic field and forces in synchronous motors accounting for the end effects using subdomain method and verified their results with numerical and experimental studies (Hu, Guo et al. 2016).

The Virtual work principle is used in this thesis for the computation of Generalised Nodal Forces and later for the forces on bodies in contact with infinitesimal air gaps. The method of the local Jacobian derivative was employed by Coulomb (1983) for the evaluation of the derivative of any integral quantity versus the parameter of motion of a rigid body, and he applied this method to calculate the magnetic force and torque using the Virtual work

principle. He proved that the numerical results of magnetic force computations based on the Maxwell stress tensor and Virtual work principle are the same; provided a good tensor integration surface is chosen in the calculations. Moreover, in Coulomb's work (1983), the computation of torque from the forces calculated by the Virtual work principle has given the same result as in the Maxwell stress-tensor method. In Fig. 2.1, a finite element mesh is depicted showing the moving and fixed nodes in an arbitrary distorted area of the mesh. The method using the Virtual work principle has been proved as fast and accurate for the finite element implementation as in the software tools devised and used by Sabonnadiere et al. (1982). In a study published five years later, Reyne et al. (1987) presented a review on difference magnetic force computation methods and concluded that the method of derivative of energy is the most appropriate one.

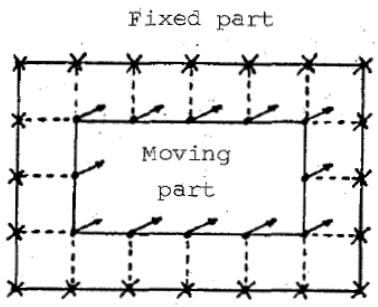

Figure 2.1. Layer of distorted finite elements demonstrated for force calculation using Virtual work principle, X - fixed nodes and . – moving nodes (Coulomb, 1983)

An edge-element based method that used differential geometry for the calculation of local forces was introduced by Bossavit (1992). In their work, Ren and Razek (1992) presented an extension of this edge-element method combined with the local Jocobian derivative method. They succeeded in calculating the nodal magnetic forces by differentiating the magnetic energy in a finite element with respect to the virtual displacement of the nodes of that element. Depending on the FE formulation, the magnetic energy was expressed either as the circulation of the magnetic field along the edges in magnetic formulation, or as the magnetic flux density across the faces in electric formulation. Delaere (1999) approached the magnetic force computation in more of a numerical way and proposed a method by presenting the magnetic

energy in terms of magnetic vector potential. In 1993, Kameari proposed computing magnetic forces using a three-dimensional finite-element method that uses the volume integration of the Maxwell stress tensor with respect to virtual displacements. This method can be implemented in FEM easily and he proved that the numerical, analytical and experimental results of the magnetic forces were in very good agreement. In Fig. 2.2, the results of force computation and comparison with the experimental results are shown. The above mentioned three methods give the same total force outputs in theoretical and numerical computations (Kameari 1993, Belahcen 2001). Moreover, the Lorentz forces in a current carrying conductor can be calculated using the same methods (Ren and Razek 1992, Kameari 1993, Delare 1999). The forces in the end-winding of an electrical motor are calculated in this thesis using the method of nodal forces. Ren et al. (1994) developed a magnetoelastic-coupled model for the computation of mechanical deformation in electrical machines, where they used the principle of virtual work in force computation and concluded that the virtual work method gives higher accuracy in local force computations.

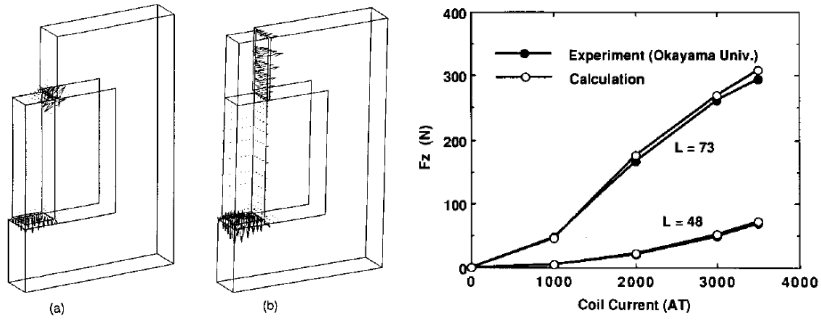

Figure 2.2. Left: Nodal force distribution in the center pole and yoke of a magnetised iron specimen, length of pole of (a) is 48 mm and (b) is 73 mm, Right: Total force comparison in the center pole (Kameari 1993)

The computation of magnetic forces in bodies in contact or in bodies with an infinitesimal air gap is carried out in this thesis using the degenerated air-gap element method. Various researchers have modeled the thin air gap problem in finite element computation using different formulations. Ren (1998) derived nodal and shell elements from the degeneration of Whitney prism elements to solve thin-structure numerical problems. The structure was modeled by a surface domain on which the scalar and vector variables are approximated by their averages (or jumps) across the thin structure. The studies by Ren et al.

presented eddy current problems and thin crack issues in conducting specimens. They have not used the shell or Whitney prism elements in magnetic force calculation of bodies in contact or having thin connecting layers. The technique of degeneration of elements is proposed in this thesis successfully for modeling nodal force computational problems. Rodger et al. (1987, 1988) modelled 3D eddy currents in thin-sheet conductors of arbitrary shape. In the finite element method, they modeled non-conducting regions in terms of magnetic scalar potential, and thin conducting sheets in terms of a scalar stream function. They have also presented only the thin conducting structure problems in their studies. Ren and Razek (1990) employed the boudary integral method to model thin conducting shell eddy current and its coupling with a mechanical model for analyzing the thin plate elastic deformation. Guerin et. al (1994) developed a magnetostatic finite-element formulation for modeling narrow gaps in an iron core and thin iron shells. The so-called shell elements were developed for air gaps in transformers or motors. Badics et al. (1994) proposed a thin-sheet finite-element crack model to study the electromagnetic interaction between probe coils and crack-type defects. Their computational and experimental results were in good agreement. Henrotte et al. (2004) developed an *eggshell* method for computing forces in rigid bodies and narrow airgaps using the method of integration of Maxwell stress tensor. They have tested this method successfully in problems where two permanent magnets are in contact and problems including movements. Krebs et al. (2009) employed the overlapping finite element method for connecting non-confirming meshes in 3D. This method consists of projecting the nodes of one surface to another and vice versa. Later, they extended this method to connect arbitrary non-planar surfaces by introducing new shape functions (Krebs et al. 2010). The overlapping method was previously developed by Tsukerman (1992) to model movement problems in finite element analysis, such as the movement of air-gap meshes. Lai et al. (2004) also have used the overlapping method for modeling 3D electromagnetic problems with continuously changing air gap sizes. Krebs and colleagues further developed this method in different formulations such as vector potential formulation (Krebs et al. 2011) and using both scalar and vector degrees of freedom with a notion of reference elements (Zaidi et al. 2012). The degenerated airgap elements method for contact problems in magnetic force

computations with experimental verification make the proposed method in thesis unique from the previously established techniques.

Knowledge of the local forces or nodal forces is imperative in the computation of vibrations in electrical machines. The nodal forces can be used directly in magneto-elastic coupled computation in numerical tools for the vibration studies. The Generalised Nodal Forces are successfully utilized in this thesis for the vibration analysis of electrical motors. In the vibration studies of this thesis, the magnetostrictive effect is included in the numerical model using a free energy-based magnetomechanical model.

2.2 Magnetostriction

2.2.1 Fundamentals of Magnetostriction

Magnetostriction is a phenomenon that causes deformations in the geometry of a ferromagnetic body, when it is subjected to an external magnetic field. This phenomenon was first discovered by Joule in 1842 (Joule 1847). The deformation in ferromagnetic materials due to magnetostriction is due to the realignment of the initial magnetic domain structure under external field, which are randomly oriented when the material is not under the influence of a magnetic field. When they are subjected to an external magnetic field, the domains position themselves to align with the magnetic field, which causes deformation thus creates a magnetostrictive strain field. The inverse effect of magnetostriction is called the Villari effect (Villari 1865), according to which an external mechanical stress can alter the magnetization behavior of ferromagnetic materials.

The presence of mechanical stress affects the magnetostriction in ferromagnetic materials. There are various studies in literature focusing on the effect of stress on the magnetostrictive behavior of ferromagnetic materials. The research works by Kittel (1949), Bozorth (1951) and Lee (1955) are significant in the literature related to magnetostriction and how mechanical stress alters this phenomenon. In general, ferromagnetic materials possess either positive magnetostriction or negative magnetostriction. Positive magnetostrictive materials expand under the influence of an external magnetic field and their magnetiza-

tion increases with tensile mechanical stress. Materials with negative magnetostriction contract when an external magnetic field is applied, and their magnetization decreases with tensile stress.

The studies done by Bozorth in 1945 were focused on the stress dependency of magnetostriction, where iron-nickel alloys were subjected to cyclic stress and inferred that the change in induction can be due to three parameters, viz, the stress dependence of saturation magnetostriction, saturation magnetization and the crystal anisotropy constant of the material. A theoretical model was formulated by Brown (1949) to portray the relationship between magnetization and mechanical stress when soft ferromagnetic materials are subjected to low cyclic stress. Three decades later, Craik et al. (1970) continued Brown's work by conducting experiments to prove how low tension and compression could affect the magnetization of ferromagnetic materials. Birss et al. (1971) have conducted experiments on the stress dependency on magnetization and studied the changes in domain structure of ferromagnetic materials under stress.

2.2.2 Magnetostriction in Rotating Electrical Machines

The effect of magnetostriction in electrical motors has been studied by many researchers in the field of electromagnetics, electrical machines and vibro-acoustics. In 1995, Låftman investigated the effect of magnetostriction on the noise produced by induction motors. He proposed an FEM model, based on actual magnetostrictive data for an electric steel sheet for the calculation of magnetostrictive deformation of the stator, although the effects of stress on magnetostriction or magnetization were not considered. Witczak (1996) developed a method for calculating the distribution of magnetostrictive forces acting on the stator core of an induction motor. He assumed the ferromagnetic continuum to be isotropic and conservative. He also studied the effect of external stress on the magnetization curve of electrical steel as shown in Fig. 2.3. The distribution of magnetostrictive forces in an induction motor is shown in Fig. 2.4.

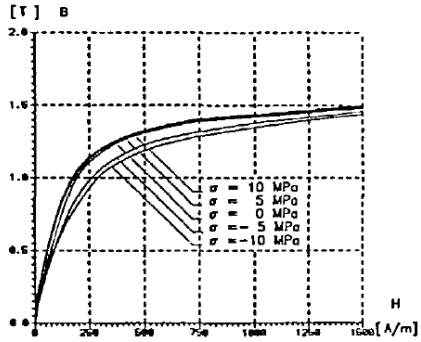

Figure 2.3. Effect of external stress on magnetization of electrical steel (Witczak, 1995)

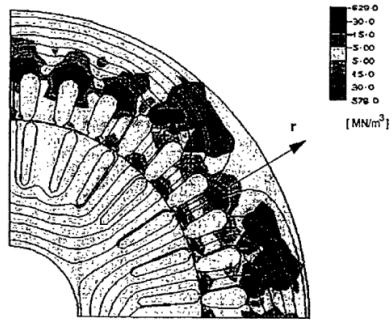

Figure 2.4. Distribution of radial component of magnetostriction force density in an induction motor (Witczak, 1995)

Delaere (2002) used the principle of Virtual work to compute the magnetic and magnetostrictive forces where he used the magnetic vector potential to obtain the magnetic energy in FE calculations. He presented the mechanical deformation caused by magnetostriction using an equivalent set of mechanical forces that gives the same deformative effect as magnetostriction (Delaere et al. 2000). Mohammed et al. (2002) presented their studies on the vibrations of a permanent magnet motor and detailed the significance of magnetostriction in the stator vibrations of the motor. Vandevelde (2002) developed a method for modeling the magnetic forces and magnetostriction in ferromagnetic materials, where magnetic forces, magnetostriction and deformation are considered simultaneously. Later, he proposed a method to separate the deformation due to magnetic forces and magnetostriction (Vandevelde and Melkebeek 2003).

2.2.3 Magnetostriction and Magnetomechanical Coupling

The interaction between magnetic and mechanical quantities in electrical machines is of high importance in machine design and analysis. Hence the modeling of magnetomechanical coupling for numerical computations has been a significant topic in the field of electrical machines. Besides, in order to include the effect of magnetostriction on magnetomechanical coupling, various modeling techniques have been adopted by researchers. In general, the coupling methods can be divided into two, viz, *local coupling* where the constitutive equations of the material are coupled that describes their interaction, and *global coupling* where the new variables are calculated in the deformed geometry. Another classification is *weak coupling* and *strong coupling*. In *weak coupling*, the magnetic and mechanical parameters are computed separately, whereas in *strong coupling*, the computation of magnetic quantities is carried out by considering the effect of the previously computed mechanical quantities. The works by Låftmann (1995) and Reyne et al. (1988a, b) can be categorized as weakly coupled problems. Belahcen (2004) proposed a strong coupling method where the constitutive equations were coupled in the numerical solver and the effect of magnetostriction has also been considered. A dynamic model for the magneto-elastic coupling was presented by Belahcen (2005), where circuit equations of the windings of an electrical motor were also coupled with the magnetic field. The simulation results of this model on a synchronous generator showed a 20% change in the amplitude of vibrations between coupled and uncoupled computations. In another study on a cage induction motor and a synchronous generator, it was inferred that the magnetostriction affects the vibration behavior of both the induction motor and large synchronous generator, while the magnetomechanical coupling is significant only in the large stators (Belahcen 2006b).

Ren et al. (1995) and Besbes et al. (1996) developed magnetomechanical coupled models based on strong coupling methods, where the governing equations of magnetic and mechanical domains were solved simultaneously. Besbes' model included the variation of permeability with stress and the anisotropic property of the material. This work showed how the strongly coupled model with the simultaneous interaction between magnetic and elastic properties is considered superior compared to the weakly coupled model as shown in Fig. 2.5.

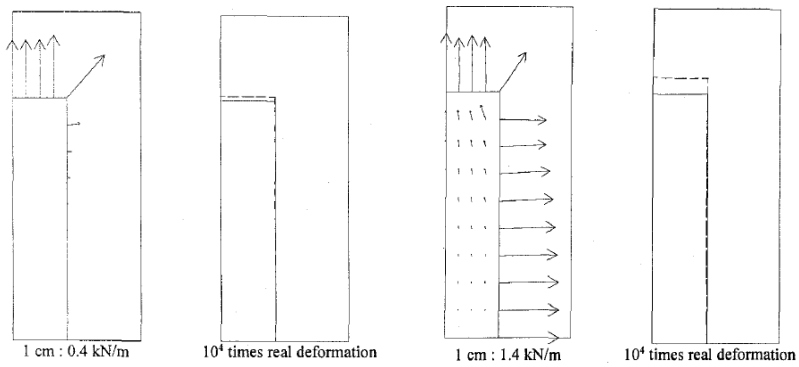

Figure 2.5. Distribution of magnetic forces and induced deformation in a magnetostrictive material, Left: Non-coupled model, Right: Strongly coupled model (Besbes 1996)

Mohammed et al. (1999) proposed a model for magnetostriction by means of coupled non-linear magneto-elastic problems in electrical devices. They derived magnetostriction curves based on analytical formulations from the magnetization curve. Later they developed a strongly coupled scheme where the dependency of permeability on mechanical stress was taken into account (Mohammed et al. 2002). Vandevelde et al. (2008) developed a magneto-elastic computation method based on two aspects, viz, the magnetic couple density, which can be represented by equivalent volume and surface force densities, and magneto-elastic interaction, which is the interaction between the magnetic and elastic behavior of the material.

Numerous studies have been conducted based on the stress-dependent magnetomechanical modeling in recent years that are different from the above-mentioned approaches of couplings. For instance, a multiaxial modeling is performed with uniaxial models using an equivalent stress concept by researchers Hubert (2011) and Yamazaki (2014). Daniel et al. (2008) proposed a multiscale approach defining a local free energy at the domain scale and obtaining macroscopic magneto-elastic behavior by homogenizing the local behavior. A simplified version of the multiscale model including magnetic hysteresis is also adopted later by Daniel et al. (2014).

In this thesis, an energy-based magnetomechanical model is used for the inclusion of magnetostriction in motor vibration studies. Fang et al. (2004) developed a phenomenological constitutive model of ferromagnetic materials for mechanical deformation behavior. They used the stress tensor and the magnetic flux density as the independent variables. The Helmholtz free energy was expressed by remanent magnetization and remanent stress. Zhou et al. (2009)

proposed a general non-linear magnetostrictive constitutive model for soft magnetic materials that can predict magnetostrictive strain and magnetization under different pre-stresses. They used the parameters maximum magnetostrictive strain, the saturation magnetization, and the maximum susceptibility for the model formulation. This model has a similar tactic to the proposed model by Liu et al. (2005) which is based on the concept that a non-linear part of the elastic strain produced by magnetic domain wall motion under a pre-stress causes the change of the maximum magnetostrictive strain due to the pre-stress. Dapino et al. (2000) developed a magnetomechanical model for the magnetostriction and strain behavior of magnetostrictive transducers including the nonlinearities and hysteresis present in the magnetic response of magnetostrictive materials and the linear elastic effects. The magnetostrictive effect is modeled by considering the rotation of magnetic moments in response to the field with the Jiles-Atherton model of ferromagnetic hysteresis in combination with a quadratic magnetostriction law. Later, Linnenmann et al. (2009) proposed a non-linear constitutive model for magnetostrictive materials. In their model, the independent variables of field strength and strain are split in a reversible and an irreversible part for the approximation of the hysteresis behavior. Fonteyn et al. (2010) developed a magnetomechanical coupling by making use of the Helmholtz free energy density, which is defined as a function of five scalar magneto-elastic invariants, where the anhysteretic mechanical behavior is obtained by minimizing this energy (Fonteyn, 2010). This method has been examined and further developed in various studies. For example, Rasilo et al. (2016) extended this model to include magnetic hysteresis. Aydin et al. (2016, 2017) further studied the magneto-elastic interactions in electrical steel sheets under multiaxial loadings using this model.

2.3 Vibrations in Electrical Machines

2.3.1 Fundamentals of Motor Vibrations

The analysis of vibrations in electrical motors mainly from an electromagnetic and magnetomechanical viewpoint is a key objective of this thesis. The literature on magnetomechanical coupling methods by various researchers given in the above section represent the fundamental computational concepts in vibration

studies. Hence, the majority of those researches deal also with the vibrational studies of electrical machines. In this section, a review on the vibrations in electrical motors is given. An extensive study by Vijayraghavan et al. (1998) provides a detailed history on the vibrations and noise in electrical machines. According to these authors, the sources of vibrations can be magnetic, mechanical, aerodynamic or electronic in origin.

In the early studies of vibrations, using an analytical method, Erdelyi (1955) calculated the natural frequencies of a motor by treating the stator as a ring. Verma et al. (1981a) treated the stator and frame as a cylinder in their studies. Ellison et al. (1968) studied the electromagnetic, mechanical and aerodynamic causes of the noise. They developed methods and techniques for the measurement of vibrations and acoustic noise in anechoic chambers (Ellison et al. 1969). Studies by Tsivitse and Weihmann (1971) on polyphase motors covered the magnetic and mechanical noise sources and their research incorporated the noise transmission paths along with the sources. Figure 2.6 portrays the stator deformation caused by magnetic forces. Verma et al. (1981) conducted an extensive study on the vibration behavior and resonance frequencies of electrical machines through experiments and theoretical studies (Verma et al. 1981a and 1981b, Girgis et al. 1981). These authors have come up with experimental results on how the resonant frequencies, different mode shapes and the coupling between components of vibrations affect the vibro-acoustics nature of the machine. Cho et al. (1998) analytically modeled the vibration behavior of small induction motors and computed the electromagnetic forces, discovering that the vibrations of the studied induction motor were excited mainly by radial forces than tangential forces.

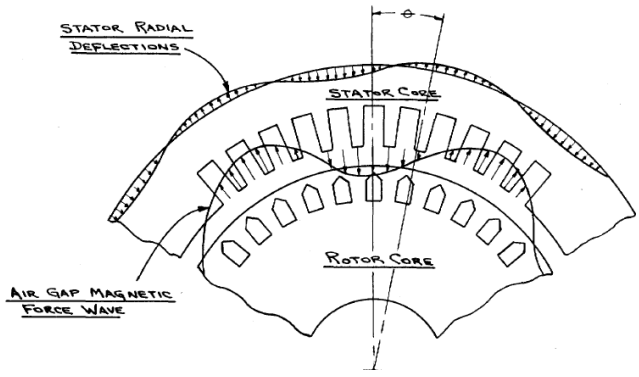

Figure 2.6. Illustration of the production of magnetic noise in an electrical motor (Tsivitse 1971)

2.3.2 Numerical and Experimental Analysis of Vibrations

The development of numerical methods such as the FEM and BEM has enabled researchers and engineers to compute the vibrations and noise in electrical machines more accurately. As mentioned in the previous section, the computation of magnetic forces and magnetomechanical computations are principally the numerical methods for vibration studies. Sections 2.1.2 and 2.2.3 address the important works done in the past related to this area. In this section, some studies that have concentrated primarily on vibrations based on numerical techniques are given. Reyne et al. (1988a) developed finite element models for computing the electromagnetically induced deformations and vibrations in DC motors where they calculated the magnetic forces and static and dynamic deformations of stator tips. In Fig. 2.7, the mechanical deformation of stator tips with a dissymmetry due to an uncompensated armature reaction is shown. Later in 1989, Reyne, Imhoff and Sabonnadiere created a finite element model to compute vibrations from electromagnetic sources using the principle of resolution based on magnetic sampling (Imhoff et al. 1989). They calculated the excitation forces using a surface distribution of the local force density on ferromagnetic materials that gives an accurate mechanical response of the structure.

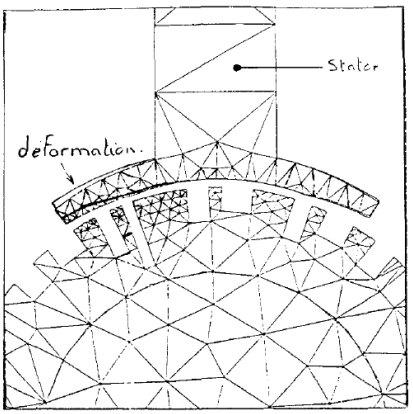

Figure 2.7. Mechanical deformation of stator tips of a DC motor (Reyne 1988)

Jang et al. (1991) studied the effect of magnet geometry on the vibrations of electrical motors using the FEM and formulated some methods for reducing the vibrations. Using modal analysis and the FEM, Benbouzid et al. investigated the mechanical and electromagnetic vibration behavior of the stator of synchronous

machines (Benbouzid et al. 1993), illustrating the modulation effect and excitation due to slots and teeth, and the vibration sources such as edge, teeth and slot effects. Ishibashi et al. studied the vibrations in small induction motors using the FEM and explained how the modes of electromagnetic force waves, natural frequencies and response vibrations are connected in low noise machines (Ishibashi et al. 1998). Wang et al. (1999) developed formulations based on finite elements for the vibro-acoustic studies of induction motors by comparing the calculated natural frequencies and the mode shapes with the experimental modal testing results. The effects of the teeth of the stator, windings, outer casing, slots, end-shields and support on the overall vibration behavior were analyzed in detail. Using 2D magnetic and mechanical finite-element models, Delaere and Hameyer developed a stator vibration spectrum of synchronous machines (Delaere et al. 2000a, 2002a). They formulated finite-element expression for local electromagnetic forces including Maxwell and Lorentz forces, and included magnetostriction as a magnetostrictive force. In their later studies, Delaere et al. used a thermal stress analogy to model magnetostriction and compared the vibration spectra of an induction motor due to reluctance forces and magnetostriction (Delaere et al. 2002b). Besides, the effect of spatial rotor harmonics on stator currents - and hence stator vibrations - were studied using transient Finite Element Analysis and the authors concluded that closed rotor geometry gives less spatial order harmonics and leads to significantly lower stator current harmonics and stator vibrations (Delare et al. 2003). Hameyer et al. (2003) combined the magnetic and mechanical finite-element systems into one magnetomechanical system including reluctance forces and magnetostrictive forces to study the mechanical deformation and vibrations using both isotropic and anisotropic materials. Nysveen et al. studied the influence of design parameters such as pole and slot combinations and slot harmonics on magnetic forces and thereby stator vibrations (Valavi, Nysveen et al. 2014a, b). Studies on controlling magnetic forces, and thus suppressing vibrations, can also be seen in the literature, for example the research by Valente et al. on permanent magnet machines (Valente, Gerada et al. 2018). Zhang et al. have done studies on advanced vibration and efficiency analysis methods by developing a low-intrusion load-evaluation method based on vibration measurements in in-service multi-motor plants (Zhang, Gerada et al. 2010). Krebs et al. developed a simplified

electromagnetic-mechanical model for rapid vibration analysis by giving the radial force look-up table in terms of current and electrical position, given by a FEM code and Virtual work method on mesh nodes. They studied different intermittent control strategies using this model to mitigate the stator vibrations (Nguyen, Krebs et al. 2019).

The studies by Belahcen on magnetostriction, magnetic forces and vibrations in electrical motors were concentrated on the effect of magnetic forces and magnetostrictive forces on the deformation of stator cores of motors. Besides, electromagnetoelastic coupling and the effect of which on vibrations was extensively investigated (Belahcen 2004). The effects of magnetic or reluctance forces and magnetostrictive forces on elastic structures were differentiated and the stress dependency of magnetization and the effect of stress-dependent magnetostriction on the vibrations of induction motors were investigated (Belahcen 2006a). The magnetic forces were calculated using the Virtual work principle and the magnetostrictive forces were computed by the magnetostrictive stress method (Belahcen 2005, 2006b). Fonteyn et al. (2010) developed a magneto-mechanical coupled model to analyze the vibrations of induction motors and studied how the magnetic forces and magnetostriction interact with each other and thereby influence the stator vibrations (Fonteyn et al. 2010a, b). They used the Helmholtz energy-based model for including magnetostriction in magneto-mechanical coupled models in the FEM. The contribution of Maxwell stress in air-iron boundary was studied and it was concluded that the inclusion of Maxwell stress in air boundary significantly increases the stator deformations (Fonteyn et al. 2012).

The effect of rotor eccentricity on motor vibrations is investigated in this thesis using a high-speed solid-rotor induction motor. Many researchers have studied motor vibrations when different kinds of faults are present in the machine. Dorrell et al. (1995) inspected the unbalanced magnetic pull in motors due to rotor eccentricity. The authors studied the variation of unbalanced magnetic pull depending on the load conditions, the position of eccentricity and type of materials that the motor is made of (Dorrell, Guo et al. 2009). Rodriguez et al. (2007) studied the vibrations occurring in an induction motor using the Maxwell stress tensor method and articulated the system behavior under dynamic eccentricity. Hamzaoui et al. (1998) investigated how the imbalance and misa-

lignment defects can contribute to the vibro-acoustic behavior of electrical motors. They proved how the noise and vibrations are higher in motors with defects compared to those without defects through experiments and theoretical studies. Han et al. (2016) formulated a magnetic equivalent circuit model to study the radial and tangential forces caused by rotor eccentricity.

2.4 Acoustic Noise in Electrical Machines

The acoustic noise in electrical machines is a complex phenomenon to analyze, because the root causes of the noise can be magnetic, mechanical or aerodynamic in nature. The electromagnetic causes of noise are of major interest in this thesis, and the aforementioned vibration studies by various researchers include noise analysis also in most of the cases. In this section, some of the studies done in the past related to electrical motor acoustic-noise computation are addressed, giving emphasis to noise calculation.

2.4.1 Acoustic Noise Computation Methods

The computation of acoustic noise produced by electrical machines can be done using analytical methods or numerical tools such as the FEM or BEM. Several studies can be seen in literature pertaining to noise analysis and its relation to the design of motors, types of motors, types of supply such as the effect of PWM on the acoustic noise and techniques to reduce them. The initial stages of the acoustic analysis of motors was mostly undertaken using analytical models. Alger developed analytical equations for decibel sound levels that motors of normal design may be expected to produce, and analyzed the variations in noise due to core and frame resonance (Alger 1954). To analyze the vibrating behavior, he characterized the induction motor by an infinitely long vibrating cylinder. As a continuation to Alger's model, Erdelyi formulated a general procedure for computing in decibels the slot frequency sound-pressure level produced by a polyphase induction motor operating at any arbitrary speed and load (Erdelyi 1955). The theoretical models were verified by sound-power level measurements and proved that the model is capable of calculating the sound-pressure levels of the magnetic noise caused by electromagnetic origin. Brauer developed

a digital computer program which predicts the acoustic noise generated by the magnetic field in an induction motor with static or dynamic eccentricities in the rotor (Brauer 1976). The computed sound power spectrum of a fractional horsepower motor with an eccentric rotor were compared with laboratory measurements and showed good agreement. Brauer's program assumed that the motor is resiliently mounted and has a simple cylindrical frame. Tilmar and Lai formulated an acoustic model for computing the change in sound power level of a variable-speed induction motor due to the change in the speed of operation (Tilmar and Lai 1994). They observed that even when there is an ideal frequency converter with no additional time harmonics, the acoustic noise radiation of electromagnetic origin can still be significantly increased by the change in speed.

Belmans et al. conducted studies on the analytical formulation of acoustic noise in squirrel-cage induction motors and validated the results with experimental results (Belmans et al. 1987). They used the rotating field theory along with Maxwell theorem for predicting the frequency spectrum components produced by the motor and for relating these components to the air-gap flux density distribution time-harmonics caused by the non-sinusoidal supply. These authors concluded that the high noise levels may be expected when one of the frequencies of the electromagnetically excited forces equals a natural frequency of the stator. Later, they developed an electromechanical-computerized scheme using finite-element calculations and modal analysis that predicts the frequency components expected in the audible noise of a three-phase induction motor fed by an inverter (Belmans et al. 1991). Through a series of experiments including the measurement of stator accelerations and acoustic noise in variable reluctance motors, Cameron et al. concluded that the stator deformation due to radial magnetic forces is the dominant electromagnetic cause of noise (Cameron et al. 1992). Using analytical and experimental studies, Besnerais et al. modeled the impact of PWM supply and switching frequencies on the magnetic noise of induction machines (Besnerais et al. 2010). The authors used mechanical and acoustic 2D ring-stator models to compute the influence of both winding space -harmonics and PWM time-harmonics in noise production (Besnerais et al. 2008). They also studied the effect of converter topologies on the magnetic forces and vibrations of electrical machines (Valavi et al. 2018). Fakam et al. coupled the finite element structural analysis results with analytical tools to

compute and compare the electromagnetic noise between surface-permanent magnet and interior-permanent magnet rotor topologies of a synchronous machine (Fakam et al. 2011). Islam et al. also developed combined structural FEA and analytical methods for computing sound-power levels in synchronous motors (Islam et al. 2010).

2.4.2 Acoustic Boundary Element Method for Noise Computation

With the advancement in numerical computational tools, the use of the BEM or combined FEM-BEM in noise computations became more prevalent, and these methods can give more accurate results in acoustic calculations, compared to analytical models. In recent years, many researchers have developed numerical methods using the BEM for acoustic studies of electrical motors. Juhl et al. created a numerical toolkit based on the BEM to compute the acoustic noise using the Helmholtz integral equation (Juhl 1993). They developed BEM-based numerical software for calculating sound fields exterior to bodies of three-dimentional shape or axisymmetric geometries (Henriquez and Juhl 2010). Wang et al. developed a BEM-based numerical model for computing sound power radiated from induction motors and effectively coupled structural FEM and acoustic BEM in their simulation studies (Wang et al. 2004). Herrin et al. formulated a high-frequency BEM and compared it with the Rayleigh approximations method, and inferred from their studies that the high-frequency BEM is more robust (Herrin et al. 2006). Roivanen has done a detailed study on the sound power calculation of electrical motors using different methods such as the BEM, high-frequency BEM and plate approximation method with extensive analytical, numerical and experimental studies (Roivainen 2009).

2.5 Summary and Conclusions

The electromagnetic, magnetomechanical and vibro-acoustic computations of electrical motors have been studied by various researchers across the globe over the last several decades. Different analytical and numerical techniques in the literature are briefly addressed in the literature review to build up a background

to the topic of this thesis and connect the relevance of different parts of the thesis with the studies from the past.

In the first section, the magnetic force computation methods in the literature were presented and how different methods such as the Maxwell stress tensor and the Virtual work principle differ and agree in terms of results accuracy. The importance of nodal magnetic forces in vibration studies is addressed and the same is presented in the thesis using the Virtual work principle. The nodal forces are then used for computing deformations by means of a direct coupling. The calculation of forces on bodies in contact is another important part in magnetic force computations and an efficient technique is proposed in this thesis using a degenerated air-gap element method. Although the use of degenerated elements has been employed in numerical tools in the past, for example in the calculation of Eddy currents, the usage of the same for magnetic-force calculation in magnets and motors using 3D FEM is presented in the thesis with experimental validation. This thesis incorporated the combination of two effectual methods, viz, force computation using the Virtual work principle (Coulomb 1984, Bossavit 1992) and the degenerated air-gap element method in finite element computations (Ren 1998) to form a proficient tool for contact force computations.

The magnetostriction in electrical steel sheets and electrical motors is modeled using different methods by various researchers, and the influence of this phenomenon on motor vibrations has been presented by referring to the previous studies. The energy-based model by Fonteyn et al. (Fonteyn et al. 2010) is employed in this thesis to slot in magnetostriction in magnetomechanical coupled analysis of motors. The effect of magnetostriction on the stator deformation of motors and the interaction of the same with magnetic forces in altering the vibration behavior of motors is explained in the thesis with numerical and experimental studies on two different motors. There are several studies available in the literature based on electrical motor vibrations and their dependency on magnetic forces and magnetostriction. However, in this thesis, the vibrations in induction motors are modeled by means of magnetomechanical coupling techniques with material models that can model the multi-axial magnetomechanical behavior of electrical steel sheets. The computation of stator deformation using such a model heightens the accuracy of the results. In addition to the electromagnetic forces and magnetostriction, the effect of rotor eccentricity and its

contribution to motor vibration is presented in the thesis with analytical, numerical and experimental studies on a high-speed induction motor.

In the final part of the thesis, the acoustic noise generated by electrical motors is briefly addressed. Several analytical models have been formulated by various researchers in the past to model the magnetic noise and total acoustic noise of electrical motors. The numerical methods based on the FEM and BEM are more accurate and a general computational method on how to calculate the sound power level generated due to the electromagnetic causes is presented in the thesis using a combined FEM-BEM method.

3. Methods

This chapter presents the methods used in the numerical computations of electromagnetic forces, magnetostriction, vibration and acoustic noise. Also, the experimental techniques employed for the measurement of magnetic forces and vibrations are explained in detail.

3.1 Computation of Electromagnetic Forces

In this section, the computation of magnetic forces in electromagnetic studies of ferromagnetic materials and electrical machines is explained. There are different formulations or methods to calculate total magnetic forces that give the same results.

3.1.1 Calculation of Magnetic Field

The magnetic field in the electrical machines used in this thesis is calculated using Finite Element Analysis. The $\boldsymbol{A}$-ϕ formulation is used in the FE studies. The electrical machines can be considered as quasi-static magnetic systems (Arkkio 1987), and according to which, the Maxwell equations are written as

$$\nabla \times \boldsymbol{E} = -\frac{\partial \boldsymbol{B}}{\partial t} \tag{3.1}$$

$$\nabla \times \boldsymbol{H} = \boldsymbol{J} \tag{3.2}$$

$$\boldsymbol{H} = \nu \boldsymbol{B} \tag{3.3}$$

$$\boldsymbol{J} = \sigma_e \boldsymbol{E} \tag{3.4}$$

where $\boldsymbol{E}$ is the electric field strength, $\boldsymbol{B}$ is the magnetic flux density, $\boldsymbol{H}$ is the magnetic field strength and $\boldsymbol{J}$ is the current density. The magnetic reluctivity is ν and σ_e is the electric conductivity of the material.

The $\boldsymbol{A}$-ϕ formulation using the vector potential $\boldsymbol{A}$ and reduced scalar potential ϕ is given by

$$\boldsymbol{B} = \nabla \times \boldsymbol{A} \tag{3.5}$$

$$\boldsymbol{E} = -\frac{\partial \boldsymbol{A}}{\partial t} - \nabla \phi \tag{3.6}$$

Assuming translational symmetry of the problem in the *z*-direction, the equation for scalar and vector potential reduces to

$$\nabla \times (\nu \nabla \times \boldsymbol{A}) = -\sigma \frac{\partial \boldsymbol{A}}{\partial t} - \sigma \nabla \phi \tag{3.7}$$

3.1.2 Magnetic Forces from Virtual Work Principle

The application of the Virtual work principle was employed for the computation of magnetic forces or more specifically *nodal forces* in various researches by Ren and Razek (1992), Kameari (1993) and Belahcen (2004). The total magnetic force $\boldsymbol{F}$ can be calculated by differentiating the magnetic energy W_S with respect to a scalar parameter S of a Virtual displacement f_S so that $\lim_{S \to 0} f_S(x) \to x$

$$\boldsymbol{F} = -\frac{dW_S}{dS} \tag{3.8}$$

where the magnetic energy is given by

$$W_S = \int_{\Omega_S} \left(\int_0^{\boldsymbol{B}} \boldsymbol{H} \cdot d\boldsymbol{B} \right) d\Omega \tag{3.9}$$

In FE analysis, this force computation can be implemented to calculate the nodal forces by differentiating the magnetic energy of the finite elements surrounding the node of an FE mesh with an elemental area Ω^e. The derivative of the energy is obtained by utilizing the change of variables and the Piola transformation for the magnetic flux density as given below

$$\frac{dW_S}{dS} = \int \boldsymbol{H}(\boldsymbol{B}) \cdot \frac{\partial}{\partial S} \boldsymbol{J}_S \cdot \boldsymbol{B} - \frac{\partial \det \boldsymbol{J}_S}{\partial S} \left(\boldsymbol{H}(\boldsymbol{B}) \cdot \boldsymbol{B} - \int_0^{\boldsymbol{B}} \boldsymbol{H} \cdot d\boldsymbol{B} \right) d\Omega \tag{3.10}$$

where $\boldsymbol{J}_S$ is the Jacobian matrix of the displacement mapping.

The integration is performed at all the elements around a given node. Choosing a deformation mapping $\boldsymbol{f}_s(\boldsymbol{x}) = \boldsymbol{x} + s\boldsymbol{u}\boldsymbol{N}(\boldsymbol{x})$, where $\boldsymbol{u}$ is a unit vector in the direction of displacement and $\boldsymbol{N}(\boldsymbol{x})$ is the nodal shape function on the computational FE mesh, the energy derivative can be written as

$$\frac{dW_S}{dS} = \int \boldsymbol{H}(\boldsymbol{B}) \cdot \boldsymbol{u}\nabla\boldsymbol{N} \cdot \boldsymbol{B} - \boldsymbol{u}\nabla\boldsymbol{N}\left(\boldsymbol{H}(\boldsymbol{B}) \cdot \boldsymbol{B} - \int_0^{\boldsymbol{B}} \boldsymbol{H} \cdot d\boldsymbol{B} \right) d\Omega \tag{3.11}$$

Considering the constitutive equation of the material, $\boldsymbol{H} = \nu(\boldsymbol{B}^2, \boldsymbol{\sigma})\boldsymbol{B}$, Eqation (3.11) can be written as

$$\frac{dW_S}{dS} = \int \nu\boldsymbol{B} \cdot \boldsymbol{u}\nabla\boldsymbol{N} \cdot \boldsymbol{B} - \frac{\nu}{2}\boldsymbol{u} \cdot \nabla\boldsymbol{N}\boldsymbol{B}^2 d\Omega \tag{3.12}$$

The output of the differentiation of the magnetic energy with respect to a Virtual displacement can be termed as Generalised Nodal Forces (GNFs). The nonlinear magnetic behavior is taken into account by considering the reluctivity as a function of $\boldsymbol{B}^2$ using the cubic spline integratoin. The GNF computation is an important part in the study of vibrations of electrical machines.

3.1.3 Maxwell Stress tensor Method

The total magnetic force on any part of a machine can be calculated by applying the Maxwell stress tensor method. The force can be calculated by integrating the Maxwell stress tensor over a closed cylindrical surface *S,* closed through the end region of the machine and with another outside cylindrical surface, as given below.

$$\boldsymbol{F} = \oint_S \left(\frac{1}{\mu_0}(\boldsymbol{B} \cdot \boldsymbol{n})\boldsymbol{B} - \frac{1}{2\mu_0}\boldsymbol{B}^2\boldsymbol{n} \right) dS = \oint_S \left(\frac{1}{2\mu_0}(B_n{}^2 - B_t{}^2)\boldsymbol{n} + \frac{1}{\mu_0}B_n B_t \boldsymbol{t} \right) dS \tag{3.13}$$

where $\boldsymbol{n}$ and $\boldsymbol{t}$ represent the outward unit vector, normal and tangential respectively to the differential surface *S*.

The Maxwell stress tensor method is a very suitable way of computing global magnetic forces. In numerical platforms, the implementation of Maxwell stress tensor method depends on the type of finite element crossed by the integration

surface and the choice of the path of this particular surface inside the finite element (Coulomb 1983, Ren 1994). According to Coulomb, in the case of triangular finite elements, the best results are attained if the integration path passes exactly through the middle of the edges of the triangles. In finite element analysis, formulating such contours could increase the computation time and complexity of implementation, because of the task of finding the edges in complex geometries.

The force equation can be separated into the normal component of traction σ_r and circumferential component of traction σ_ϕ.

$$\sigma_r = \frac{1}{2\mu_0}(B_r^2 - B_\phi^2) \tag{3.14}$$

$$\sigma_\phi = \frac{1}{\mu_0}(B_r B_\phi) \tag{3.15}$$

To examine the spatial distribution and time dependence of the radial stress, it can be developed into a two-dimensional Fourier series (Belahcen, 2004).

$$\sigma_r = \sum_{m=0}^{\infty}\sum_{n=0}^{\infty}\lambda_{mn}\begin{bmatrix} a_{mn}\cos(mp\varphi)\cos(n\omega t) + \\ b_{mn}\cos(mp\varphi)\sin(n\omega t) + \\ c_{mn}\sin(mp\varphi)\cos(n\omega t) + \\ d_{mn}\sin(mp\varphi)\sin(n\omega t) \end{bmatrix} \tag{3.16}$$

where m and n represent the space and time harmonic numbers, p is the pole pair number of the machine and ω is the rotational speed of the magnetic field, t and φ are the time and angular position respectively. The other constants are calculated as

$$a_{mn} = \frac{p\omega}{2\pi^2\mu_0 r^2}\int_0^{\frac{2\pi}{p}}\int_0^{\frac{2\pi}{\omega}}\sigma_r\cos(mp\varphi)\cos(n\omega t)\,d\varphi dt \tag{3.17}$$

$$b_{mn} = \frac{p\omega}{2\pi^2\mu_0 r^2}\int_0^{\frac{2\pi}{p}}\int_0^{\frac{2\pi}{\omega}}\sigma_r\cos(mp\varphi)\sin(n\omega t)\,d\varphi dt \tag{3.18}$$

$$c_{mn} = \frac{p\omega}{2\pi^2\mu_0 r^2}\int_0^{\frac{2\pi}{p}}\int_0^{\frac{2\pi}{\omega}}\sigma_r\sin(mp\varphi)\cos(n\omega t)\,d\varphi dt \tag{3.19}$$

$$d_{mn} = \frac{p\omega}{2\pi^2 \mu_0 r^2} \int_0^{\frac{2\pi}{p}} \int_0^{\frac{2\pi}{\omega}} \sigma_r \sin(mp\varphi)\sin(n\omega t)\, d\varphi dt \tag{3.20}$$

$$\lambda_{mn} = \begin{cases} (1/4) \text{ for } m=n=0 \\ (1/2) \text{ for } m=0,\ n>0 \text{ and } m>0,\ n=0 \\ 1 \text{ for } m>0,\ n>0 \end{cases} \tag{3.21}$$

The radial stress can be expressed as a sum of waves circulating in the clockwise and anticlockwise direction with respect to the rotational direction of the motor. Then the radial stress can be described as

$$\sigma_r = \sum_{m=0}^{\infty} \sum_{n=0}^{\infty} \begin{bmatrix} \frac{1}{2}\lambda_{mn}\left\{(a_{mn}+d_{mn})^2 + (b_{mn}-c_{mn})^2\right\}^{\frac{1}{2}} \\ \cos(-mp\varphi + n\omega t + \gamma_+) + \\ \frac{1}{2}\lambda_{mn}\left\{(a_{mn}-d_{mn})^2 + (b_{mn}+c_{mn})^2\right\}^{\frac{1}{2}} \\ \cos(mp\varphi + n\omega t + \gamma_-) \end{bmatrix} \tag{3.22}$$

In the radial stress equation, m is the mode or the spatial frequency and n represents the temporal frequency of these components.

3.1.4 Motor Imbalances and Forces

If there is an imbalance, in the form of static or dynamic rotor eccentricity, there can be additional force components in stress distribution (Pöyhönen et. al. 2003). The dynamic eccentricity is illustrated in Fig. 3.1. The resultant radial force acting between the two cylindrical bodies, the stator and rotor is zero, if there is no eccentricity. The rotor eccentricity creates an unbalanced magnetic pull (Dorrel 1995) that can pull the rotor further from the concentric position.

In a motor with dynamic eccentricity, the air gap length is no longer constant and can be expressed as (Rodríguez et al. 2008, Dorrell et al. 1997),

$$g(\varphi, t) = g[1 - d_e \cos(2\pi f_r - \varphi)] \tag{3.23}$$

where g is the average air-gap length, d_e is the degree of dynamic eccentricity and f_r is the rotor rotational frequency. For small values of dynamic eccentricity, the air-gap permeance Λ can be denoted as (Dorrell 1997),

$$\Lambda(\varphi,t) = \frac{1}{g}\mu_0[1 + d_e \cos(2\pi f_r - \varphi)] \tag{3.24}$$

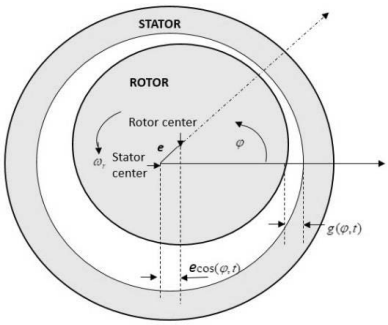

Figure 3.1 Dynamic eccentricity in a motor

Although there is eccentricity, magnetic flux passes through the air gap. With this assumption, the magnetic flux density can be expressed as

$$b(\varphi,t) = \Lambda(\varphi,t)\int_0^{\varphi} j_S(\theta,t)d\theta \tag{3.25}$$

where j_s is the stator current density given by

$$j_S(\theta,t) = J\sin(2\pi f_S t - p\varphi) \tag{3.26}$$

where f_s is the fundamental supply frequency. By substituting (3.24) and (3.26) in (3.25) gives

$$\begin{aligned} b(\varphi,t) &= {B_S}^p \cos(2\pi f_S t - p\varphi) \\ &+ {B_S}^{p-1}\cos[(2\pi f_S - 2\pi f_r)t - (p-1)\varphi] \\ &+ {B_S}^{p+1}\cos[(2\pi f_S + 2\pi f_r)t - (p+1)\varphi] \end{aligned} \tag{3.27}$$

where $${B_S}^p = \frac{\mu_0 J_S}{pg}; \qquad {B_S}^{p\pm1} = \frac{\mu_0 J_S}{2pg} d_e \tag{3.28}$$

The radial force per unit area can be expressed as

$$f(\varphi,t) = \frac{1}{2\mu_0} b^2(\varphi,t) \tag{3.29}$$

Replacing (3.27) in (3.29) gives

$$f(\varphi,t)=\frac{1}{2\mu_0}\{(B_S{}^p)^2\cos(4\pi f_s t+2p\varphi) \quad (3.30a)$$

$$+B_S{}^{p-1}B_S{}^{p+1}\cos(4\pi f_r t-2\varphi) \quad (3.30b)$$

$$+B_S{}^{p}B_S{}^{p-1}\cos(2\pi f_r t+2p\varphi) \quad (3.30c)$$

$$+B_S{}^{p-1}B_S{}^{p}\cos[(4\pi f_s+2\pi f_r)t-\varphi] \quad (3.30d)$$

$$+B_S{}^{p+1}\cos[(4\pi f_s-2\pi f_r)t-\varphi]\} \quad (3.30e)$$

$$+\left(B_S{}^{p+1}\right)^2\cos[2(2\pi f_s+2\pi f_r)t-2(p+1)\varphi] \quad (3.30f)$$

$$+\left(B_S{}^{p-1}\right)^2\cos[2(2\pi f_S-2\pi f_r)t-2(p-1)\varphi] \quad (3.30g)$$

Equation (3.30) represents the frequency components when dynamic eccentricity is present in an induction motor. Dynamic eccentricity may produce other vibrations than twice the supply frequency $2f_S$, in addition to the rotational frequency f_r. Those components are $2f_r$ (3.30b) which is twice the rotor frequency, $2f_S \pm f_r$ given in (3.30d) and (3.30e), $2(f_S \pm f_r)$ as presented in (3.30f) and (3.30g). In general, the additional frequency components can be quantified as $2f_{r,k}$, $2f_{s,k} \pm f_r$ and $2(f_{s,k} \pm f_r)$ where k is an integer. These frequency components are affected by the slip and hence an additional +/- sf_s term will be reflected in these frequencies.

The radial stress in Equation (3.22) can be written as

$$\sigma_r=\sum_{m=0}^{\infty}\sum_{n=0}^{\infty}\lambda_{mn}\cos(mp\varphi\pm n\omega t+\phi_{m,n}) \quad (3.31)$$

Because of the existence of dynamic eccentricity, the air-gap permeance will have an additional term $\Lambda_{rd}=\frac{g}{e_d}\cos(\varphi-\omega t-\alpha_d)$ where α_d is the original position of the eccentricity. The radial air-gap flux density is

$$B_r=\varepsilon_m\cdot(\Lambda+\Lambda_{rd})=\varepsilon_0\cos(p(\varphi-\omega t)-\phi)\cdot\frac{\mu_0}{e}[1+\frac{g}{e_d}\cos(\varphi-\omega t-\alpha_d)] \quad (3.32)$$

where $e_d=e\cos(\omega t)$, ε_m is the m.m.f produced by the stator and rotor windings, ε_0 is the amplitude of the m.m.f and ϕ is the phase angle of the m.m.f. wave. Equation (3.32) can be further developed as

$$B_r=B_0\cos(p(\varphi-\omega t)-\phi)+B_e\cos[(p\pm1)(\varphi-\omega t)-(\phi\pm\alpha_d)] \quad (3.33)$$

where $B_e = B_0 \times \frac{g}{2e_d}$ is the amplitude of eccentric magnetic flux density and $B_0 = \frac{\varepsilon_0 \mu_0}{g}$ is the amplitude of the classical flux density.

Now, from the relation $\sigma_r = B^2{}_r / 2\mu_0$, the stress can be written as

$$\begin{aligned}\sigma_r = [&B_0{}^2 \cos(2p(\varphi - \omega t) - 2\phi) \\ &+ B_e{}^2 \cos(2(p \pm 1)(\varphi - \omega t) - 2(\phi \pm \alpha_d)) \\ &+ 4B_0 B_e \cos((2p \pm 1)((\varphi - \omega t) - (2\phi \pm \alpha_d)) \\ &+ 4B_0 B_e \cos(\pm(\varphi - \omega t) \pm \alpha_d)] / 4\mu_0\end{aligned} \tag{3.34}$$

Therefore, without any rotor eccentricity, there is only a stress wave rotating at $n\omega = 2p\omega$ speed and with a spatial order of $m = 2p$. When there is eccentricity, new spatial temporal waves arise and these terms are modulations at $2(p \pm 1)$, $2p \pm 1$ and ± 1 of the spatiotemporal waves. Thus, rotor dynamic eccentricities in a motor will yield modulations of the magnetic forces that are non-multiples of the number of pole pairs of the motor.

It can be inferred from the aforementioned analytical models that the dynamic eccentricity can induce additional force frequencies and consequently the same frequencies will be present in the stator deformation and vibrations. The application results of the Virtual work principle for force calculation in an induction motor and on the end winding of another motor are given in Section 4.1.1. The effect of rotor eccentricity on forces and motor vibration explained in the above Section 3.1.3 will be shown in the vibration study of a solid rotor induction motor given in Section 4.2.4.

3.1.5 Degenerated Air-gap Elements

The conventional method of computing nodal magnetic forces from the Virtual work principle is described in section 3.1.2, in which the FE implementation can be used for the nodal force computation at any part of a machine. However, there are cases in electrical machines and devices where two bodies are in contact, which creates an infinitesimally thin air-gap between them. The GNF approach can be applied to these parts with the cost of heavy meshing and a costly computational burden. This scenario can be tackled by using the degenerated air-gap element method for force computation.

The conventional GNF calculation is given in Eq. (3.12). For infinitesimally small air gaps, by employing the shell element or the air-gap element method, this equation can be written as

$$\boldsymbol{F} = -\frac{\partial \boldsymbol{W}_S}{\partial S} \approx \int_S \nu B_n \cdot \boldsymbol{u} N_S \boldsymbol{n} \cdot B_n - \frac{\nu}{2} \boldsymbol{u} \cdot \boldsymbol{n} B_n^{\,2} N_S dA \tag{3.35}$$

where N_s is the restriction of nodal shape function N to the air-gap surface S and $\boldsymbol{B}_n$ is the normal component of the flux density $\boldsymbol{B}$. The volume integral is replaced by surface integral by considering the field discontinuity across the thin structure. The thin air gap is modeled by the surface domain on which the scalar and vector variables are approximated by their averages across the structure.

Consider a thin air gap as shown in Fig 3.2, where K is a boundary element and its extrusion in normal direction K_d is a prism or hexahedral polygonal domain. The change of magnetic energy in K_d is given by

$$\frac{\partial \boldsymbol{W_S}}{\partial S} = \int_{K_d} \nu \boldsymbol{B} \cdot \partial_S J_S . \boldsymbol{B} - \frac{1}{2} \nu \boldsymbol{B}^2 \partial_S |J_S| dx = \int_{K_d} \nu \boldsymbol{B} \cdot \nabla N \boldsymbol{u} . \boldsymbol{B} - \frac{1}{2} \nu \boldsymbol{B}^2 \nabla N . \boldsymbol{u} dx \tag{3.36}$$

where J_S is the Jacobian ascending from the Virtual displacement and $|J_s|$ is its determinant.

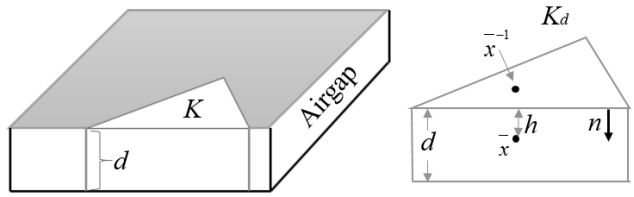

Figure 3.2. Degeneration of air-gap boundary element or shell element

In Fig. 3.2, $\bar{x}$ is a point in the air gap at a distance h from the boundary element. Then the nodal shape function at that point is

$$N(\bar{x}) = N_k(1 - \frac{h}{d}) = \frac{d - h(\bar{x})}{d} N_k\left(\bar{x}^{-1}\right) \tag{3.37}$$

where $N_k\left(\bar{x}^{-1}\right)$ is the shape function at a point $\bar{x}^{-1}$ which is the projection of $\bar{x}$ at the element K.

$$\nabla N = \frac{-\boldsymbol{n}}{d} N_k(\bar{x}) + \frac{d - h(\bar{x})}{d} \nabla N_k(\bar{x}) \tag{3.38}$$

Substituting (3.38) in (3.36) gives

$$\frac{\partial \boldsymbol{W}_s}{\partial S} = \int_{K_d} \nu \boldsymbol{B}.\left(\frac{-\boldsymbol{n}}{d}\right) \boldsymbol{u} \cdot \boldsymbol{B} N_k(\bar{x}) - \frac{1}{2} \nu \boldsymbol{B}^2 \left(\frac{-\boldsymbol{n}}{d}\right).\boldsymbol{u} N_k(\bar{x}) dx \tag{3.39}$$

where $h = \boldsymbol{n}.\bar{x}$ and $\boldsymbol{B} \cdot \nabla N_k = 0$

If the air gap is very small so that $\boldsymbol{B} \| \boldsymbol{n}$ and is constant in $\boldsymbol{n}$ direction,

$$\frac{\partial \boldsymbol{W}_s}{\partial s} = d \int_K \nu \boldsymbol{B} \cdot (-N_k \boldsymbol{n}) \boldsymbol{u}.\boldsymbol{B} - \frac{1}{2} \nu \boldsymbol{B}^2 (-N_k \boldsymbol{n}).\boldsymbol{u} dx \tag{3.40}$$

This implies that $\boldsymbol{B} = \nabla \times_K \boldsymbol{A}$ (3.41)

From the above equation, it can be deduced that

$$\boldsymbol{n}.\boldsymbol{B} = \boldsymbol{n}.\nabla \times A = \boldsymbol{n}.\nabla \times_K \boldsymbol{A} \tag{3.42}$$

where $\nabla \times_K$ denotes the boundary curl operator on the element *K*. On a boundary whose exterior normal is directed along *z*, it is given by $\nabla \times_K \boldsymbol{A} = \boldsymbol{u}_z(\partial_y \boldsymbol{A}_x - \partial_x \boldsymbol{A}_y)$. For an infinitesimal air gap, it avails to consider only the normal component of the flux density. Then the magnetic force can be formulated as

$$\boldsymbol{F} = -\frac{\partial \boldsymbol{W}_s}{\partial s} = \int_K -\nu N_k \nabla \times_k \boldsymbol{A}.\boldsymbol{n}.\boldsymbol{u} \nabla \times_k \boldsymbol{A} + N_k \frac{1}{2} \nu (\nabla \times_k \boldsymbol{A})^2 \boldsymbol{n}.\boldsymbol{u} dx \tag{3.43}$$

The FE computation using the degenerated air gap requires modeling the thin airgap as a layer with the same mesh density as other parts of the geometry with no additional mesh refining. The application results of this method can be seen in Section 4.1.2, where the simulation results are compared with measurements and the degenerated air-gap element method is applied in a permanent magnet motor simulation for force calculation.

3.1.6 Measurement of Magnetic Forces

The magnetic forces acting between two permanent magnets are measured using an experiment set-up as show in Fig. 3.3. There are two concentric cylindri-

cal permanent magnets and the airgap length d between them is varied for different sets of force measurements. The structure supporting the magnets is amagnetic and the distance is varied by using an accurate positioning vertical gauge. A laser displacement sensor monitored the air-gap length, and a precision force sensor (0-200 N) measured the magnetic force. The permanent magnets used in the study were sintered NdFeB (NEOFLUX-GSN35) with a remanent magnetic flux density of B_r = 1.24 T for the fixed magnet and 1.04 T for the moving magnet, and a relative permeability of μ_r = 1. The heights of the magnets were different, as the fixed one has 10 mm height while the moving magnet has 40 mm, and both have the same diameter of 14 mm.

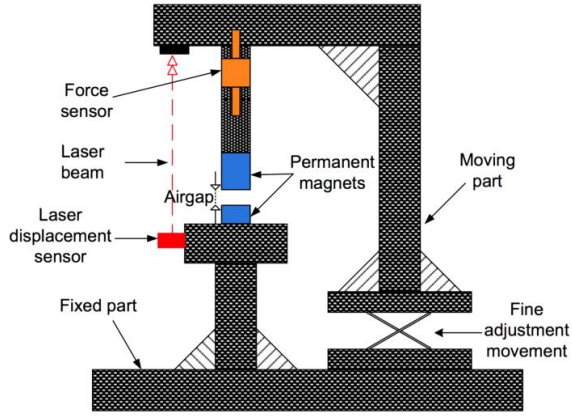

Figure 3.3. Schematic diagram of the magnetic force measurement set-up

3.2 Vibrations and Magneto-mechanical Coupling

This section deals with the deformations and vibrations in electrical machines due to electromagnetic causes and the magnetomechanical coupling methods to compute the vibrations. The magnetic forces and magnetostriction are the major electromagnetic sources of vibrations in electrical machines. These two phenomena can induce deformations, that causes the vibration and, finally, these vibrations produce acoustic noise. The magneto-elastic or magnetomechanical coupling using FE tools is an efficient method to calculate the vibrations.

3.2.1 Magneto-elastic Coupling

The deformations occurring in an electrical machine due to electromagnetic forces can be modeled and computed by a weak magneto-elastic coupling method. This is a simple and direct coupling approach by utilizing the Navier equation for linear elasticity. The dynamic equations for elastic deformation of solids is

$$\rho \frac{\partial^2 \boldsymbol{d}}{\partial t^2} - \nabla \cdot \tau = \vec{\boldsymbol{f}} \tag{3.44}$$

where ρ is the mass density, $\boldsymbol{d}$ is displacement field, $\vec{\boldsymbol{f}}$ is the given volume force and τ is the stress tensor. The stress tensor is given by

$$\tau^{ij} = C^{ijkl} \varepsilon_{kl} - \beta^{ij} (T - T_0) \tag{3.45}$$

where $\boldsymbol{\varepsilon}$ is the strain and $\boldsymbol{C}$ is the elastic modulus.

Thermal stresses may be considered by giving the heat expansion tensor $\boldsymbol{\beta}$ and the reference temperature of the stress-free state T_o. The linearized strain is given by

$$\varepsilon = \frac{1}{2}(\nabla \boldsymbol{d} + (\nabla \boldsymbol{d})^T) \tag{3.46}$$

The stress tensor in terms of Lamé parameters is

$$\tau = 2G\varepsilon + \lambda \nabla \cdot \vec{d}\boldsymbol{I} - \beta(T - T_0)\boldsymbol{I} \tag{3.47}$$

where G and λ are the first and second Lamé parameters respectively and $\boldsymbol{I}$ is the unit tensor.

In the numerical computation, the magneto-elastic model is simulated hierarchically, assuming that the coupling is weak, first solving the magnetic system and then providing the elasticity solver with the magnetic nodal forces as the volume force on the right side of Eq. (3.44). The application results of this kind of coupling in an induction motor are given in section 4.2.1.

3.2.2 Magnetostriction and Magnetomechanical Coupling

In section 3.2.1, the calculation of mechanical deformation due to magnetic forces using a weak coupling is explained. In order to include the effect of magnetostriction, a more complex and strongly coupled magnetomechanical model

is needed to model it accurately. The magnetomechanical coupling using the Helmholtz free energy principle is employed in this thesis to incorporate magnetostriction in the FE computations.

The constitutive equations of the material are formulated from a Helmholtz free energy density ψ (Fonteyn et. al 2010, Aydin et. al 2016-2017), which enables the coupling of the magnetic and elastic properties of the material. For an isotropic magneto-elastic material, ψ is articulated as a function of five scalar invariants, in terms of the magnetic flux density vector $\boldsymbol{B}$ and the total strain tensor $\boldsymbol{\varepsilon}$

$$I_1 = \mathrm{tr}(\boldsymbol{\varepsilon}),\ \ I_2 = \frac{1}{2}\mathrm{tr}(\boldsymbol{\varepsilon}^2),\ I_4 = \frac{\boldsymbol{B}\cdot\boldsymbol{B}}{\boldsymbol{B}_{\mathrm{ref}}^2},\ \ I_5 = \frac{\boldsymbol{B}\cdot(\tilde{\boldsymbol{\varepsilon}}\boldsymbol{B})}{\boldsymbol{B}_{\mathrm{ref}}^2},\ \ I_6 = \frac{\boldsymbol{B}\cdot(\tilde{\boldsymbol{\varepsilon}}^2\,\boldsymbol{B})}{\boldsymbol{B}_{\mathrm{ref}}^2} \tag{3.48}$$

where $\boldsymbol{B}_{\mathrm{ref}}$ = 1 T. The first two invariants define the elastic behavior of the material, and I_3 is not used, because linear elasticity is presumed in this model. The fourth invariant depicts the single-valued magnetization behavior and the fifth and sixth invariants stand for the magneto-elastic coupling. The deviatoric part of the strain $\tilde{\boldsymbol{\varepsilon}} = \boldsymbol{\varepsilon} - \boldsymbol{\varepsilon}_{Hyd}$ where $\boldsymbol{\varepsilon}_{Hyd}$ the hydrostatic strain is used in the fifth and sixth invariants, since the variation in permeability is not depending on the hydrostatic pressure. The equation for the Helmholtz free energy density is then expressed as

$$\psi = \frac{1}{2}\lambda I_1^2 + 2GI_2 - \nu_0\left(\frac{I_4}{2} + \sum_{i=0}^{n_\alpha-1}\frac{\alpha_i}{i+1}I_4^{i+1} + \sum_{i=0}^{n_\beta-1}\frac{\beta_i}{i+1}I_5^{i+1} + \sum_{i=0}^{n_\gamma-1}\frac{\gamma_i}{i+1}I_6^{i+1}\right) \tag{3.49}$$

Here λ and G are the Lamé constants of the material, ν_0 is the reluctivity of free space and α_i, β_i, γ_i are the fitting parameters to be identified from measurements. The magneto-elastic stress and magnetization are obtained as

$$\boldsymbol{\sigma}_{me}(\boldsymbol{B},\boldsymbol{\varepsilon}) = \frac{\partial\psi(\boldsymbol{B},\boldsymbol{\varepsilon})}{\partial\boldsymbol{\varepsilon}} \ \text{ and } \ \boldsymbol{M}(\boldsymbol{B},\boldsymbol{\varepsilon}) = -\frac{\partial\psi(\boldsymbol{B},\boldsymbol{\varepsilon})}{\partial\boldsymbol{B}} \tag{3.50}$$

The magnetic field strength vector is then calculated by $\boldsymbol{H} = \nu_0\boldsymbol{B} - \boldsymbol{M}$. The magneto-elastic stress tensor $\boldsymbol{\sigma}_{me}$ consists of elastic and MS-related stress tensors.

The studied material was 0.5 mm non-oriented Fe-Si electrical sheets. A total of fifteen parameters were required to model the properties of the material, and they were determined using the experimental data obtained from a custom-built uniaxial single sheet tester developed by A. Belahcen, D. Singh and U. Aydin

(2016-2017). In the experimental procedure, the material was loaded with different stresses varying from 50 MPa compression (–) to 80 MPa tension (+) parallel to the flux density, and the magnetization curves were measured. Then, the initial fitting of the single-valued model parameters to the ***H***-averaged measured magnetization curves was comprehended at various stress values, as shown in Fig. 3.4. It was observed that magnetic materials show reduced permeability under compression and high tension. This behavior of magnetic materials is modeled efficaciously using the model. In addition, increased permeability is noticed under low tensile stress as reported by Singh et al. (2015).

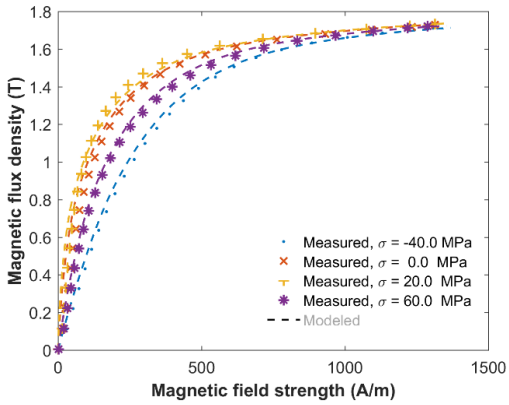

Figure 3.4. The fitting results of the single-valued model parameters

3.2.3 Measurement of Deformation due to Magnetic Forces and Magnetostriction

The electromagnetic causes of deformations and vibrations in electrical machines are magnetic forces and magnetostriction. The knowledge of how these two phenomena cause the deformation and interact with each other is important for the design of electromagnetic machines and devices. An original experiment was performed to segregate the deformations contributed by magnetic forces and magnetostriction in electrical steel sheets.

In the experiment, an iron sheet of 0.5 mm thickness is selected as the test specimen, and analytical and numerical computations were used to design the specimen, in order to get ample magnetic flux density and mechanical deformation. The test sheet is rectangular shaped with curved corners and has an air gap of 0.4 mm in the right limb. Two current-carrying copper coils having 700

turns each, as shown in Fig. 3.5, were used for the excitation of the sheet. The excitation coils produce a magnetic flux in the iron core, which sequentially introduces mechanical strain and deformation in the sheet. The thin air gap in the flux path facilitates larger magnetic forces than in the case of a completely closed-loop core. The magnetic field itself can produce magnetostrictive strain in the sheet, while the total deformation is due to both the magnetic forces and MS. In the case of a closed-loop sheet with no airgap, the magnetic forces will be negligibly small. It will not be possible to segregate the effects with the proposed measurement set-up.

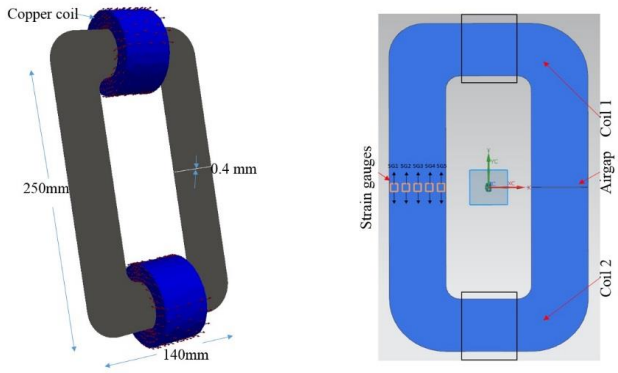

Figure 3.5. Iron sheet with copper coils and strain gauges (SG1 to SG5 from left to right)

Three different supply currents with frequency of 1 Hz were used to excite the coils: 6.26 A (excitation voltage: 64.2 V) resulting in 1.68 T flux density in the left limb, 3.14 A (31.7 V) resulting in 1.59 T flux density and 1.31 A (13.2 V) resulting in 1.49 T flux density. A search coil measured the flux density, while five strain gauges, SG1 to SG5, placed in the left limb were used for measuring the strain. To avoid the induction in the strain gauge grid, non-inductive foil strain gauges were used. The main part of the experimental setup where the test specimen is placed is shown in Fig. 3.6. The iron sheet was fitted between two glass fiber plates, to avert out-of-plane displacements. Thin Teflon sheets between the plates and the iron sheet were used to minimize the friction. The objective of this experiment was to measure and separate the bending of the iron caused by magnetic forces from the air gap, and the uniform tension and compression due to magnetostriction. The individual measurements were done five times to assess repeatability and uncertainty in the measurements.

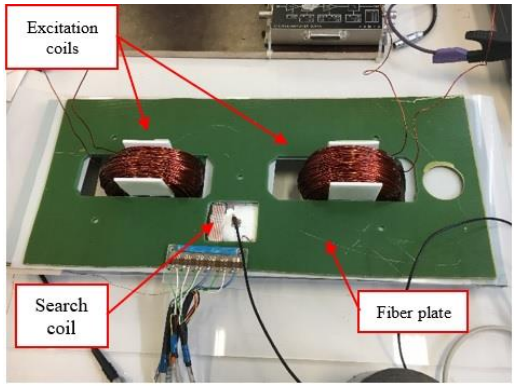

Figure 3.6. Experimental set-up for iron sheet deformation measurement

3.2.4 Motor Vibration Measurements

In this section, the measurements of vibrations of two induction motors are explained. The first one is a three-phase squirrel cage induction motor and the second motor is a high-speed solid rotor induction motor (SRIM). These vibration measurement spectra were later post-processed to analyze the frequency components present in them and to study the causes behind the vibrations.

For the first machine, which is a four-pole squirrel cage induction motor, the measurement set up consisted of the motor under investigation and a similar loading machine. The chief parameters of the machine are given in Table 3.1. The two machines are mounted on the same mechanical support and arranged with a back-to-back shaft coupling.

Table 3.1. Parameters of the Induction Motor under Study

Parameter	Value
Number of poles	4
Number of phases	3
Connection	Star
Number of stator slots	48
Number of rotor slots	40
Terminal voltage	415V@60 Hz; 325V@50 Hz
Rated slip	0.055
Rated power	22kW@60 Hz; 18kW@50 Hz
Stack length	0.23m
Stator outer diameter	0.22 m
Stator inner diameter	0.125 m

The investigated motor was supplied by an autotransformer and loaded by an identical motor fed from a frequency converter to confirm different loading levels appropriately. The laboratory set up is shown in Fig. 3.7 and the schematic

diagram of the measurement set up is shown in Fig. 3.8. The coupling between the two motors is finely implemented and properly balanced to avoid any undesirable effects from the loading machine that can cause disturbances in the measured machine's vibrations. Five triaxial accelerometers corresponding to 15 vibration channels are distributed around the machine frame as shown in Fig. 3.9. The *x*, *y* and *z* axes represent radial, tangential and axial vibrations respectively. The measured signals were recorded by a digital multi-channel recorder synchronized with a sampling frequency of 10 kHz and the data is stored in the computer. The phase voltages, currents, and rotational speed were also measured.

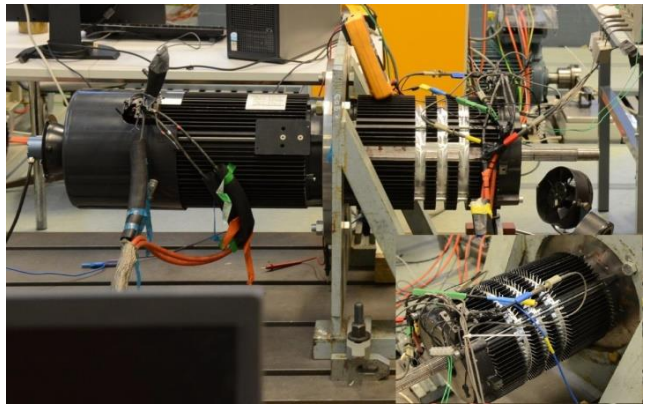

Figure 3.7. Experimental set-up for induction motor vibration measurement

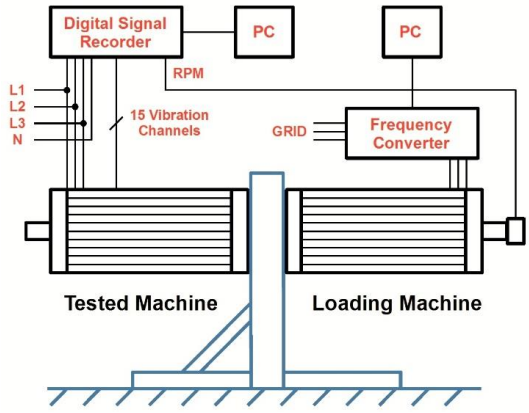

Figure 3.8. Experimental set-up schematic

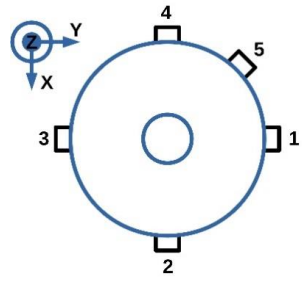

Figure 3.9. Five triaxial accelerometers

The second machine was a high-speed solid rotor induction motor in an industrial installation. The specifications of the motor are given in Table 3.2. For

measuring the acceleration, eight tri-axial accelerometers of Brüel&Kjær type 4524B were used simultaneously. A multi-axial Brüel&Kjær LAN-XI type 3050-A-060 real-time PULSE analyzer was used for multi-channel sound and vibration data acquisition. The eight accelerometers were attached at different positions around the motor set-up to measure the vibrations. Two accelerometers were attached on the top of the motor frame in bearing planes and four were closely next to the fitting points. One accelerometer recorded the vibrations in the inlet duct of cooling air and the final one in the outlet duct. The acceleration was measured in all the three directions, X-vertical, Y-horizontal, and Z-axial. In Fig. 3.10, a schematic diagram showing the placement of accelerometers around the motor structure is given.

Table. 3.2. Parameters of the Solid Rotor Induction Motor

Specifications	Unit	Value
Power	kW	300
Voltage (line-to-line)	V	400
Rated speed	rpm	60 000
Number of poles		2
Stator outer diameter	mm	250
Stator inner diameter	mm	116

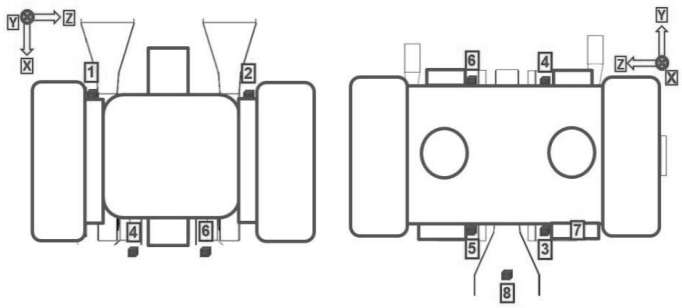

Figure 3.10. Schematic digram of accelerometer placement around the motor structure

3.3 Acoustic Noise in Electrical Machines

In the previous sections, the magnetic forces, magnetostriction and the deformations and vibrations caused by them are explained. In an electrical motor, these vibrations can cause unwanted acoustic noise. This section deals with the acoustic noise in electrical motors and methods to model and compute the generated noise. The noise generation in electrical machines is a complex scenario,

as there can be several sources of noise in a power train of a system that the electrical motor is part of. This thesis concentrates only on the electromagnetically-induced noises and their modeling.

3.3.1 Vibro-acoustics

The term vibro-acoustics can be interpreted as the acoustic noise generated by a source that vibrates and makes changes in the pressure in the surrounding medium and these pressure variations are assimilated to noise. In the electric power train of a motor, the acoustic noise can be divided into three different transfer sources viz, electromagnetic noise, mechanical noise and aerodynamic noise. Fig. 3.11 portrays these three noises according to their sources.

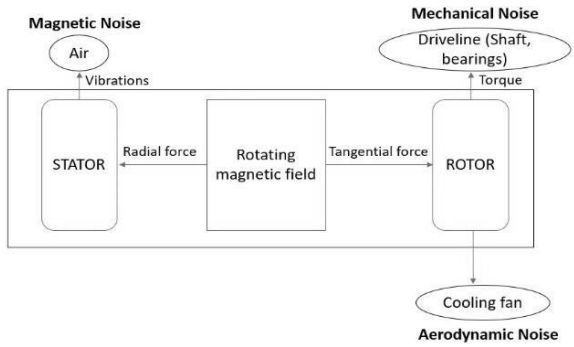

Figure 3.11. Three kinds of noise in an electrical motor power train

The electromagnetic or magnetic noise is essentially the noise produced by vibrations due to magnetic forces and magnetostriction. The magnetic flux density fluctuations in the air gap arise due to the permeability difference between the iron core and air in the air gap translates into forces that excite the stator core and hence cause vibrations. The mechanical noise is produced primarily by the mechanical contact of different parts of the motor that create vibratory responses and consequentially produce noise. The bearings and gears, rotor imbalances and shaft whirling are examples of the causes of mechanical noise. Finally, the aerodynamic noise is originated by the motor cooling fans that cause air flow turbulences. The sound-pressure level of aerodynamic noise increases with the increase in rotational speed.

3.3.2 Boundary Element Method

The numerical computation of acoustic noise in terms of sound pressure or sound level employs the Boundary Element Method (BEM) in this thesis. In the electromagnetic and mechanical domain, the FEM is used for the computation of different parameters, while in the case of acoustic noise, the domains are of infinite extent and the use of the FEM is impractical because the finite element computation requires the discretization of the entire domain. Besides, for a wide variety of acoustic problems, the frequency ranges are so high that a very large number of elements will have to be used to get a reliable solution. Due to these conditions, the FEM is only used in acoustic studies of relatively small enclosures. The BEM based on the surface Helmholtz integral equation is the major numerical tool in acoustic studies and the same is used in this thesis also.

3.3.3 BEM Approach to Acoustic Studies

The Boundary Element Method requires the discretization of only the domain boundary, saving computing time and storage. In the BEM, the *direct collocation method* deals directly with the acoustic variables (sound pressure and particle velocity) and boundary conditions. The development of a numerical computational technique for sound level or pressure comprises the incorporation of different fundamental theories and equations in physics. The steps involved in formulating acoustic pressure computation equations are described below.

For modeling vibro-acoustics in an electrical motor, the vibrating stator boundary can be used as the acoustics FEM-BEM boundary to couple the acceleration from the FEM computation to the BEM interface. This methodology facilitates modeling in a FEM-BEM framework, using the assets of both the formulations efficiently. The wave equation can be solved in the frequency domain for one frequency at a time. The acoustics computations solve the Helmholtz equation for constant-valued material properties and uses the pressure as the dependent variable. The governing Helmholtz equation for the boundary element interface is given by

$$-\frac{1}{\rho_c}\nabla^2 p_t - \frac{k_{cq}^{\ 2}}{\rho_c} p_t = 0 \tag{3.51}$$

$$k_{cq}^{\ 2} = \left(\frac{\omega}{c_c}\right)^2 \text{ and } p_t = p + p_b \tag{3.52}$$

where p_t is the total acoustic pressure, p_b is the background pressure, K_{cq} is the wave number, ρ_c is the density, ω is the angular frequency and c_c is the speed of sound.

The acoustic pressure computation problem comprises solving for small acoustic pressure variations p in the surrounding medium of a sound source, on top of the stationary background pressure p_0. This scenario can be construed as a linearization of the dependent variables around the stationary quiescent values. The fluid flow problems in a compressible lossless fluid can be analyzed using the three governing equations, viz, the mass conservation equation or the continuity equation, the momentum conservation equation or Euler's equation, and the energy equation or the entropy equation. They are given by

$$\frac{\partial \rho}{\partial t} + \nabla \cdot (\rho \boldsymbol{v}) = \boldsymbol{M} \tag{3.53}$$

$$\frac{\partial \boldsymbol{v}}{\partial t} + (\boldsymbol{v} \cdot \nabla)\boldsymbol{v} = -\frac{1}{\rho}\nabla p + \boldsymbol{F} \tag{3.54}$$

$$\frac{\partial s}{\partial t} + \nabla \cdot (s\boldsymbol{v}) = 0 \tag{3.55}$$

where ρ is the total density, p is the total pressure, $\boldsymbol{v}$ is the velocity field, s is the entropy, $\boldsymbol{M}$ and $\boldsymbol{F}$ are the possible source terms representing body forces if any.

In conventional pressure acoustics settings, all thermodynamic processes are assumed to be isentropic in nature (both reversible and adiabatic). The small parameter expansion is executed on a stationary fluid ($v_0 = 0$) of density ρ_0 (kg/m^3) and at pressure p_0 (Pa) such that $p = p_0 + p_1$ with $p_1 \ll p_0$, $\rho = \rho_0 + \rho_1$ with $\rho_1 \ll \rho_0$, $\boldsymbol{u} = 0 + \boldsymbol{u}_1$ with $\boldsymbol{u}_1 \ll c$, and $s = s_0 + s_1$. The small acoustic variations are characterized by the variables with subscript 1. Inserting these values in the governing equations gives

$$\frac{\partial \rho_1}{\partial t} + \nabla \cdot (\rho_0 \boldsymbol{v}_1) = \boldsymbol{M} \tag{3.56}$$

$$\frac{\partial \boldsymbol{v}_1}{\partial t} = -\frac{1}{\rho_0}\nabla p_1 + \boldsymbol{F} \tag{3.57}$$

$$\frac{\partial p_1}{\partial t} = c_S^{\,2}\left(\frac{\partial \rho_1}{\partial t} + \boldsymbol{v}_1 \cdot \nabla \rho_0\right) \tag{3.58}$$

where c_s is the isentropic speed of sound. The pressure time differential in the last equation is derived from the entropy equation. If the material parameters are constant, the last equation reduces to

$$p_1 = c_s^{\,2}\rho_1 \tag{3.59}$$

This expression of acoustic pressure gives a condition that needs to be fulfilled for the linear acoustic equations to hold

$$|p_1| \ll c_s^{\,2}\rho_0 \tag{3.60}$$

In a lossless medium, the wave equations for pressure waves can be obtained by reorganizing Equations (3.56)-(3.58) and dropping the subscripts

$$\frac{1}{\rho c^2}\frac{\partial^2 p}{\partial t^2} + \nabla \cdot \left[-\frac{1}{\rho}(\nabla p - q_d)\right] = Q_m \tag{3.61}$$

where the source term Q_m is a monopole domain source that corresponds to a mass source and q_d is a dipole domain source representing a domain force source. The speed of sound (c) and the density (ρ) may in general be space dependent. The combination term ρc^2 is the adiabatic bulk modulus (K_s) with unit Pa, associated to the adiabatic compressibility coefficient $\beta_s = 1/K_s$. In the frequency domain, the Helmholtz equation can be written as

$$\nabla \cdot \left[-\frac{1}{\rho_c}(\nabla p_t - q_d)\right] - \frac{k_{cq}^{\,2} p_t}{\rho_c} = Q_m \tag{3.62}$$

Acoustic fields typically involve simple harmonic waves such as sinusoidal waves. In acoustic-structure interactive numerical calculations, the structural

analysis can be coupled to acoustics by imposing acceleration as a source in the boundaries of the structure in the form of normal acceleration, indicated as

$$-\boldsymbol{n}\cdot[-\frac{1}{\rho_c}(\nabla p_t - q_d)] = -\boldsymbol{n}\cdot a_0 \tag{3.63}$$

where a_0 is the normal acceleration and q_d is the external force term.

Sound is measured by changes in air pressure from normal atmospheric pressure or reference pressure to the pressure disturbance produced by the sound. Sound pressure is measured in the unit pascals. A pascal (Pa) is equal to a force of one newton per square meter. The smallest sound pressure a human ear can hear is 20 μPa, which corresponds to zero dB. The sound pressure level (SPL) in dB can be calculated by

$$SPL = 20\ log_{10}\left(\frac{p}{p_{ref}}\right) dB \tag{3.64}$$

where p_{ref} is the reference pressure 20 μPa in the case of audible sound calculations.

The application results of BEM-based acoustic computation of an induction motor is given in section 4.3.1.

4. Application and Results

In this chapter, the results obtained using the methods given in Chapter 3 are explained and organized based on the results presented in the publications. The numerical simulation results and experimental results are presented and compared when they are relevant.

4.1 Electromagnetic Forces

In this section, the computational and experimental results of magnetic forces are explained in detail. The computation of magnetic forces is a fundamental process in the magnetic and vibro-acoustic studies presented in this thesis. The force computations are part of the Publications I, II and III.

4.1.1 Generalised Nodal Forces

The Generalised Nodal Forces or GNF are computed based on the Virtual work principle, described in section 3.1.2. The numerical model for the nodal force computation is implemented in the open-source finite element software *Elmer*. In Fig. 4.1, the *Elmer* computational result of nodal forces on the stator of a three-phase four-pole squirrel cage induction motor is given. The specifications of the motor are given in Table 3.1. The time-stepping simulation was done for 6000 time-steps with 0.0002 seconds as a time-step interval, which corresponds to 1.2 seconds of motor running time. The finite element mesh contains 89892 elements and 45003 nodes. The nodal forces are majorly distributed on the stator teeth. The visualization of the nodal forces is done using the open-source software *ParaView*. In Fig. 4.2, the nodal magnetic forces acting on the node of a stator tooth are plotted as a function of time.

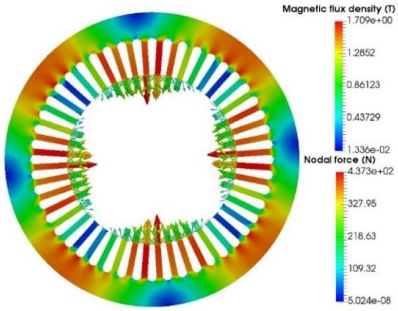

Figure 4.1. Nodal magnetic forces on stator teeth.

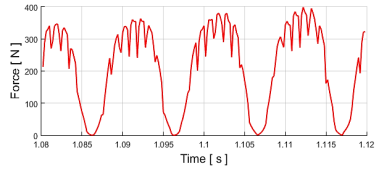

Figure 4.2. Amplitude of a nodal force as function of time.

The Virtual work principle is employed in the calculation of magnetic forces on the end winding of a high voltage three-phase induction motor. The specifications of the induction motor are given in Table 4.1. In Fig. 4.3, the nodal forces acting on the ending windings are given, that are theoretically the Lorentz forces due to the interaction between the circulation of currents and the leakage flux. The end-winding shown in Fig. 4.3 and the airgap forces in Fig. 4.1 are of different motors. The magnetic forces in the inner layer are higher than that in the outer layer of the winding. The forces on different parts of the same coil are different in magnitude. The simulation corresponds to a state where there is high current flow in the windings during the starting mode. The results shown here are from a static FE simulation, where the currents are imposed as a body force in the winding.

Table 4.1. Specifications of the Induction Motor

Parameter	Value
Number of poles	2
Number of phases	3
Connection	Star
Number of stator slots	42
Number of rotor slots	34
Rated voltage	6.6 kV
Rated power	660 kW
Rated current	138 A

The above two examples of nodal force calculations using the Virtual work principle depict a fundamental and significant computational aspect in the electromagnetic analysis of electrical motors. The nodal forces can be directly used in the structural analysis such as stress and vibration studies of motors.

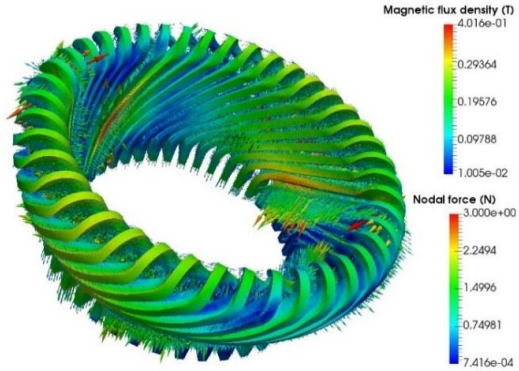

Figure 4.3. Distribution of flux density and nodal magnetic force vectors in the end winding

4.1.2 Nodal Forces from Degenerated Air-gap Element Method

The application of conventional nodal force calculation based on the Virtual work principle is given in the previous section. In the case of the stator or end winding of a motor, the generalized nodal forces can be calculated efficiently as shown in the results. However, if there is an infinitesimal air gap in the body where the nodal forces need to be calculated, the conventional method would require very thin mesh and thereby heavy finite element computations. In such scenarios, the use of degenerated air-gap elements in force calculation is an excellent choice. The theory behind the degenerated air-gap elements is given in section 3.1.4, and an experimental set up to measure the magnetic forces between two permanent magnets is explained in section 3.1.5. The numerical simulation and experimental results are presented and compared in this section.

The nodal forces are calculated by FE simulations by adjusting the air-gap length between the two magnets and the results were compared with the measurement data. In Table 4.2, comparison between the results of 3D simulations with first order tetrahedral elements, the measured forces and the eggshell method are given, and the same is portrayed graphically in Fig. 4.4. The distribution of nodal forces on the magnets is shown in Fig. 4.5, where the nodal forces are concentrated at the edges near the air gap. The number of degrees of freedom and the maximum size of the finite element of the mesh are taken as norms of references in the convergence behavior study of the degenerated air-gap element method, shown in Fig. 4.6.

Table 4.2. Experimental and 3D simulation results

Experimental		Numerical Simulation	
d [mm]	F [N]	Degenerated air gap F [N]	Eggshell F [N]
0.095	64.7	64.1	63.8
0.274	60.9	60.0	59.7
0.477	57.1	55.9	54.6
0.745	52.8	51.3	49.9
1.009	48.9	47.5	46.9

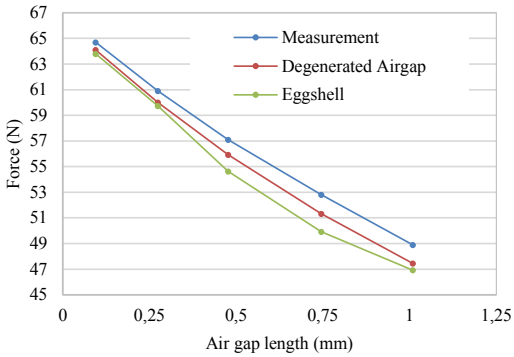

Figure 4.4. Numerically calculated magnetic forces and measurement results

Fig. 4.4 shows that the degenerated air-gap method and eggshell method have given very close results of magnetic forces, although the measurement values are somewhat higher than the calculated forces. This slight mismatch is due to an error in the measurement set-up, where the laser displacement sensor estimates the air-gap distance as the distance between the magnet supports instead of the distance between the two magnets. The support assembly of the measurement setup is not entirely rigid, and hence a minor decrease of the air gap is anticipated due to the support stretching, that can result in recording higher magnetic forces.

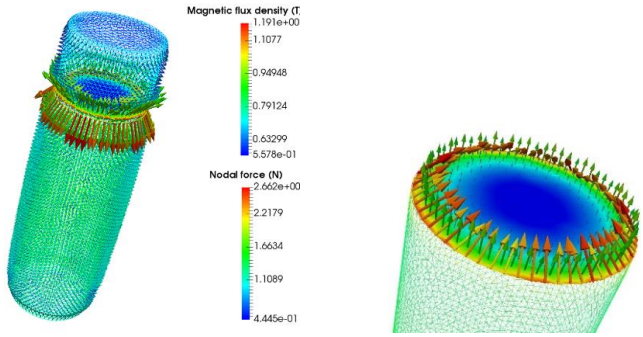

Figure 4.5. Left: Nodal magnetic forces on permanent magnets. Right: Forces at one side of the contact surface of the magnets

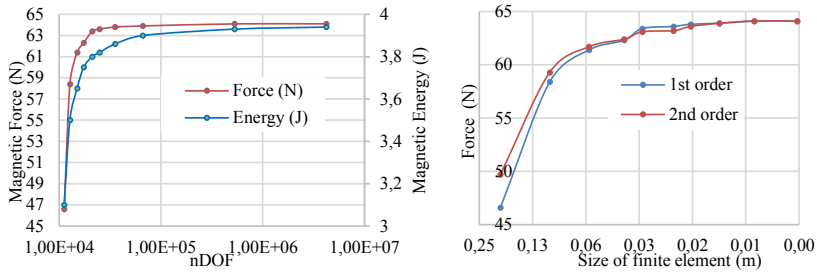

Figure 4.6. Convergence behavior Left: with respect to the number of degrees of freedom, Right: with respect to the maximum size of the finite element in the mesh at the air-gap length 0.095 m

The magnetic energy and the forces have the same rate of convergence from Fig. 4.6. The magnetic force solution is studied with respect to the maximum size of the finite element in the mesh at an air-gap length of 0.095 m. It was observed that, after a certain limit, the size of the elements does not affect the solution, because the force values remain the same after a certain element size.

The degenerated air-gap element method can be applied to several practical applications such as force computation in certain parts of electrical machines. Two such examples are given in Fig. 4.7 and in Fig. 4.8. In conventional FEA, the computation of magnetic forces acting on the magnets and rotor core in permanent magnet motors requires dense meshing at the contact surface between the magnet and the rotor core. The degenerated air-gap element method can be employed in this case without the addition of an extra dense air-gap mesh. In the presented case in Fig. 4.7, the air gap is of 0.1 mm thickness. In real machines, this thin air gap represents an adhesive layer that glues the magnets to the rotor. In linear permanent magnet synchronous motors with Halbach arrays as shown in Fig. 4.8, the analysis of magnetic forces on the contact surfaces of the magnets is very important. The Halbach array of magnets enables better usage of magnetic flux and provides higher torque and performance compared to radial magnet structures, using a spatially rotating magnetisation pattern. This orientation augments the magnetic field on one side of the array and cancels the field to nearly zero on the other side. The magnetic contact forces are distributed on the contact surface between the magnets.

The similarity of results with the eggshell force computation method and the convergence results show the consistency and reliability of the proposed degen-

erated air-gap method for force calculation of bodies in contact. Also, the practical application of this method in a permanent magnet motor and linear motors makes it an efficient and cost-effective tool for the engineering design of motors.

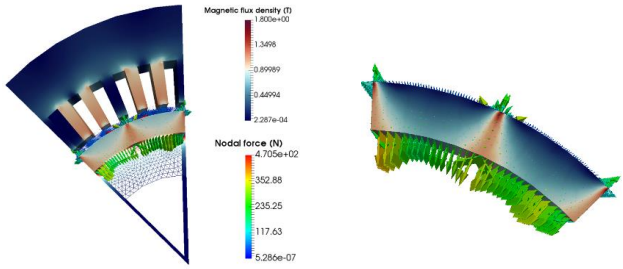

Figure 4.7. Left: Magnetic forces on the permanent magnet edges, Right: Nodal forces on the magnet surface

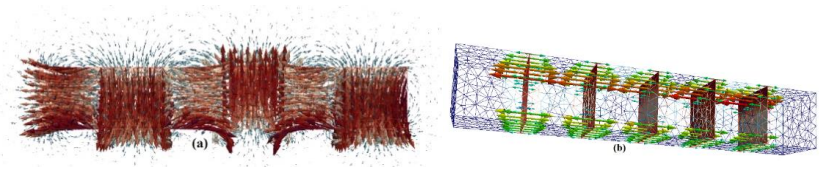

Figure 4.8. (a) Magnetic flux path on Halbach arrayed permanent magnets, (b) Nodal magnetic forces on the contact layer between the magnets

4.2 Deformation from Magnetomechanical Coupling

The computational and experimental results of magnetic forces and their applications are described in the previous section 4.1. Magnetic forces are the major electromagnetic cause of deformation in electrical motors, besides magnetostriction. The magnetic forces or electromagnetic stresses are the sources of the mechanical deformation of ferromagnetic parts of an electrical machine, and this scenario can be modeled in numerical analysis using magnetomechanical coupled models. These models can compute the mechanical effect of magnetic forces and magnetostriction on electrical machines and calculate the displacements or deformations and the consequent vibrations due to these deformations. In this section, two such magnetomechanical coupled FE models described in sections 3.2.1 and 3.2.2 are explained with their application results.

4.2.1 Weak Magneto-elastic Coupling

The nodal magnetic forces calculated using the Virtual work principle can be applied as the excitation to the mechanical solver in the FE simulation. This is done by feeding the nodal forces as the input volume force to the elastic solver. The elastic solver computes the stress caused by the magnetic forces and the resulting mechanical deformation. This kind of coupling is implemented in *Elmer* and the application results of two such cases are given in Fig. 4.9 and Fig. 4.10. The deformation of the stator core of an induction motor described in section 4.1.1 is shown in Fig. 4.9 where the deformed geometry is compared with the original geometry. The plot of displacement at an arbitrary timestep at a node on the stator outer surface is also shown in Fig. 4.9. In the radial displacement computation, the tangential displacement was set to zero as the boundary condition in the elastic solver.

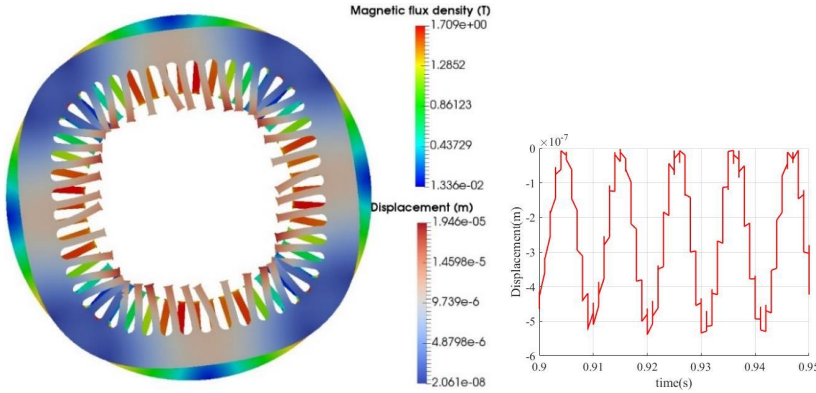

Figure 4.9. Left: Deformation of stator due to magnetic forces. Displacements are zoomed by a factor of 1000, Right: Radial displacement at a node on stator surface.

The nodal forces acting on the end winding of a high voltage induction motor are presented in section 4.1.1. These magnetic nodal forces are coupled to the elastic solver in *Elmer* and the consequential stress and deformation of the winding is portrayed in Fig. 4.10. In this simulation also, the displacements in the required direction is set free and the other directions are set to zero in mechanical boundary conditions. In the case of small motors like in Fig. 4.9, the end-windings are so small that they would not affect the vibrations. Besides, the forces on the end windings are very small compared with the ones on the iron.

The windings themselves can be modeled as either a mass or a mass and damping, but the effect of these issues has been shown only in large machines. The insulation is hard to model, but its effect also could be very marginal.

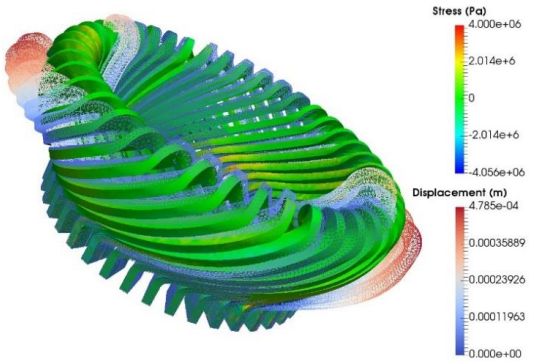

Figure 4.10. Stress distribution and displacement in end-winding. Displacements are zoomed by a factor of 200.

The application of nodal magnetic forces in magneto-elastic coupled computations is a simple yet reliable technique for the structural analysis of both the core and the windings of electrical motors. Especially in the case of low and medium power machines where magnetostriction does not considerably affect the mechanical deformation of the core, this mode of calculating the deformations and stress comes conveniently in the design stages of the motor.

4.2.2 Magnetomechanical Coupling and Magnetostriction

The magnetomechanical coupling described in the previous section considers only the magnetic forces. In electrical machines, the magnetostriction also plays an important role in the production of stress, mechanical deformations and vibrations. The magnetostriction is included in the magnetomechanical coupling using the free-energy-based coupled model explained in section 3.2.2. The experiment to study the deformation of iron, explained in section 3.2.3 is simulated using the free-energy-based numerical model, where the magnetomechanical material model is implemented. The experimental results have provided light on how the magnetic forces and magnetostriction affected the mechanical deformation of the iron sheet under investigation.

In Fig. 4.11, the magnitude of the measured strains is plotted from the five strain gauges SG1 to SG5, that are placed from left to right at the center of one

limb of the iron sheet. This strain is caused by both the magnetic forces and magnetostriction. The magnitude of the total strain on the left side at SG1 is higher compared to that on the right side at SG5. This difference is due to the torque and force relationship $T = \boldsymbol{F} \times r$, where r is the distance from the air gap to the location where torque is calculated, or the strain gauge is located. Henceforth, on the left, the distance from the air gap is more than that to the right and the torque becomes higher on the left. This causes the increased total strain on the left side. The strain measured by SG1 is plotted against the magnetic flux density variation, which is also given in Fig. 4.11, where the increase in the strain is seen, as the flux density increases.

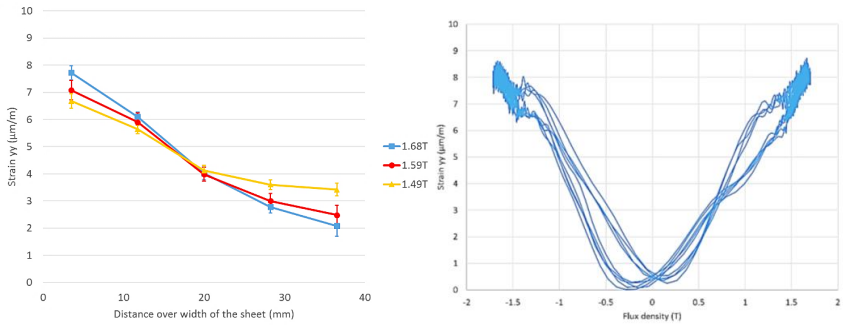

Figure 4.11. Left: The strains measured by strain gauges SG1 to SG5 at three different flux densities, Right: Strain measured by SG1 as a function of flux density

The numerical implementation of the energy-based magnetomechanical material model is done in the open-source software *Elmer*. In Fig. 4.12, the deformation due to the magnetic forces are shown. The HB curve was extracted from the energy-based model by generating field-flux-strain relations. The boundary at the topside of the air gap is fixed in all directions in the FE mechanical simulation. The magnetic flux density at the air gap is approximately 0.5 T and the maximum displacement of the sheet edge is around 7 μm near the air gap. The deformation produced by magnetic forces and magnetostriction is shown in Fig. 4.13. The supply current used in the simulations is 1.3 A at 1 Hz.

The magnetic forces near the air gap produce mainly a bending-type strain, which is tensile on the left and becomes compressive at the right end. Additionally, a very small uniformly distributed compressive strain is also caused by the air-gap forces. The result of a mechanical FEA study by applying uniform distributed pressure of 1 N on the iron sheet on the top side of the air gap is given in Fig. 4.14. At the center of the left limb, the strain is not zero, but has a small

negative offset. This uniformly distributed negative strain due to the air-gap forces is about 5.2 % of the bending-type strain at SG1 and about 4.2% of the bending type component at SG5. The magnetostrictive strain is obtained by subtracting this component from the measured total uniformly distributed strain. The measured maximum strain can be separated into pure-uniform and bending-type strain distributions.

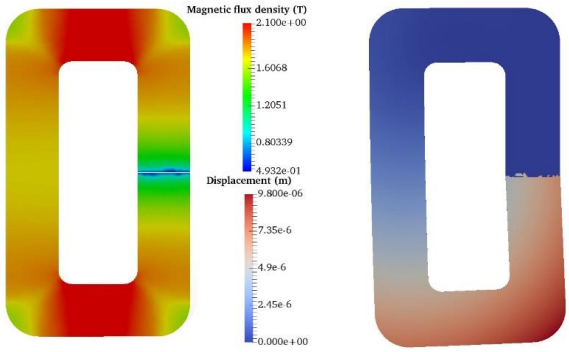

Figure 4.12. Left: Magnetic flux density in the iron sheet, Right: Deformation due to magnetic forces only (scale factor: 500)

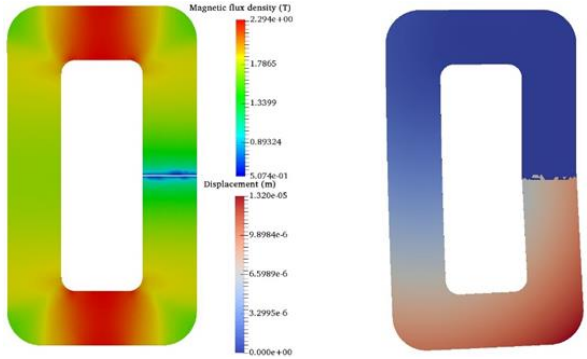

Figure 4.13. Left: Magnetic flux density in the iron sheet, Right: Deformation due to both magnetic forces and magnetostriction (scale factor: 500)

The separated strain components are given in Table 4.3 that are obtained by linear regression fitting. Regarding the magnetostrictive component, the correction due to air-gap forces has already been considered in the values in the table. Due to linear regression curve fitting and correction due to air-gap forces, the obtained magnetostrictive strain is higher than the measured strain value at the center of the limb. The bending-type strain is half of the difference between the fitted values of SG1 and SG5 and the same at the SG5 location has almost the

same amplitudes as the SG1 location, but the opposite sign.

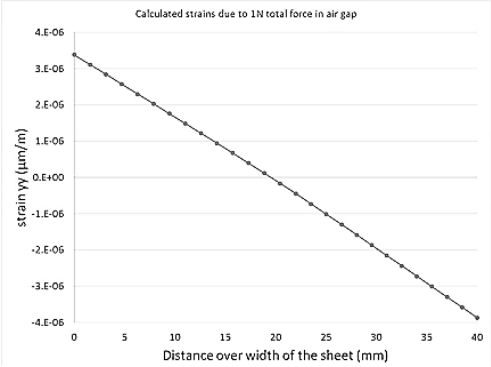

Figure 4.14. Bending strain due to air-gap forces

Table 4.3. Measured strain components segregated

Flux density	Bending-type strain at SG1 due to air-gap forces	Strain due to magnetostriction
1.68 T	2.8 µm/m	4.7 µm/m
1.59 T	2.3 µm/m	4.6 µm/m
1.49 T	1.6 µm/m	4.8 µm/m

The experiments by U. Aydin, D. Singh and A. Belahcen showed that the tensile stress decreases the maximum magnetostriction, while the compressive stress increases it (Takagi et al. 1997, Singh et al. 2015, Aydin et al. 2016). The shape of the test specimen and the magnetization of the sheet in the experiment have resulted in some difficulties in recreating the magnetic flux density and strain in simulations the same as in the measurement. The copper coils for giving supply to the specimen are located at the top and bottom limbs. This causes the magnetization along the rolling direction in top and bottom limbs, while it is normal to the rolling direction in the left and right limbs. The strain measurements were done in the left limb where the rolling direction is opposite to the magnetization, while the strains were measured in the magnetization direction. The magnetomechanical model is formulated for materials magnetized in the rolling direction and with an assumption that the material is isotropic. However, the measurements by Singh et al. (2015) had showed that the magnetostriction in transverse direction is much higher than in the rolling direction. In the part of the specimen where the strain measurements were done, the magnetostriction produces only tensile strain. The simulated strain in the sheet due to both magnetic forces and magnetostriction, and the distribution of the magnetostrictive strain in the measurement area are shown in Fig. 4.15. The magnetic

forces cause tension in the y-direction on the left side at SG1, and compression on the right side at SG5. The computed strains from the locations of the gauges SG1 to SG5 are plotted in Fig. 4.16 corresponding to 1.49 T flux density, resulting from only magnetic forces and from both magnetic forces and magnetostrictoin respectively.

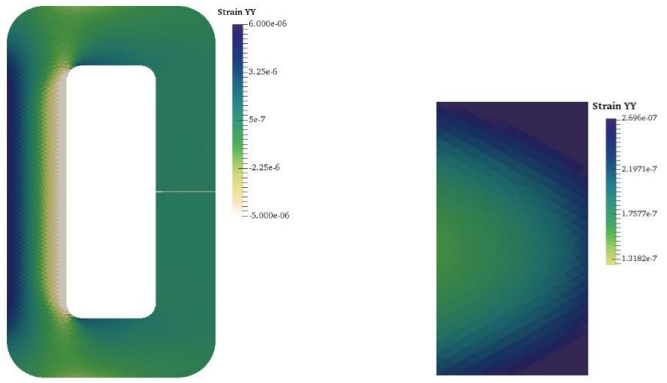

Figure 4.15. Left: Strain (m/m) in y-direction due to both magnetic forces and magnetostriction, Right: Magnetostrictive strain over the width of the sheet.

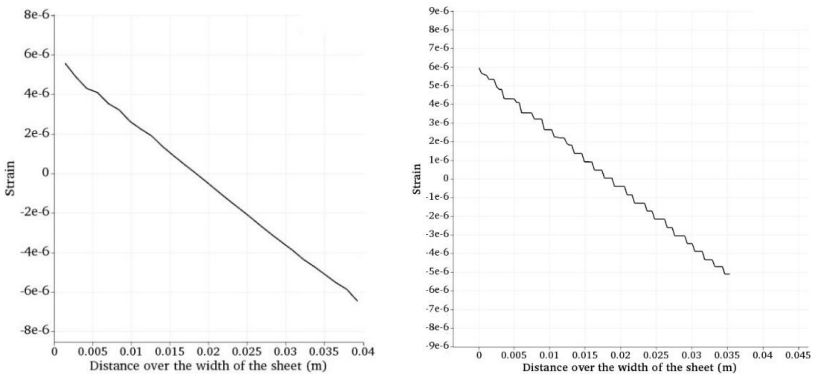

Figure 4.16. Simulated strain (m/m) in y-direction (from Sg1 to SG5), Left: Due to magnetic forces, Right: Due to both magnetic forces and magnetostriction

The strain due to air-gap forces is smaller in measurement compared to the simulation. The magnetization of the sheet is in transverse to the rolling direction at the limb where the air gap is located, which causes lower flux density at the airgap and consequently lower strain. On the other hand, the measured magnetostrictive strain is higher compared to the simulation, because the magnetostrictive strain in the transverse direction to magnetization is higher compared to that in the parallel direction.

4.2.3 Effect of Magnetic Forces and Magnetostriction on Vibrations

In the previous section, the mechanical deformation caused by magnetic forces and magnetostriction in an iron sheet and their interaction are explained. In an electrical motor, these two phenomena cause deformations and vibrations, and the effect of their interaction and the resulting vibrations depend on many factors such as the number of poles and the rotor and stator design. The vibration studies are part of the Publications IV and V.

The energy-based magnetomechanical model is used for the vibration studies of the induction motor described in sections 4.1.1 and 4.2.1. The results shown in Fig. 4.17 are from Matlab time-stepping simulations with a simulation time of 0.6 sec (6000 time-steps) and a timestep length of 0.0001 sec. The mesh has 694 nodes and 1162 triangular elements. The deformations of the stator in three different cases viz., due only to magnetic forces, due only to magnetostriction and due to both magnetic forces and magnetostriction are shown in Fig. 4.18. The effect of magnetic forces on the stator core is introducing contraction, whereas the magnetostriction expands the core. In radial displacement simulation, the displacements of the outer nodes of the stator and inner nodes of the rotor were fixed to zero in the tangential direction, and those were fixed in the radial direction for the tangential displacement simulation.

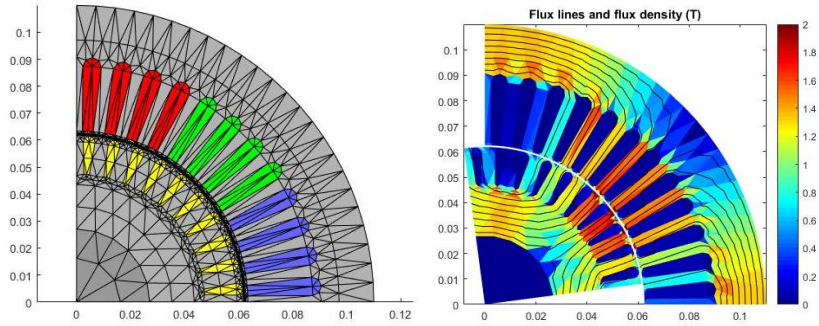

Figure 4.17. Left: FE mesh in Matlab, Right: Magnetic flux density in rotor and stator

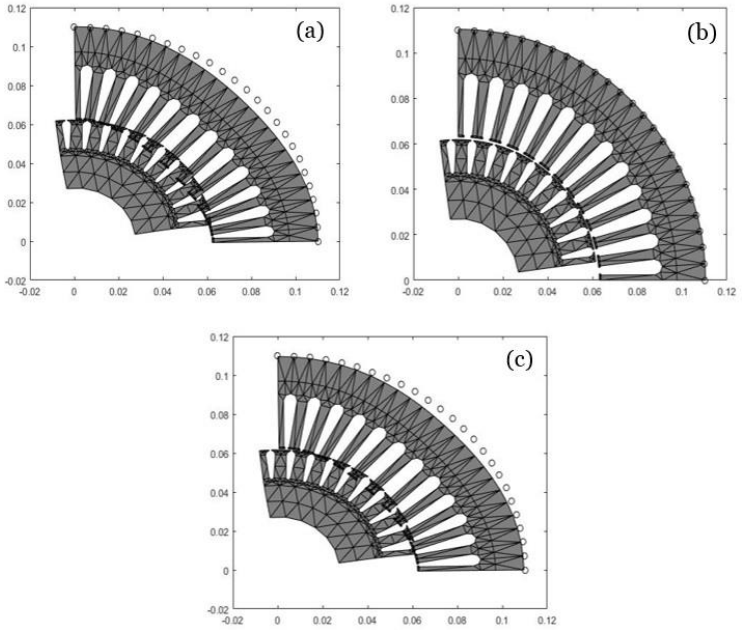

Figure 4.18. Deformation of the stator of four-pole motor due to (a) magnetic forces only, (b) magnetostriction only and (c) both magnetic forces and magnetostriction. Displacement scale factor: 1e4. The dotted line represents the original stator outer boundary before deformation.

In Fig. 4.19, the displacements at a point on the stator outer surface are compared for three different cases and it is inferred that the displacements due to magnetic forces and magnetostriction are opposite in phase, which results in the attenuation of the final displacement because they oppose each other's effect. For more accurate results and avoiding the locking effect of FE elements, simulations were done using second order elements also. From Fig. 4.20, the second-order simulation results are shown, where the displacements are bigger, compared to the first-order simulations.

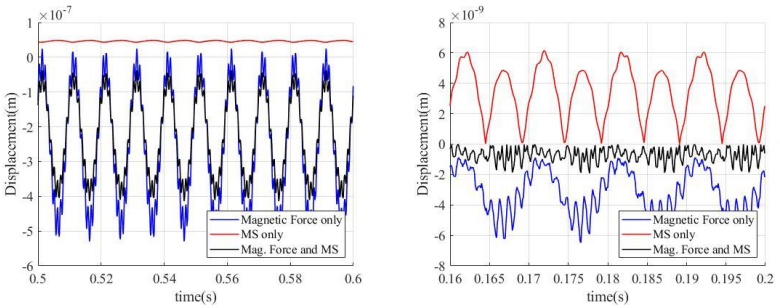

Figure 4.19. Simulated displacements at a point on the stator outer surface of the four-pole motor. Left: Radial displacements, Right: Tangential displacements

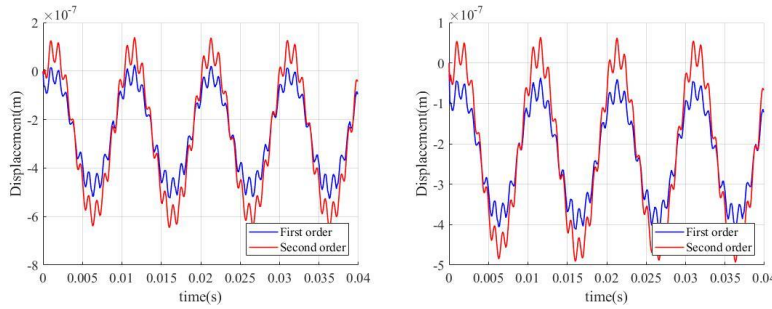

Figure 4.20. Comparison of radial displacements between first-order and second-order simulations. Left: Displacement due to only magnetic forces, Right: Displacement due to both magnetic forces and magnetostriction

The same induction motor was simulated with a two-pole configuration to study how the magnetic forces and magnetostriction behave in a two-pole motor. The results are shown in Fig. 4.21. Unlike the four-pole configuratiofn, the magnetic forces and magnetostriction are in phase and the final displacement becomes strengthened, because the contributions of magnetic forces and magnetostriction add together in this case. The stator deformation of the two-pole motor in three different cases is shown in Fig. 4.22.

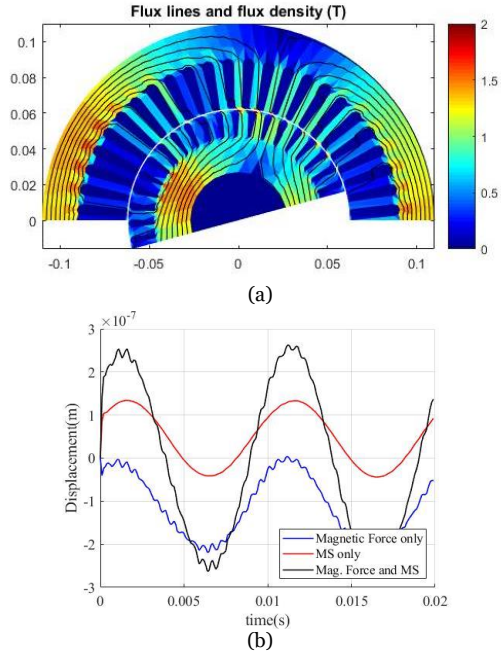

Figure 4.21. (a) Flux density distribution in the two-pole motor, (b) Simulated radial displacements at a node on the outer surface of stator

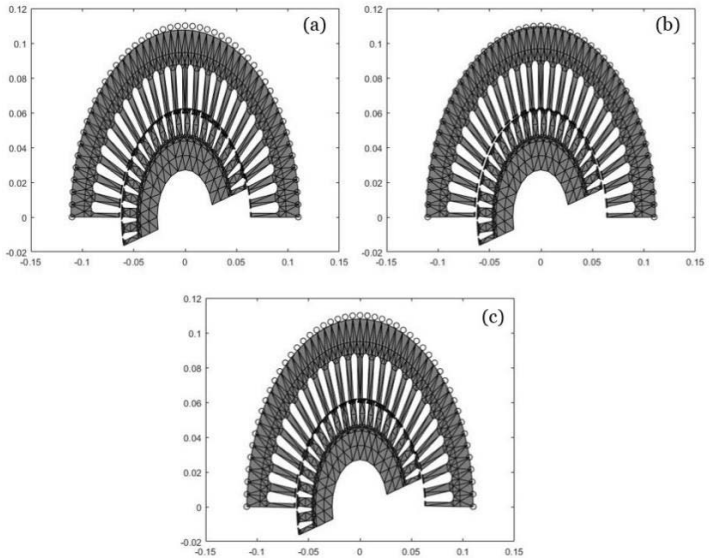

Figure 4.22. Deformation of the two-pole stator core due to (a) magnetic forces only, (b) magnetostriction only and (c) both magnetic forces and magnetostriction. Displacement scale factor: 1e4. The dotted line represents the original stator outer boundary before deformation

4.2.4 Vibrations and Frequency Spectra Analysis

The deformation of the stator due to magnetic forces and magnetostriction causes unwanted vibrations in electrical motors. The computational results of magnetomechanical numerical models are presented in this section and compared with the vibration measurements for detailed frequency spectra analysis. The vibration measurements of two different induction motors are explained in section 3.2.4. For the squirrel-cage induction motor, the measured vibration spectra are given in Fig. 4.23. The same motor is simulated and the radial displacements were computed, as explained in section 4.2.3. The Fourier analysis of these displacements showing the frequency spectra is given in Fig. 4.24.

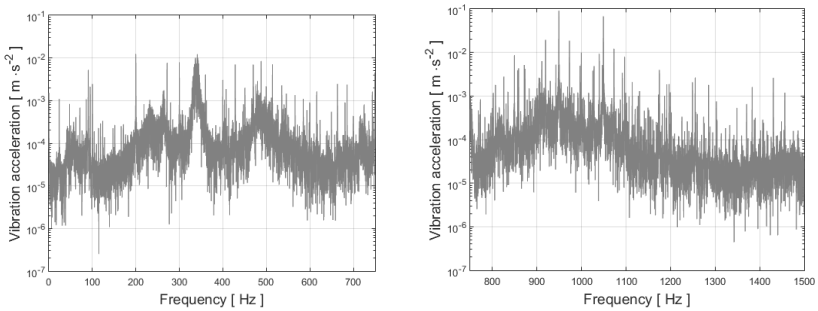

Figure 4.23 Measured radial vibration frequency spectra of induction motor

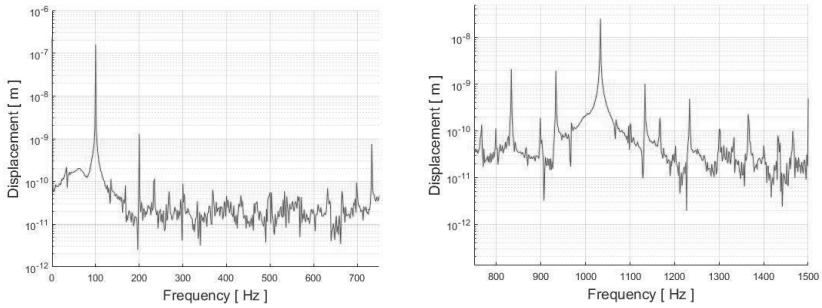

Figure 4.24 Simulated radial vibration frequency spectra of induction motor

The frequency spectra show that, the most important frequencies present are the rotational speed frequency f_{1x} = *rotational speed*/60 = 1400/60 = 23.3 Hz, and the twice-line frequency $2f_L$ (100 Hz) and their harmonics. Natural frequencies f_{res} 271 Hz and 423 Hz are also present in the spectrum. The magnetic forces acting on the stator teeth and core produce the twice line frequency $2f_L$. For the sinusoidal magnetising current, these nodal forces have two peak values at each current period, which implies that vibrations caused by this force will have a frequency equal to double the supply current frequency. There are spikes in the vibration spectra at frequencies $2f_L$ (100 Hz) and its integer multiples. In the high frequency regions, the highest amplitudes of vibrations are caused by the rotor-bar passing frequency f_{QR}, given by, f_{1x}***number of rotor slots* = 932 Hz. The rotor-bar passing frequency (f_{QR}) vibrations are the result of the magnetic field around the rotor bars. This magnetic field generated by the rotor-bar currents produces forces that act on the stator teeth and create vibrations in the teeth and core of the stator. The frequency of these vibrations is usually higher than 1 kHz and it increases with load. The sidebands of f_{QR} at $\pm$ 2 f_L, 4 f_L, 6 f_L and 8 f_L corresponding to 832 Hz, 1032 Hz, 732 Hz, 1132Hz, 632 Hz, 1232 Hz, 532 Hz and 1332 Hz are also present in the spectrum. At 341 Hz in Fig. 4.23, a relatively high magnitude of acceleration is seen in the frequency spectrum, which is caused by the structural vibration of the entire machine set-up. The frame of the motor is not modeled and hence the magnitude of the vibrations will be different in simulations compared to that of measurement. Because the rigid body motion is not included in the simulation. This is why the simulated accelerations were not separately calculated. The simulation solves primarily the displacements. However, the frequency components should be the same in both displacement and acceleration. The damping value was given as 1.2%,

which was obtained from modal testing of the motor (not done within this thesis).

The second study on vibration measurements was done for a high-speed solid rotor induction motor, the specifications of which are given in Table 3.2 of section 3.2.4. The Fourier analysis of the measured vibrations is given in Fig. 4.25, showing the frequency components in the measured accelerations at sensor 1, in the radial and tangential directions respectively. There are higher values of the acceleration components at frequencies 1000 Hz, 2000 Hz, 3000 Hz, 4000 Hz, 5000 Hz, 6000 Hz and 7000 Hz.

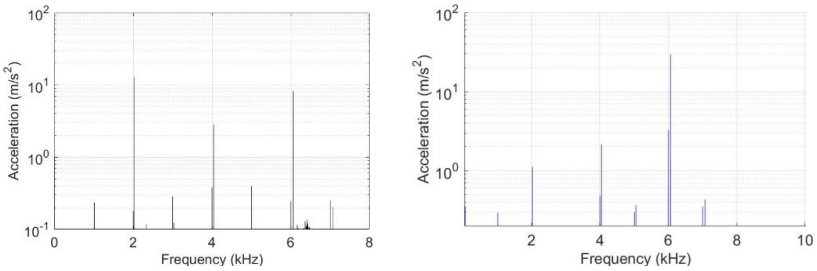

Figure 4.25 Measured vibration frequency spectra of solid rotor induction motor at a motor speed of 60000 rpm and a motor load of 51 Nm. Left: Radial acceleration, Right: Tangential acceleration

The energy-based model is employed for the magneto-mechanical simulation of the motor in Matlab. The motor was simulated with a PWM supply as in the original measurement. The results shown are from time-stepping simulations with a simulation time 0.015 s and have a time-step length of $5e^{-6}$ s. The mesh of the simulated motor and the flux density distribution are shown in Fig. 4.26. The radial displacement at a point on the stator surface due to magnetic forces and magnetostriction is given in Fig. 4.27.

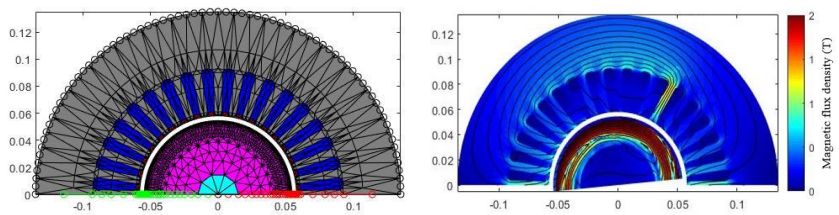

Figure 4.26. The FE mesh of the solid rootr motor and the magnetic flux density distribution

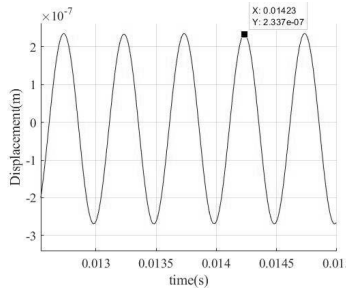

Figure 4.27. Simulated radial displacement at a point on the stator surface

The simulated displacements are used for the Fourier analysis and the frequency spectra of the displacements are shown in Fig. 4.28, where there are high magnitudes of displacements at 2000 Hz and 4000 Hz. Since the measured frequency spectra are different from the simulated ones, the motor was simulated again after introducing dynamic eccentricity in the rotor. The radial and tangential frequency spectra of the motor under dynamic eccentricity are shown in Fig. 4.29. It is worth noting that, the objective of this analysis is not to determine the amplitude of the induced deformation or vibration, but to investigate the frequency components present in them and to find out how they were initiated. For different types of motors in terms of size and power, the amplitude of the deformations and vibrations also vary (Verma et al. 1975).

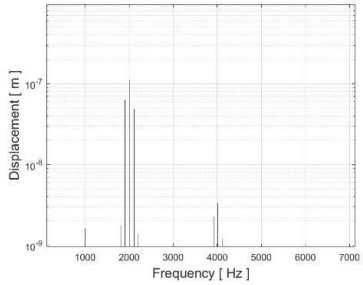

Figure 4.28. Frequency spectrum of simulated radial displacement (normal operation)

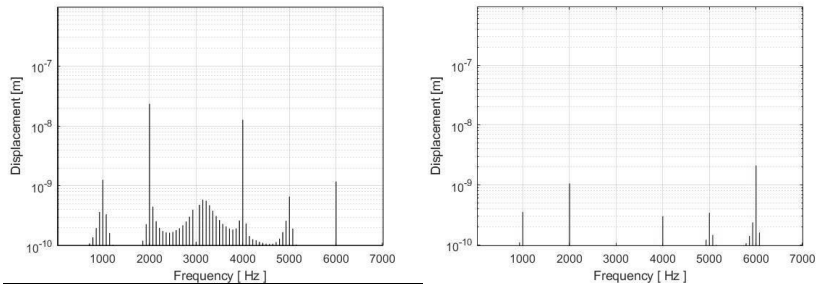

Figure 4.29. Frequency spectrum of simulated displacement under dynamic eccentricity. Left: Radial and Right: Tangential displacements

For this high-speed motor, the rotor rotational frequency f_r is 1000 Hz, the supply frequency f_s is 1008.7 Hz for a slip of 0.00875. Fig. 4.30 shows the major radial acceleration amplitudes above 1 m/s² around 2000 Hz, 4000 Hz and 6000 Hz frequencies, and the tangential components are given in Fig. 4.31. In Table 4.4, the origination of different frequency components from the measurement shown in Fig. 4.30 are detailed.

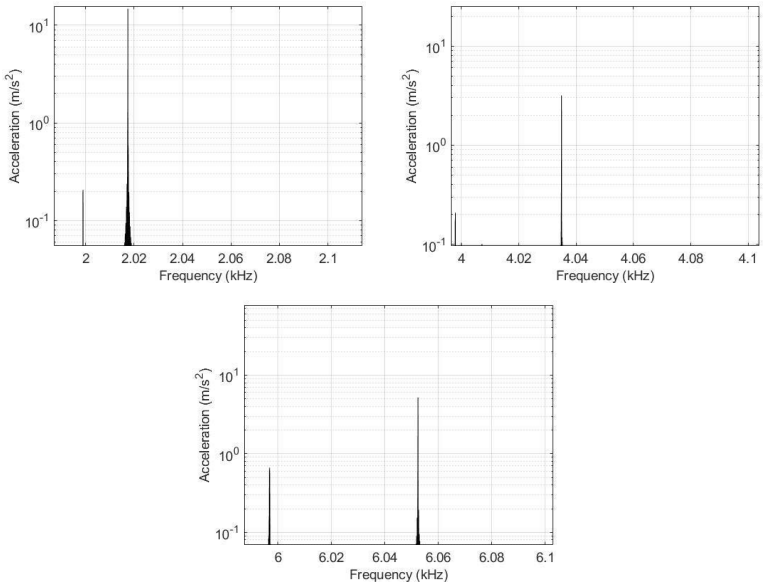

Figure 4.30. Frequency spectra of measured radial accelerations

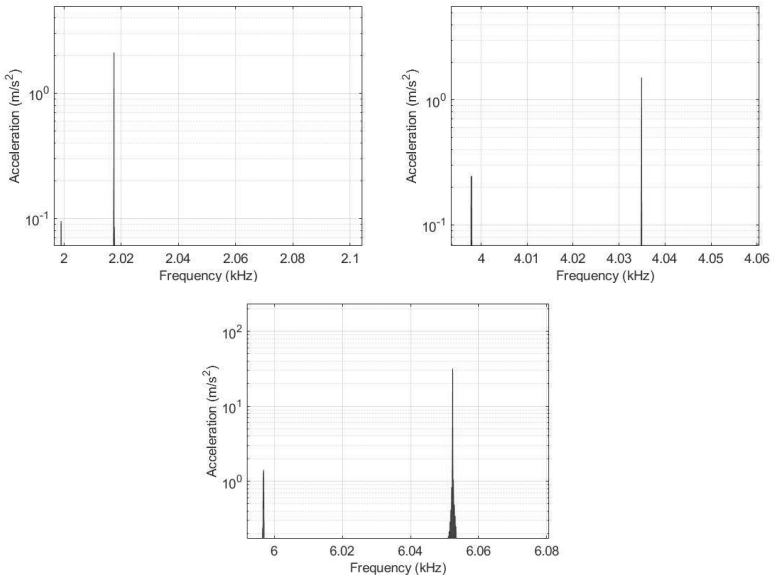

Figure 4.31. Frequency spectra of measured tangential accelerations

In Fig. 4.32, the simulated results of the major radial frequency components at 2017 Hz, 4035 Hz and 6052 Hz are given. It can be seen that the theoretically proven components explained in section 3.1.4 are present in this simulated spectra at the same frequencies as in the measurement shown in Fig. 4.30. The same results were achieved for tangential frequency spectra also. Hence, it can be concluded from the simulation and measurement results that the supply frequency, rotor frequency and the additional components due to dynamic eccentricity are the major contributing factors of the motor deformation and thereby the accelerations. In the simulation, the rigid- body motion including the frame of the motor is not modeled, and hence the simulated acceleration will not have the effect of rigid-body motion. This is the reason behind the difference in the amplitude between the measured and simulated accelerations. The measurement data can also be influenced by the damping and resonance of the housing and support structures of the motor.

Table 4.4. Origination of different frequencies in the acceleration spectrum

Frequency	**Value (Hz)**	**Sideband**	**Value (Hz)**
f_s	**1008.75**		
$2f_s$	**2017.5**	**$2(f_s\text{-}sf_s)$**	2*(1008.75-(1008.75*0.00875)=**1999**
$2p*2f_s$	(2*1)*2017.5=**4035**	**$2p*2(f_s\text{-}sf_s)$**	2*(1008.75-(1008.75*0.00875)=**3998**
$(2p+1)*2f_s$	(2+1)*2017.5=**6052**	**$(2p+1)*2(f_s\text{-}sf_s)$**	3*2*(1008.75-(1008.75*0.00875)=**5999**

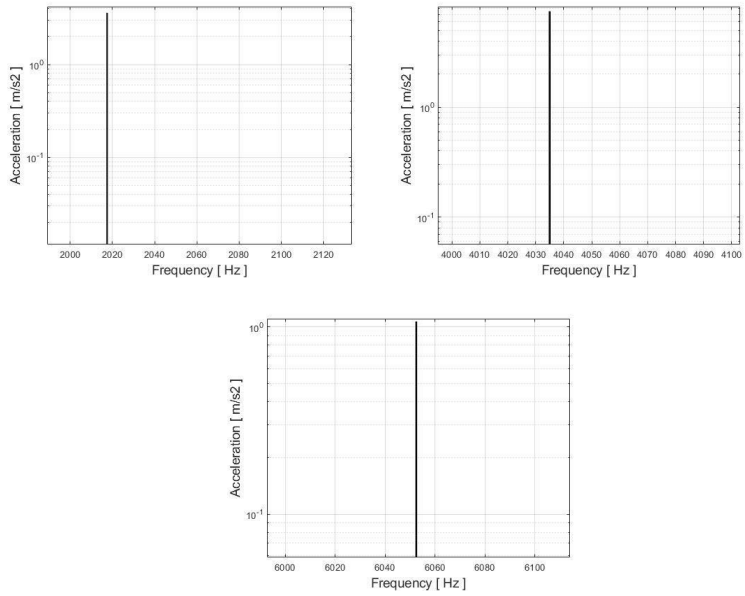

Figure 4.32. Radial frequency spectra of simulated acceleration showing 2017 Hz, 4035 Hz and 6052 Hz

The major inference from the study is that when a dynamic eccentricity is present in the motor, the frequencies in both measurement and simulation are similar. This is a noteworthy result in terms of condition monitoring, motor assembly and acoustic noise problems. The results indicate the existence of dynamic eccentricity in the motor according to this study. This needs to be investigated further to discover the root causes of eccentricity such as the calibration of magnetic bearings that keeps the rotor at the center of the motor.

4.3 Noise Analysis

The computational and experimental analysis and results of electromagnetic phenomena including magnetic forces, magnetostriction, and their mechanical effects such as deformation and vibrations are explained in the previous sections. The final part of this study is the consequence of vibrations, which is acoustic noise. The Boundary Element Method (BEM) is used in this thesis for the acoustic studies. The application results of the BEM in the noise computation of an induction motor are given in the following sections. The acoustic analysis is part of the publication VI.

4.3.1 Acoustic Noise produced by an Induction Motor

Numerical modeling of noise generation in an electrical motor involves three stages: first modeling the electromagnetic forces, then the structural deformation and vibration behavior and, lastly, the resulting acoustic response of the motor. The magnetic force can be calculated from the Maxwell stress tensor as given in Equation (3.15) in section 3.1.3. The magnetic forces are used as the excitation for the structural simulation of the stator core of the motor. The elastic model is shown in section 3.2.1. In the final step, the acoustic BEM model explained in section 3.3.3 is employed for acoustic pressure calculations.

The simulations were done in the COMSOL multiphysics software. The specifications of the solid-rotor induction motor are given in Table 3.2 in section 3.24. From the finite-element-based electromagnetic analysis, the magnetic forces of electromagnetic origin are taken into the structural mechanics domain to compute the deformation and vibrations. The supply frequency was 1008 Hz

and three time periods were simulated in the electromagnetic 2D computation. There were 19750 linear triangular elements in the 2D mesh as shown in Fig. 4.33(a) and the structural 3D mesh of the stator had 104931 tetrahedral elements, given in Fig. 4.33(b). In the structural simulation, the deformation of the stator core is calculated as shown in Fig. 4.34.

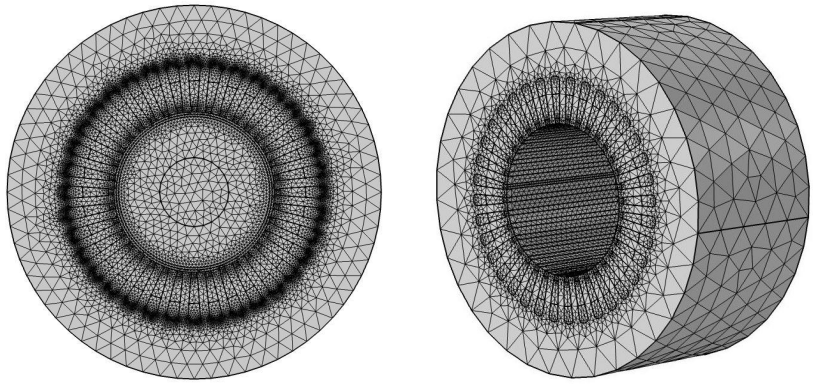

Figure 4.33. The finite element mesh. (a) 2D triangular mesh of rotor and stator, (b) 3D tetrahedral mesh of the stator

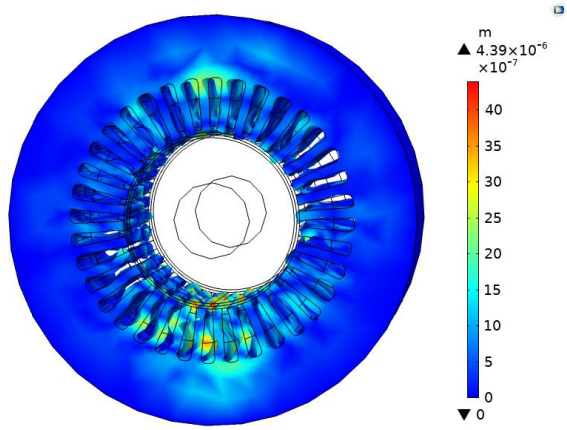

Figure 4.34. Deformation of the stator due to magnetic forces. Displacement scale factor: 5000

In the acoustic simulation, the accelerations computed in the FE structural mechanics domain are taken as the boundary condition in the FEM-BEM interface, where it is imposed at the stator outer boundaries, and thereby couples the acoustics with structural analysis to create an acoustic-structure interface. For the acoustics computations, the air surrounding the motor is modeled as an in-

finite void. The BEM simulation computes the acoustic pressure in the surrounding air of the motor due to the stator vibrations and the consequential sound pressure level corresponding to different frequencies. The acoustic pressure distribution outside the motor at 2016 Hz frequency is shown in Fig. 4.35. The sound-pressure level produced by this acoustic pressure difference in the air is given in Fig. 4.36. The same parameters for 4032 Hz are portrayed in Fig. 4.37. The sound-pressure level at the far field in different planes is given in Fig. 4.38. The far-fields plots of the sound pressure level offer an indication about the directivity of the noise radiation in different planes around the motor at a specific frequency.

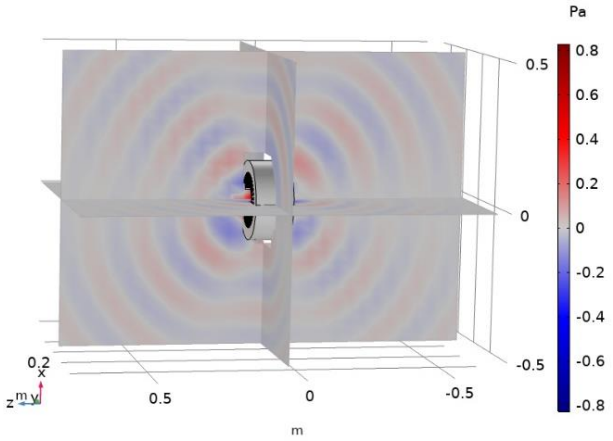

Figure 4.35. Acoustic pressure distribution in Pa outside the motor at a frequency of 2016 Hz

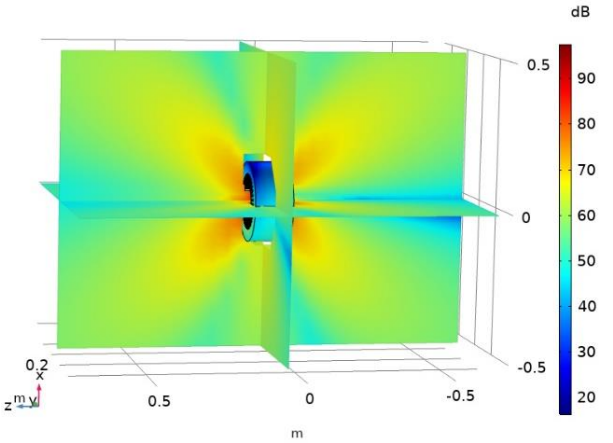

Figure 4.36. Sound pressure level in dB outside the motor at a frequency of 2016 Hz

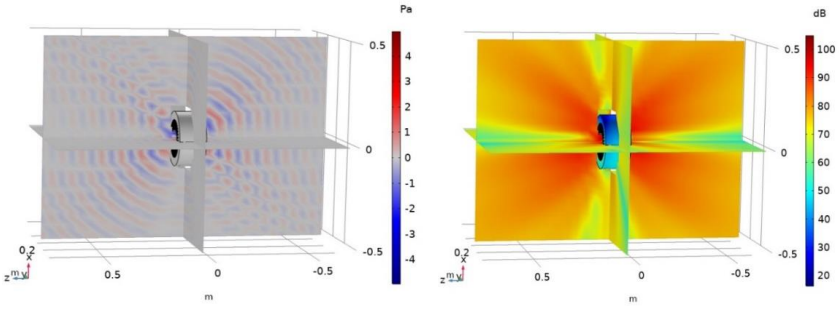

Figure 4.37. Left: Acoustic pressure distribution in Pa outside the motor at 4032 Hz, (b) Sound pressure level in dB outside the motor at 4032 Hz

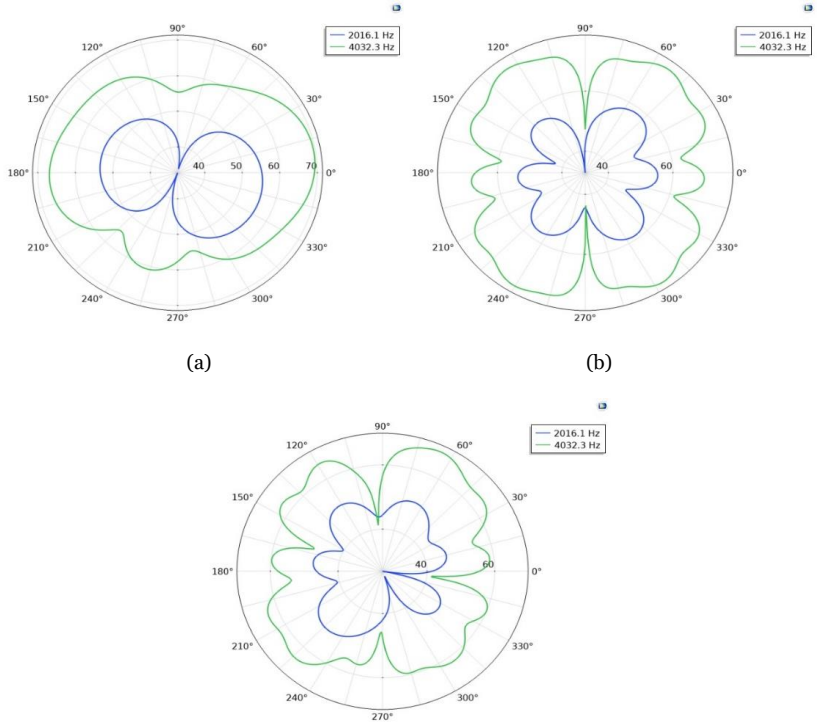

Figure 4.38. Far-field sound pressure level in dB at a distance of 1 m around the motor in the (a) xy-plane, (b) xz-plane and (c) yz-plane

The results of the combined electromagnetic, structural and acoustic simulation show that how the magnetic forces produce acoustic sound in an electrical motor. This multi-level method conjoining two numerical methods and three different physics into a single finite-element tool is an efficacious scheme for acoustic analysis of electrical motors. The future part of this study is to conduct laboratory experiments to measure the sound levels. Besides, to compare the

measurement results with the numerical simulations, the whole structure of the motor with the frame and bearings needs to be modeled in the forthcoming stages.

5. Discussion and Conclusions

This thesis focuses on the electromagnetic, magnetomechanical and vibro-acoustic computations of electrical machines. In this chapter, the developed methods, results and findings are discussed and summarized. The scope of continuation of the work done during this thesis, as well as suggestions for future research, are presented and, finally, the thesis is concluded.

5.1 Discussion of the Methods and Results

5.1.1 Summary of the Findings

Magnetic Force Computations

The computation of magnetic forces is a key factor in most of the stages of this thesis. The magnetic force calculation using the Virtual work principle is an efficient method that facilitates the analysis of local forces or nodal forces. Compared to other methods like the Maxwell stress-tensor method, which computes the total forces, the knowledge of nodal forces is an imperative factor in vibration studies. Besides, the Generalized Nodal Forces can be used for calculating deformation and the analysis of frequency components in vibrations of electrical motors using a direct magneto-elastic coupling. This method has proven to be accurate by comparative studies with measurements and other magnetomechanical coupling methods. The implementation of Generalised Nodal Forces computation in an open-source tool, which was done as part of this thesis facilitates the cost-effective study of magnetomechanical properties of different kinds of materials and electrical devices. The GNF computation is employed in an induction motor for computing the nodal forces and the stator vibrations, and in the stress analysis of end-windings in a high-voltage induction motor.

From the stress distribution pattern in the winding, one can compare the magnitudes of the maximum stress with the yield stress of copper, insulations and supporting materials. This data are decisive in the mechanical design including insulation and supporting rings. Besides, the amplitude of vibrations is vital in the design of the retaining structure.

The degenerated air-gap element method for magnetic force computation is another important and original outcome of this thesis. This is an accurate and effective technique for computing magnetic forces, where thin air gaps are presented in bodies in contact. The comparative study of results with the force measurements and the *eggshell* method, and the convergence results show the consistency of the degenerated air-gap method. Some of the applications of this method are in permanent magnet motors, where magnets are glued in the iron core in the motor and in linear synchronous motors with Halbach arrayed magnets. Moreover, the degenerated air-gap element method significantly decreases the finite element computational load of heavy meshing and expensive simulations. In situations where accurate magnetic force computations are crucial, this method is a brilliant option, as it eliminates the need for intricate meshing at the contacts of complex structures and the forces can be computed in any part or boundaries of machines or devices.

Magnetomechanical Coupling

The effect of electromagnetic phenomena such as magnetic forces and magnetostriction on the mechanical properties of ferromagnetic materials, and thereby the deformation and vibrations of electrical motors, are studied using magnetomechanical coupling methods. Different simulations and measurement based studies that are done for this thesis using the energy-based magnetomechanical material model developed by extensive experiments and mathematical modeling by different researchers prove that, it is an efficient and accurate tool for studying the interaction between electromagnetic and magnetomechanical domains in an electrical machine. The magnetostriction is included in the coupling model and the studies on induction motors showed that the interaction of magnetic forces and magnetostriction affects the amplitude of mechanical deformations and hence the vibrations. An original experiment was done to measure the mechanical deformation in an iron sheet due to magnetic forces and magnetostriction. The strain measurements were compared with the

simulation results and separated the effects of magnetic forces and magnetostriction on the deformation of the iron specimen. The interactive effects of the magnetic forces and magnetostriction depend significantly on the structure of the material and the method of excitation. In stationary devices like transformers, the noise due to vibration is caused mainly by magnetostriction, which is an intrinsic property of iron, whereas in rotating electrical machines like electrical motors, the presence of air-gaps produces magnetic forces that chiefly contribute to stator vibrations.

Vibrations in Electrical Motors

In the vibration studies, the electromagnetic causes were the major point of interest in this thesis, even though there are mechanical and aerodynamic factors that affect the vibration and noise in an electrical machine. A simple magneto-elastic coupling method by using nodal magnetic forces as input to an elasticity calculation solver in an open-source finite element software tool that was carried out specifically for this thesis was proven to be an economic yet effective method for computing deformations and studying the frequency components in the vibration spectra of an induction motor. The same vibration measurements were used in another study using energy-based magnetomechanical coupling to include magnetostriction. The inclusion of magnetostriction did not affect the frequencies present in the vibrations, while there was a difference in the amplitude of the deformations. The results from the numerical studies using the magnetomechanical coupled models show that, in different kinds of machines, the effect of magnetic forces and magnetostriction can be different, because they can either strengthen or counteract each other and thereby change the nature of deformation and vibrations. The influence of pole numbers in an induction motor is analyzed in one of the studies in this thesis, and studies need to be done for other types of machines to comprehend the effect of magnetic forces and magnetostriction in different kinds of motors. An investigation of vibrations of a high-speed induction motor using the energy-based magnetomechanical model is another important contribution as part of this thesis. An extensive study with the aid of measurements and numerical simulations in a high-speed solid rotor motor for industrial applications is an innovative element of this study. From the measurement and simulation results, it has been discovered that the faults in electrical motors such as rotor eccentricity can significantly

contribute to the origination of vibrations and acoustic noise. The stress dependency of magnetostriction is included in the magnetomechanical model and hence this study also takes into account the effect of stress in high-speed motors, which facilitates more accurate computation of deformations and vibrations.

Vibro-acoustics and Noise

In the final part of the thesis, the acoustic noise in electrical machines due to vibrations is studied. The Boundary Element Method is used for noise computations, which is an efficient and cost-effective numerical tool in acoustic studies. The sound level generated by an induction motor due to electromagnetic forces is modeled successfully using a joint FEM-BEM based numerical computational technique. The energy conversion process in an electrical motor is illustrated by presenting how the electrical energy is converted into acoustic energy. The proposed method explains how the electromagnetic, mechanical and acoustic domains can be examined and coupled in a simulation tool, formulated originally for the presented study. This tool delivers a convenient and useful means for researchers to conduct magnetomechanical and vibro-acoustic studies.

5.1.2 Significance of the Work

This thesis focuses on the computational aspects and experimental studies on three different multiphysical or, in other words, coupled entities. The first part is the electromagnetics in electrical machines that includes mainly the electromagnetic forces in machines. The development of numerical computational methods for magnetic forces based on the Virtual work principle is a substantial feature in the technology of electrical machines. The accurate computation of magnetic forces is an essential part of machine design and analysis. The proposed Generalised Nodal Forces method facilitates the calculation of deformation and vibrations in electrical machines by magneto-elastic coupling methods. The degenerated air-gap element method for magnetic force computation in bodies in contact is another significant outcome of this thesis. This method can be applied in wide areas of electrical machines and devices where accurate force computation is required. Moreover, the implementation of these numerical methods in open-source software is a remarkable development. This enables

the use of the developed methods for further studies and improvement of the models in a cost-effective way.

The second part is the magnetomechanical computations where the magnetic forces and magnetostriction are coupled to the mechanical domain to study how these phenomena affect the mechanical properties of ferromagnetic materials and electrical machines. The energy-based magnetomechanical coupling, developed by Fonteyn, Rasilo, Deepak, Aydin and Belahcen (2010-2018) is an imperative tool in the vibration studies of this thesis. This model is proficiently used in this thesis and proved to be an accurate method for vibration analysis. The application of a well-studied and proven magnetomechanical coupling method in electrical motor vibration studies is a unique characteristic of this thesis. The interaction of magnetic forces and magnetostriction and the effect of this phenomenon on mechanical deformation are vital outcomes of the studies conducted for this thesis. This interactive effect can significantly affect the magnetomechanical properties of electrical machines such as vibrations and acoustic noise. Besides, this is a crucial factor, which needs to be considered during the design phase of electrical machines and devices. This is because the lack of magnetostriction and the interaction of the same with magnetic forces could result in inaccurate calculation of design parameters of parts of the machines and supporting structures.

In the end, the vibro-acoustic analysis concluded the flow of energy through the magnetic, mechanical and acoustic trail in an electrical machine system to the final product, which is the acoustic noise. The knowledge of vibrations and frequency spectra from the magnetomechanical studies can be used in the noise analysis by means of the Boundary Element Method.

5.2 Suggestions for Future Work

There are some potential topics that can be further investigated related to the subjects studied in this thesis. Some suggestions for future work are summarized as follows:

Local Magnetic Force Measurement

The computation of nodal magnetic forces is one of the key factors in this thesis. The magnetic force measurements were done in a permanent magnet set-up and

the results were compared with simulations. However, the measurement of local magnetic forces is a potential experiment that can be done as a continuation of these studies. The conducted experiment measured the total magnetic force and the comparison of the measurement values with the total simulated forces was successful. If we can obtain the nodal or local forces from a measurement, it can establish the accuracy of the nodal force calculations. More complex experimental methods like electron microscopy would be needed for such a measurement system.

Segregating Magnetic Forces and Magnetostriction in Motors

The effect of magnetic forces and magnetostriction on the mechanical deformation of iron sheets was studied in an experiment as part of this thesis. In practical applications such as electrical motors, these two phenomena can have a substantial effect on the mechanical properties and overall performance of the machine. The measurement and segregation of the deformation caused by magnetic forces and magnetostriction in an electrical motor is a potential topic for laboratory experiment that would shed light on the correctness of the application of the developed magnetomechanical models in motor vibration studies. The measurement of deformations or strains in active parts of a motor while the motor is running is rather a difficult task. The placement of strain gauges and other measurement devices is challenging in such an experiment set up. The mode of operation of the motor and placement of rotor and stator need to be calibrated to facilitate accurate measurements without compromising the real-time operating conditions of the motor.

Digital Vibro-acoustic Measurement Applications

The measurements of vibrations were conducted for two different types of induction motors in this thesis. Accelerometers were used for the measurement of vibrations. With the advancement in digital platforms such as mobile phone applications, it is possible to develop applications to measure the nature of vibrations and acoustic noise from a motor and analyze the frequency components in the spectra. These kinds of digital devices and applications enable fast and frequent diagnosis and condition-monitoring of electrical motors in an economic

way, without setting up complex laboratory measurement systems. The proposed magnetomechanical and vibro-acoustic computational models can be used in these applications with the help of advanced software programming.

Fault Prediction from Noise

As a continuation of the above mentioned vibro-acoustic measurement applications, devices and applications for fault prediction and detection in electrical motors are another potential topic having wide scope in condition-monitoring. A study on the vibrations of a high-speed induction motor revealed that, rotor eccentricity is a major cause of vibration in the investigated motor. The theoretical analysis of this fault agrees with the simulation and measurement results. If the tools used for the study can be implemented in a digital platform, it would facilitate fault detections from noise recording.

5.3 Conclusions

The modeling and study of magnetic, mechanical and acoustic domains in an electrical motor are imperative in the design and analysis of machine systems. Decades of research and studies by scientists and engineers have developed efficient tools for optimizing the performance of electrical machine systems in terms of their electromagnetic and magnetomechanical behavior. The excitation of a machine by applying electrical power, the journey of the power, and the conversion of energy from electrical energy to acoustic pressure includes different physical phenomena. This thesis has succeeded in addressing these domains of energy conversions and their effects in electrical machines by developing reliable and efficient computational tools and experimental methods. The research conducted for this thesis resulted in the formulation and implementation of successful numerical and experimental tools for the computation and analysis of magnetic forces, magnetostriction, vibrations and acoustic noise in an intuitive manner, and largely using open-source platforms.

References

Alger, P.L., 1954, 'The magnetic noise of polyphase induction motors [includes discussion', *Trans. of the American Institute of Electrical Engineers. Part III: Power Apparatus and Systems,* vol. 73, Issue: 2, pp. 118-125.

Arkkio, A. 1987, 'Analysis of induction motors based on the numerical solution of the magnetic field and circuit equations', *Doctoral thesis*, Acta Polytechnica Scandinavia, Electrical Engineering Series No. 59, 97 p.

Arkkio, A. 1995, 'Unbalanced magnetic pull in a four-pole induction motor with an odd number of rotor slots', *Proceedings of CICEM'95*, Hangzhou, 31 Aug. - 2 Sept. 1995, China, pp. 343–348.

Aydin, U., Rasilo, P., Martin, F., Singh, D., Daniel, L., Belahcen, A., Kouhia, R., Arkkio, A., 2017, 'Modeling the Effect of Multiaxial Stress on Magnetic Hysteresis of Electrical Steel Sheets: A Comparison', *IEEE Trans. Magn.* 53, pp. 1–4.

Aydin, U., Rasilo, P., Singh, D., Lehikoinen, A., Belahcen, A., Arkkio, A., 2016, 'Coupled Magneto-Mechanical Analysis of Iron Sheets Under Biaxial Stress' *IEEE Trans. Magn.* 52, 1–4.

Badics, Z., Komatsu, H., Matsumoto, Y., Aoki, K., Nakayasu, F., Miya, K., 1994, 'A Thin Sheet Finite Element Crack Model in Eddy Current NDE', *IEEE Trans. Magn.* 30, pp. 3080–3083.

Barkhausen H., Woschni E. G., 1960, 'Lehrbuch der elektronenröhren und ihrer technischen anwendungen'*, Gebundenes Buch*. Publisher: Hirzel; Edition: 9th.

Belahcen, A., Arkkio, A., Klinge, P., Linjama, J., Voutilainen, V., Westerlund, J. 1999, 'Radial forces calculation in a synchronous generator for noise analysis', *Proceedings of CICEM'99*, Xi'an, China, 29-31 August 1999, pp. 119–122.

Belahcen, A., 2006a, 'Effect of stress-dependent magnetostriction on vibrations of an induction motor', *Recent Developments of Electrical Drives. Springer, Dordrecht.* pp. 201-210.

Belahcen, A., 2006b, 'Vibrations of rotating electrical machines due to magnetomechanical coupling and magnetostriction', *IEEE Trans. Magn.* 42, pp. 971–974.

Belahcen, A., 2004, 'Magnetoelasticity, magnetic forces and magnetostriction in electrical machines', *Doctoral thesis*, Helsinki University of Technology, Lab. of Electromechanics, report. 72.

Belahcen, A., 2005, 'Magnetoelastic Coupling in Rotating Electrical Machines', *IEEE Tran. Mag*., Vol. 41, No. 5, pp. 1624–1627.

Belahcen, A., 2001, 'Review of the methods for local forces calculation in electrical apparatus', *Proceedings of Xth International Symposium on Electromagnetic Fields*, 20-22 September 2001, Cracow, Poland, pp. 339–342.

Belmans, R.J.M., D'Hondt, L., Vandenput. A., and Geysen, W., 1987, 'Analysis of the audible noise of three phase squirrel cage induction motors supplied by inverters', *IEEE trans. ind. app*., vol. 23, pp. 842-947.

Belmans, R. J. M., Verdyck, D., Geysen, W., and Findlay, R. D., 1991, 'Electromechanical analysis of the audible noise of an inverter-fed squirrel-cage induction motor', *IEEE Trans. Ind. Applicat*., vol. 27, pp. 539–544.

Benbouzid, M.E.H., Reyne, G., Dérou, S., Foggia, A., 1993. 'Finite element modeling of a synchronous machine: electromagnetic forces and mode shapes', *IEEE Trans. Magn*. vol. 29, pp. 2014–2018.

Besbes, M., Ren, Z., Razek, A. 1996, 'Finite element analysis of magneto-mechanical coupled phenomena in magnetostrictive materials', *IEEE Transaction on Magnetics*, Vol. 32, No. 3, May 1996, pp. 1058–1061.

Besnerais, J. Le, Lanfranchi, V., Hecquet, M., Brochet, P., Friedrich, G., 2008, 'Acoustic noise of electromagnetic origin in a fractional-slot induction machine', *COMPEL - Int. J. Comput. Math. Electr. Electron. Eng*. 27, pp. 1033–1052.

Besnerais, J. Le, Lanfranchi, V., Hecquet, M., Brochet, P., 2010, 'Characterization and reduction of audible magnetic noise due to PWM supply in induction machines', *IEEE Trans. Ind. Electron*. 57, pp. 1288–1295.

Birrs, R., 'Magnetomechanical effects in the Rayleigh region', 1971, *IEEE Trans. Magn.* 7(1), pp. 113 – 133.

Bloch, F., 1932, 'Zur theorie des austauschproblems und der remanenzerscheinung der ferromagnetika', Zeit. Physik 74, pp. 295–335.

Bossavit, A., 1992, 'Edge-element computation of the force field in deformable bodies' *IEEE Trans. Magn*. 28, pp. 1263–1266.

Boughanmi, W., Henrotte F., Benabou, A., Le Menach, Y., 2016, 'Finite element implementation and experimental validation of 2-D/3-D magnetic force formulas', *IEEE Trans. Magn*., vol. 52, no. 3, article 7402604.

Bozorth, R. M. , 1951, Ferromagnetism, Van Nostrand.

Bozorth, R. M. and Williams, H. J. (1945), 'Effect of small stresses on magnetic properties', *Rev. Mod. Phys*. 17(1), pp. 72–80.

Brauer, J.R., 1976, 'Magnetic noise of induction motors', *IEEE trans. Power Apparatus and Systems*, vol. 95, issue 1, pp. 66-75.

Brown, W. F. , 1949, 'Irreversible magnetic effects of stress', *Phys. Rev*. 75(1), pp. 147–154.

Cameron, D. E., Lang, J. H., and Umans, S. D., 1992, 'The origin and reduction of acoustic noise in doubly salient variable reluctance motors', *IEEE Trans. Ind. Applications*, vol. 28, pp. 1250–1255.

Carpenter, C. J., 1959, 'Surface-Integral Methods of Calculating Forces on Magnetized Iron Parts', *The Institution of Electrical Engineers Monograph*, No. 342, pp. 19–28.

Cho, D.-H., Kim, K.J., 1998, 'Modelling of electromagnetic excitation forces of small induction motor for vibration and noise analysis', *IEE Proc. - Electr. Power Appl.* vol. 145, no. 199.

Coulomb, J.L., 1983, 'A methodology for the determination of global electromechanical quantities from a finite element analysis and its application to the evaluation of magnetic forces, torques and stiffness', *IEEE Trans. Magn.* 19, pp. 2514–2519.

Coulomb, J. L., and Meunier, G., 1984 , 'Finite element implementation of virtual work principle for magnetic or electric force and torque computation', *IEEE Trans. Magn.*, vol. 20, no. 5, pp. 1894–1896.

Craik, D. J. and Wood, M. J., 1970, 'Magnetization changes induced by stress in a constant applied field', J. Phys. D App. Phys. 3(7), pp. 1009–1016.

Daniel, L. , Hubert, O., Buiron, N., and Billardon, R., 2008 , 'Reversible magnetoelastic behavior: A multiscale approach', *J. Mech. Phys. Solids*, vol. 56, no. 3, pp. 1018–1042.

Daniel, L. , Rekik, M., and Hubert, O., 2014, 'A multiscale model for magnetoelastic behavior including hysteresis effects', *Arch. Appl. Mech.*, vol. 84, nos. 9–11, pp. 1307–1323.

Dapino, M.J., Smith, R.C., Faidley, L.E., Flatau, A.B., 2000, 'Coupled structural-magnetic strain and stress model for magnetostrictive transducers', *J. Intell. Mater. Syst. Struct.* 11, pp. 135–152.

Delaere, K., Heylen, W., Belmans, R., and Hameyer, K.,2000, 'Finite element analysis of electrical machine vibrations caused by Lorentz, Maxwell and magnetostriction forces', *IEE Seminar on Current Trends in the Use of Finite Elements (FE) in Electromechanical Design and Analysis (Ref. No. 2000/013)*, pp. 9/1-9/4.

Delaere, K., 2002, 'Computation and experimental analysis of electrical machine vibrations caused by magnetic forces and magnetostriction', *doctoral thesis*, Publication of the Katholiek Universiteit Leuven, 223 p.

Delaere, K., Belmans, R., Hameyer, K., Heylen, W., Sas, P., 1999, 'Coupling of magnetic analysis and vibrational modal analysis using local forces', *Xth International Symposium on Theoretical Electrical Engineering ISTET'99*, Magdeburg, Germany, 6-9 September 1999, pp. 417–422.

Delaere, K., Belmans, R., Hameyer, K., 2003, 'Influence of rotor slot wedges on stator currents and stator vibration spectrum of induction machines: A transient finite-element analysis', *IEEE Trans. Magn.* vol. 39, pp. 1492–1494.

Delaere, K., Heylen, W., Hameyer, K., Belmans, R., 2000, 'Local magnetostriction forces for finite element analysis', *IEEE Trans. Magn.* 36, pp. 3115–3118.

Delaere, K., Heylen, W., Belmans, R., Hameyer, K., 2002, 'Comparison of induction machine stator vibration spectra induced by reluctance forces and magnetostriction', *IEEE Trans. Magn.*, Vol. 38, No. 2, pp. 969-972.

Dorrell, D. G. , 1995, 'The influence of rotor skew on unbalanced magnetic pull in cage induction motors with eccentric rotors', *Proc. 7th Int. Conf. Elect. Mach. Drives*, pp. 67–71.

Dorrell, D. G., 1996, 'Calculation of unbalanced magnetic pull in small cage induction motors with skewed rotors and dynamic rotor eccentricity', *IEEE Trans. Energy Convers.*, vol. 11, no. 3, pp. 483–488.

Dorrell, D.G., Thomson, W.T., Roach, S., 1997, 'Analysis of airgap flux, current, and vibration signals as a function of the combination of static and dynamic airgap eccentricity in 3-phase induction motors', *IEEE Trans. Ind. Appl.*, vol. 33, no. 1, pp. 24–34.

Dorrell, D.G., Hsieh, M.F., Guo, Y., 2009, 'Unbalanced magnet pull in large brushless rare-earth permanent magnet motors with rotor eccentricity', *IEEE Trans. Magn.,* vol. 45, pp. 4586–4589. doi:10.1109/TMAG.2009.2022338.

Elmer – *Open source finite element software for multiphysical problems.* [Online]. Available: https://www.csc.fi/web/elmer

Ellison A. J., and Moore, C.J., 1968, 'Acoustic noise and vibration of rotating electric machines', Proc. IEE, vol. 111, issue.11, pp. 1633-1640

Ellison, A. J., Moore, C. J., and Yang, S. J. , 1969, 'Methods of measurement of acoustic noise radiated by an electric machine', *Proc. lEE*, vol. 116, pp. 1419-1431.

Erdelyi, E., 1955, 'Predetermination of Sound Pressure Levels of Magnetic Noise of Polyphase Induction Motors', *Trans. Am. Inst. Electr. Eng. Part III Power Appar. Syst.* 74, pp. 1269–1280.

Fakam, M., Verbeke, D ., Hecquet, H. et al., 2011, 'Electromagnetic noise comparison between ' spm ' and ' ipm ' concentrated winding synchronous machine', *ISEF 2011-XV Int. Symp. Electromagn. Fields Mechatronics, Electrical Electron. Eng.*

Fang, D.N., Feng, X., Hwang, K.C., 2004. 'Study of magnetomechanical non-linear deformation of ferromagnetic materials: Theory and experiment', *Proc. Inst. Mech. Eng. Part C J. Mech. Eng. Sci.* 218, pp. 1405–1410.

Fonteyn, K., Belahcen, A., Kouhia, R., Rasilo, P., Arkkio, A., 2010a. 'FEM for directly coupled magneto-mechanical phenomena in electrical machines', *IEEE Trans. Magn.* 46, pp. 2923–2926.

Fonteyn, K. A., 2010b, 'Energy-based magneto-mechanical model for electrical steel sheets', Doctoral thesis, Aalto University, Espoo/Finland.

Fonteyn, K.A., Belahcen, A., Rasilo, P., Kouhia, R., Arkkio, A., 2012, 'Contribution of maxwell stress in air on the deformations of induction machines', *J. Electr. Eng. Technol.* vol. 7, pp. 336–341.

Girgis, R.S., Vermas, S.P., 1981, 'Method for accurate determination of resonant frequencies and vibration behavior of stators of electrical machines', *IEE Proc. B*

Electr. Power Appl. vol. 128, no. 1.

Gros, L., Reyne, G., Body, C., Meunier, G., 1998, 'Strong coupling magneto mechanical methods applied to model heavy magnetostrictive actuators', *IEEE Trans. Magn.*, Vol. 34, No. 5, pp. 3150-3153.

Guerin, C., Tanneau, G., Meunier, G., Brunotte, X., Albertini, J.-B., 1994, 'Three dimensional magnetostatic finite elements for gaps and iron shells using magnetic scalar potentials', *IEEE Trans. Magn.* 30, pp. 2885–2888.

Hameyer, K., Henrotte, F., Katholieke, D., 2003, 'Electromagnetically excited audible noise in electrical machines', *J. KSNVE* 13, pp. 109–118.

Hamzaoui, N., Boisson, C., and Lesueur, C. , 1998a, 'Vibro-acoustic analysis and identification of defects in rotating machinery, Part I: Theoretical model', *Journal of Sound and Vibration*, 216(4), pp. 553-570, article no. sv951713.

Hamzaoui, N., Boisson, C., and Lesueur, C. , 1998b, 'Vibro-acoustic analysis and identification of defects in rotating machinery, Part II: Experimental study', *Journal of Sound and Vibration*, 216(4), pp. 571-583, article no. sv951714.

Han, X. , Palazzolo, A. , 2016, 'Unstable force analysis for induction motor eccentricity', *Journal of Sound and Vibration,* vol. 370, pp. 230-258.

Henriquez, V.C., and Juhl, P.M., 2010, 'OpenBEM – An open source boundary element method software in acoustics', *Proc. of internoise 2010, noise and sustainability*, pp 1-10.

Henrotte, F., Deliége, G., Hameyer, K., 2004, 'The eggshell approach for the computation of electromagnetic forces in 2D and 3D', *COMPEL - Int. J. Comput. Math. Electr. Electron. Eng.* 23, pp. 996–1005.

Herrin, D.W. & Martinus, F. & Wu, T.W. & Seybert, A.F., 2006, 'An Assessment of the High Frequency Boundary Element and Rayleigh Integral Approximations', *Applied Acoustics*, 67(8), pp.819-833.

Hubert, O. and Daniel, L., 2011, 'Energetical and multiscale approaches for the definition of an equivalent stress for magneto-elastic couplings', *J. Magn. Magn. Mater.*, vol. 323, no. 13, pp. 1766–1781.

Hu, H., Zhao, J., Liu, X., Guo, Y., 2016, 'Magnetic Field and Force Calculation in Linear Permanent-Magnet Synchronous Machines Accounting for Longitudinal End Effect', *IEEE Trans. Ind. Electron.* vol. 63, pp. 7632–7643.

IEC 60027-1 1992, 'Letter symbols to be used in electrical technology', Corrected and reprinted 1995-03-31, - Part 1: General, 111 p.

IEC 61672-1 'Electroacoustics, Sound level meters - Part 1: Specifications', pp.5.

Imhoff, J.F , Meunier, G., Reyne, G., Foggia. A., Sabonnadiere, J.C., 'Spectral analysis of eletcromagnetic vibrations in D.C: machines using the finite element method', 1989, *IEEE Trans. Magnetics*, vol. 25, pp. 3590-3592.

Ishibashi, F., Noda, S., and Mochizuki, M., 1998, 'Numerical simulation of electromagnetic vibration of small induction motor', IEE Proc. Electr. Power Appl., Vol. 145, No. 6, pp. 528–534.

Islam, R., Husain, I., 2010, 'Analytical model for predicting noise and vibration in permanent-magnet synchronous motors', *IEEE Trans. Ind. Appl.* 46, pp. 2346–

2354.

Jang, G.H. and Lieu, D.K., 1991, 'The effect of magnetic geometry on electric motor vibration', *IEEE Trans. Magn.*, Vol. 27, No. 6, pp. 5202–5204.

Jover Rodríguez, P.V., Belahcen, A., Arkkio, A., Laiho, A., Antonino-Daviu, J.A., 2008, 'Air-gap force distribution and vibration pattern of Induction motors under dynamic eccentricity', *Electr. Eng.* 90, pp. 209–218.

Joule, J.P., 1847, 'On the effects of magnetism upon the dimensions of iron and steel bars', *Philosophical Magazine*, Vol. 30, pp. 76.

Juhl, P.M., 1993, 'The boundary element method for sound field calculations', PhD Thesis, report 55, The acoustic laboratory, Technical university of Denmark.

Kameari, A., 1993, 'Local force calculation in 3D FEM with edge elements', *Int. J. Appl. Electromagn. Mater.* 3, pp. 231–240.

Kittel, C., 1949, 'Physical theory of ferromagnetic domains', *Reviews of Modern Physics*, Vol. 21, No. 4, pp. 541-583.

Krebs, G., Clénet, S., Abakar, A., Locment, F., Piriou, F., 2009, 'Method to connect non-conforming mesh in 3-D with the overlapping method', *IEEE Trans. Magn.* 45, pp. 1420–1423.

Krebs, G., Clénet, S., Tsukerman, I., 2010, 'Overlapping finite elements for arbitrary surfaces in 3-D', *IEEE Trans. Magn.* 46, pp. 3473–3476.

Krebs, G., Henneron, T., Clénet, S., Le Bihan, Y., 2011, 'Overlapping finite elements used to connect non-conforming meshes in 3-D with a vector potential formulation', *IEEE Trans. Magn.* 47, pp. 1218–1221.

Lai, H.C., Rodger, D., Coles, P.C., 2004, 'A 3-D overlapping finite-element scheme for modeling movement', *IEEE Trans. Magn.* 40, pp. 533–536.

Landau, L., Lifshitz, E., 1935, 'On the theory of the dispersion of magnetic permeability in ferromagnetic bodies', *Physikalische Zeitschrift der Sowjetunion,* vol. 8, pp. 153-169.

Låftman, L., 1995, 'Magnetostriction and its contribution to noise in a PWM inverter fed induction machine', Journal *de Physique IV (Proceedings)* 08(PR2), DOI: 10.1051/jp4:19982130.

Låftman, L., 1995, 'The contribution to noise from magnetostriction and PWM inverter in an induction machine', *Doctoral thesis*, IEA Lund Institute of Technology, Sweden, 94 p.

Lee, E. W., 1955, 'Magnetostriction and magnetomechanical effects', *Rep. Prog. Phys.* 18, pp. 185–229.

Lehikoinen A., Davidsson, T., Arkkio , A., and Belahcen, A., 2018, 'A high-performance open-source finite element analysis library for magnetics in MATLAB', *Proceedings of the IEEE XIII International Conference on Electrical Machines (ICEM)*, pp. 486-492.

Linnemann, K., Klinkel, S., Wagner, W., 2009, 'A constitutive model for magnetostrictive and piezoelectric materials', *Int. J. Solids Struct.* 46, pp. 1149–1166.

Liu, X., Zheng, X., 2005, 'Nonlinear constitutive model for magnetostrictive materials', *Acta Mech. Sin. Xuebao* 21, pp. 278–285

Melcher, J. R. 1981, 'Continuum Electromechanics', MIT Press, Cambridge, MA, 640 p.

Mohammed, O.A., Calvert, T., and McConnell, R., 1999, 'A model for magnetostriction in coupled nonlinear finite element magneto-elastic problems in electrical machines', *Proceedings of the International Conference on Electric Machines and Drives*, pp. 728–735.

Mohammed, O.A., Calvert, T., McConnell, R., 2001, 'Coupled magneto-elastic finite element formulation including anisotropic reluctivity tensor and magnetostriction effects for machinery applications', *IEEE Trans. Magn.*, Vol. 37, No. 5, pp. 3388-3391.

Mohammed, O.A., Calvert, T. E., and McConnell, R., 2002, 'Transient modeling of coupled magnetoelastic problems in electric machines', *Proceedings of the Power Engineering Society Summer Meeting*, 21-25 July 2002, vol. 1, pp. 281–287.

Muller, W., 1990, 'Comparison of different methods of force calculation', *IEEE Trans. Magnetics*, vol. 26, no. 2, pp. 1058-1061.

Nguyen, D.M., Bahri, I., Krebs, G., Berthelot, E., Marchand, C., 2019, 'Vibration study of the intermittent control for a switched reluctance machine', *Math. Comput. Simul.,* vol. 158, pp. 308–325.

Pöyhönen, S., Negrea, M., Jover, P., Arkkio, A., Hyötyniemi, H., 2003, 'Numerical magnetic field analysis and signal processing for fault diagnostic of electrical machines', *COMPEL Int. J. Comput. Math. Elect. Eng.* 22(4), pp. 969–981.

Rasilo P. et al., 2016, 'Modeling of hysteresis losses in ferromagnetic laminations under mechanical stress', *IEEE Trans. Magn.*, vol. 52, no. 3, Art. no. 7300204.

Ren, Z., and Razek, A., 1990, 'A coupled electromagnetic-mechanical model for thin conductive plate deformation analysis', *IEEE Trans. Mag.*, vol. 26, issue 5, pp. 1650-1652.

Ren, Z., 1998, 'Degenerated Whitney Prism Elements - General Nodal and Edge Shell Elements', *IEEE Trans. Magn.*, vol. 34, no. 5, pp. 2547-2550.

Ren, Z., Razek, A., 1992, 'Local Force Computation in Deformable Bodies using Edge Elements', *IEEE Trans. Magn.* 28, pp. 1212–1215.

Ren, Z., 1994, 'Comparison of different force calculation methods in 3-D finite element modelling', *IEEE Trans. Magn.*, Vol. 30, No. 5, pp. 3471-3474.

Ren, Z., Ionescu, B., Razek, A., 1995, 'Calculation of mechanical deformation of magnetic materials in electromagnetic devices', *IEEE Trans. Magn.*, Vol. 31, No. 3, pp. 1873-1876.

Reyne, G., Sabonnadière, J.C., Imhoff, J.F., 1988a, 'Finite element modelling of electromagnetic force densities in DC machines', *IEEE Trans. Magn.*, Vol. 24, No. 6, pp. 3171-3173.

Reyne, G., Meunier, G., Imhoff, J.F., Euxibie, E., 1988b, 'Magnetic forces and mechanical behavior of ferromagnetic materials - presentation and results on the theoretical, experimental and numerical approaches', *IEEE Trans. Magn.*, Vol. 25, No. 1, pp. 234-237.

Reyne, G., Sabonnadière, J.C., Coulomb, J.L., Brissoneau, P., 1987, 'A Survey of the main aspects of magnetic forces and mechanical behavior of ferromagnetic materials under magnetization', *IEEE Trans. Magn.*, Vol. MAG-23, No. 5, pp. 3765-3767.

Rodger, D., Atkinson, N., 1987, '3D eddy currents in mutliply connected thin sheet conductors', *IEEE Trans. Magn.* 23, pp. 3047–3049.

Rodger, D., Atkinson. N., and Leonard p.J., 1988, 'Transient 3D eddy currents in thin sheet conductors', *IEEE Trans Mag,* Vol 24, No 6, pp. 2691-93.

Rodríguez, P. V. J., Belahcen, A., Arkkio, A. Laiho, A., and Antonino-Daviu, J. A., 2007, 'Air-gap force distribution and vibration pattern of Induction motors under dynamic eccentricity', *Elect. Eng.*, vol. 90, no. 3, pp. 209–218.

Roivainen, J. 2009, 'Unit-wave response-based modeling of electromechanical noise and vibration of electrical machines', Ph.D. Thesis, Helsinki University of Technology, Espoo, Finland.

Sabonnadiere, J.C., Meunier, G., Morel, B., 1982. 'FLUX: A general interactive finite elements package for 2D electromagnetic fields', *IEEE Trans. Magn.* 18, pp. 624–626.

Singal, RK., Williams, K. and Verma, S.P., 1990, 'The Effect of windings, frame and impregnation upon the resonant frequencies and vibrational behavior of an electrical machine stator', *Experimental Mechanics***,** no. 30, pp. 270-280.

Singh, D., Rasilo, P., Martin, F., Belahcen, A., Arkkio, A., 2015, 'Effect of mechanical stress on excess loss of electrical steel sheets', *IEEE Trans. Magn.* 51, pp. 1–4.

Takagi, T. et al., 1997, 'Nondestructive residual stress management in butt welded steel plates using stress dependence of magnetostriction', *Electromagnetic nondestructive evaluation*, pp. 87-90.

Tilmar, P.L., and Lai J.C.S., 1994, 'Acoustic noise of electromagnetic origin in an ideal frequency-converter-driven induction motor', *IEEE proc. – Electric Power Applications'*, vol. 141, issue 6, pp. 1350-2352.

Tsivitse, P. J. , and Weihsmann, P. R., 1971, 'Polyphase induction motor noise', *IEEE Trans. Ind. Gen. Appl.*, vol. IGA-7, pp. 339-359.

Tsukerman, I., 1992, 'Overlapping finite elements for problems with movement', *IEEE Trans. Magn.* 28, pp. 2247-2249.

Valavi, M., Nysveen, A., Nilssen, R., Lorenz, R.D., Rølvåg, T., 2014a, 'Influence of pole and slot combinations on magnetic forces and vibration in low-speed PM wind

generators', *IEEE Trans. Magn.* 50. doi:10.1109/TMAG.2013.2293124.

Valavi, M., Nysveen, A., Nilssen, R.D., Rølvåg, T., 2014b, 'Slot harmonic effect on magnetic forces and vibration in low-speed permanent-magnet machine with concentrated windings', *IEEE Trans. Ind. Appl.,* vol. 50, pp. 3304–3313. doi:10.1109/TIA.2014.2309717

Valavi, M., Devillers, E., Besnerais, J. Le ,Nysveen, A., Nilsen, R., 2018, 'Influence of Converter Topology and Carrier Frequency on Airgap Field Harmonics, Magnetic Forces, and Vibrations in Converter-Fed Hydropower Generator', *IEEE Trans. Ind. Appl.*, vol. 54, pp. 2202–2214. doi:10.1109/TIA.2018.2801859.

Valente, G., Papini, L., Formentini, A., Gerada, C., Zanchetta, P., 2018, 'Radial Force Control of Multisector Permanent-Magnet Machines for Vibration Suppression', *IEEE Trans. Ind. Electron.* 65, pp. 5395–5405. doi:10.1109/TIE.2017.2780039

Vandevelde, L, Hilgert, T.G.D, and Melkebeek, J.A.A, 2008, 'Magnetic force and couple densities and magnetoelastic interaction', *IET 7th Int. Conf. Comp. Electromagn.*, Brighton, pp. 26-28.

Vandevelde, L., and Melkebeek, J.A.A., 2003, 'Magnetic forces and magnetostriction in electrical machines and transformer cores'*, IEEE Trans. Magn., vol. 39, no.3*, pp. 1618-1621.

Vandevelde, L., and Melkebeek, J.A.A., 2002, 'Modeling of magnetoelastic material'*, IEEE Trans. Magn.* 38, pp. 993–996.

Verma, S. P., and Girgis, R. S., 1975, 'Considerations in the choice of main dimensions of stators of electrical machines in relation to their vibration characteristics'*, IEEE Trans. Power App. Syst.*, vol. 94, no. 6, pp. 2151–2159.

Verma, S.P., and Girgis, R.S., 1981a, 'Experimental verification of resonant frequencies and vibration behavior of stators of electrical machines. Part 1: Models, experimental procedure and apparatus', *IEE Proc. B Electr. Power Appl.* vol. 128, no. 12.

Verma, S.P., and Girgis, R.S., 1981b, 'Experimental verification of resonant frequencies and vibration behavior of stators of electrical machines. Part 2: Experimental investigations and results'*, IEE Proc. B Electr. Power Appl.* vol. 128,no. 22.

Verma, S.P., Singal, R.K., and Williams, K., 1987a, 'Vibration behavior of stators of electrical machines, part I: theoretical study', *Journal of Sound and Vibration*, Vol. 115, No. 1, pp. 1-12.

Verma, S.P., Singal, R.K., and Williams, K., 1987b, 'Vibration behavior of stators of electrical machines, part II: experimental study', *Journal of Sound and Vibration*, Vol. 115, No. 1, pp. 13-23.

Vijayraghavan, P., and Krishnan, R., 1998, 'Noise in electric machines: A review', *IEEE Trans. Ind. Appl.* 35, pp. 1007–1013.

Villari, E. (1865), 'Ueber die aenderungen des magnetischen moments, welche der zug und das hindurchleiten eines galvanischen stroms in einem stabe von stahl oder eisen hervorbringen', *Ann. Phys. Chem. (Ann. Poggendorf)* 126, pp. 87–122.

Wang C., Lai J.C.S., and Astfalck A., 2004, 'Sound power radiated from an inverter driven induction motor II: numerical analysis', *IEE proc. – electric power applications*, vol. 151, issue 3.

Wang, C. and Lai, J.C.S. , 1999, 'Vibration analysis of an induction motor', *Journal of Sound and Vibration*, vol. 224, issue 4, pp. 733-756.

Weiss, Pierre; Foëx, Gabrie, 1926, 'Le *Magnétisme*', par Pierre Weiss et Gabriel Foëx, 2e édition, revue et corrigée (in French). libr. Armand Colin.

Weiss, P., 1907, 'L'hypothèse du champ moléculaire et la propriété ferromagnétique', *J. Phys. Theor. Appl.* 6(1), pp. 661–690.

Witczak, P., 1995. 'The magnetostriction forces in the induction motor', *COMPEL*, Vol. 14, No. 4, pp. 229–232.

Witczak, P., 1996, 'Calculation of force densities distribution in electrical machinery by means of magnetic stress tensor', *Archive of Electrical engineering*, vol. XLV, No. 1, pp. 67–81.

Yamazaki, K., and Kato, Y.,2014, 'Iron loss analysis of interior permanent magnet synchronous motors by considering mechanical stress and deformation of stators and rotors', *IEEE Trans. Magn.*, vol. 50, no. 2, Art. no. 7022504.

Zaidi, H., Santandrea, L., Krebs, G., Le Bihan, Y., Demaldent, E., 2012, 'Use of overlapping finite elements for connecting arbitrary surfaces with dual formulations', *IEEE Trans. Magn.* 48, pp. 583–586.

Zhang, H., Zanchetta, P., Bradley, K.J., Gerada, C., 2010, 'A low-intrusion load and efficiency evaluation method for in-service motors using vibration tests with an accelerometer', *IEEE Trans. Ind. Appl.*, vol. 46, pp. 1341–1349. doi:10.1109/TIA.2010.2049550.

Zhou, H.M., Zhou, Y.H., Zheng, X.J., Ye, Q., Wei, J., 2009, 'A general 3-D nonlinear magnetostrictive constitutive model for soft ferromagnetic materials', *J. Magn. Magn. Mater.* 321, pp. 281.

Publication Errata

Publication I

In Section IV. A second paragraph, in the last sentence, “The change of the force error…” is incorrectly placed. It should come before the last sentence of the third paragraph “When the length of the airgap…”

In Section IV. B second paragraph, in the first sentence, “In permanent magnet synchronous motors the Halbach magnet array…” should be read as, “In permanent magnet synchronous motors where Halbach magnet array…”

Publication IV

In section 2.1, the last sentence of the last pargraph ends as “.. right side of (2).” The (2) means the second equation in that section 2.

Aalto-DD 34/2020

When an electrical machine is supplied by electrical energy, various multi-physical phenomena take place during the initial startup phase and at different operational stages of the machine. One major pathway of the energy is from electrical energy to magnetic energy, magnetic to mechanical and mechanical to acoustic energy. Modeling various parameters related to these different domains is challenging and numerical computational tools are vital in such tasks.

From the design phase to condition-monitoring and fault-diagnostics of electrical motors, the knowledge of electromagnetic forces, vibration patterns and acoustic noise is imperative, as these variables provide substantial information on the behavior of the machine under different operating conditions. This thesis successfully addresses and models the fascinating journey of energy in electrical machines and proposes efficient computational and experimental schemes for calculating the associated electromagnetic, magnetomechanical and vibro-acoustic parameters.

ISBN 978-952-60-8969-0 (printed)
ISBN 978-952-60-8970-6 (pdf)
ISSN 1799-4934 (printed)
ISSN 1799-4942 (pdf)

Aalto University
School of Electrical Engineering
Electrical Engineering and Automation
www.aalto.fi

BUSINESS + ECONOMY

ART + DESIGN + ARCHITECTURE

SCIENCE + TECHNOLOGY

CROSSOVER

DOCTORAL DISSERTATIONS